

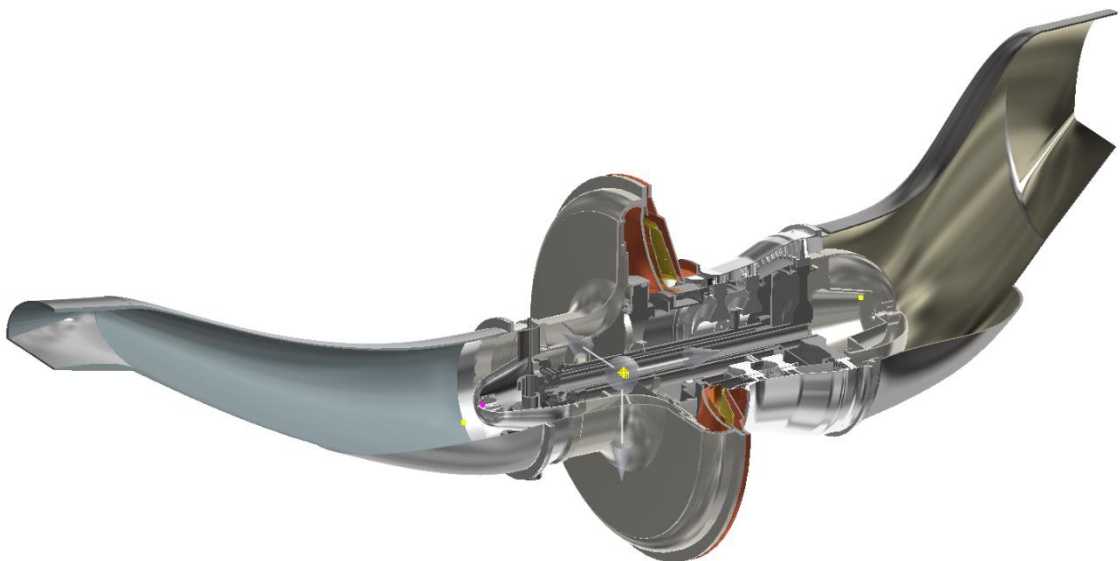


**Military  
University  
of Technology**

Team: Total Incredible Technical Solutions

# PFF-63 - Candidate Engine for a Hybrid Electric Medium Altitude Long Endurance Search and Rescue UAV

AIAA Foundation Student Design Competition 2018/19  
Undergraduate Team – Engine



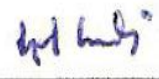
# Signature page

## Design team:

Karol Kozdrowicz	
karol.kozdrowicz@student.wat.edu.pl	#904279
Maciej Spychała	
	#921050
Damian Maciorowski	
	#919069
Karolina Pazura	
	#919607

## Faculty Advisor:

dr hab. inż. Ryszard Chachurski

  
#920758

## **Abstract**

The following report details the design of PFF-63 turboshaft, as a replacement for the TPE331-10, candidate engine for a Hybrid Electric Medium Altitude Long Endurance Search and Rescue UAV.

The PFF-63 incorporates modern engine architecture, advanced solutions and technologies including:

1. High efficiency architecture
2. Higher cycle pressure ratio
3. Successful usage of birotational compressor
4. Higher turbine inlet temperature
5. Usage of ceramic matrix composite
6. Elimination of nozzle stage in power turbine
7. No active cooling for turbine
8. Significant decrease of mass

The primary requirements for this engine were to lower fuel burn, while provide decrease of weight and greater efficiency. Advanced, modern materials with great thermal properties are used to eliminate turbine cooling. Also usage of birotational compressor significantly increase efficiency of a cycle and lowers mass.

The PFF-63 offers a 29 % lower SFC at loiter, an 42 % decrease in mass and increase of 313 °R temperature at the exit of combustion chamber.

# Contents:

Nomenclature.....	5
1. Introduction.....	9
2. Cycle analysis.....	10
2.1. Parametric design concept.....	10
2.1.1. Engine cycle constraints and assumptions.....	11
2.2. Engine concepts for PFF-63.....	12
2.3. Concepts analysis.....	12
2.3.1. Compression efficiency.....	12
2.3.2. Compressors geometry comparison.....	14
2.3.3. Concepts of mass comparison.....	16
2.4. Analysis of results.....	17
3. Inlet design.....	22
3.1. Inlet construction technical description.....	23
4. Compressor.....	24
4.1. Gas-dynamic analysis.....	24
4.1.2. The centrifugal compressor.....	24
4.1.3. The centrifugal compressors diffuser.....	26
4.1.4. Planetary gear.....	30
4.1.5. Compressor construction technical description..	31
5. Combustion system.....	32
5.1. Combustor inlet analysis.....	32
5.2. Combustor flow analysis.....	32
5.3. Combustion efficiency.....	32
5.4. Temperature profile.....	33
5.5. Used materials.....	34
6. Turbine design .....	34
6.1. Projecting assumptions.....	34
6.2. Gas-dynamic analysis of HPT.....	35
6.3. Gas-dynamic analysis of PT.....	39
6.4. Blade-profile design.....	40
6.5. Material selection.....	40
6.6. Cooling system.....	41
6.7. Tensile calculations.....	41
6.8. Locking piece design.....	44
6.9. Tensile calculation of blades.....	44
6.10. Turbine construction technical description.....	46
7. Diffuser design.....	47
7.1. Diffuser construction technical description.....	47
8. Additional systems.....	48
8.1. Control system.....	48
8.2. Fuel system.....	48
8.3. Bearings.....	48
8.4. Lubrication system.....	49
8.5. Anti-icing system.....	50

8.6. Fire detection and extinguishing system.....	50
9. Summary.....	50
10. References.....	53
Appendix 1. Assembly drawing of the inlet.....	54
Appendix 2. Assembly drawing of the compressor.....	55
Appendix 3. Assembly drawing of the turbine.....	56
Appendix 4. Assembly drawing of the diffuser.....	57
Appendix 5. Assembly drawing of the PFF-63 engine.....	58
Appendix 6. Three dimensional model of the PFF-63 engine.....	59

## Nomenclature

### *Normal*

Aphy	Cross-section area
Afs	Free stream area
Ath	Throat area
B	Supporting coefficient
Cfg	Gross thrust coefficient
CdTh	Discharge or flow coefficient
Cv	Velocity coefficient
D	Supporting coefficient
Fg	Gross thrust
MNth	Throat mach number
N1	Power shaft rotational speed
N2	High pressure shaft rotational speed
NP	Post-gear shaft rotational speed
P	Pressure
PR	Pressure ratio
Rt	Gas constant
$T_{4.1}$	Turbine rotor inlet temperature
$T_s$	Static temperature
$T_t$	Total temperature
TtOut	Exit temperature
$U$	Peripheral velocity
Vact	Gas exit velocity
VTAS	Vehicle true aircraft speed
$W$	Air mass flow rate
$W_c$	Corrected air mass flow rate
$W_{fuel}$	Fuel mass flow rate
$W_{fuelHR}$	Fuel mass flow rate per hour

### *Normal lowercase*

$a$	Local sound velocity; coefficient depended on kind of vibrations
$b$	Impeller width; chord of blade
$c$	Tip clearance
$c_p$	Specific heat
$e$	Polytropic efficiency
$F_1$	Force
$f$	Vibration frequency
$f$	Bend of blade
$f_d$	Dynamic vibrations
$g$	Thickness of blade
$h$	Height of teeth
$h_f$	Height of teeth feet
$h_h$	Height of teeth head

$i$	Transmission ratio
$j$	Side shake
$p$	Width of wheel
$p_{t1...n}$	Total pressure in diffuser
$\frac{p_{tn-1}}{p_{tn}}$	Shock total pressure recovery
$M$	Module pitch
$M_{0...n}$	Mach number
$M_1$	Moment
$Re$	Reynolds number
$R_0$	Hole radius
$R$	Disk radius
$r$	Radius; running radius
$x$	Parameter safety record along to radius

*Greek characters*

$\beta$	Shock move angle
$\beta_{1k}$	Angle of blade setup
$\eta$	Efficiency, kinematic viscosity
$\eta_c$	Adiabatic efficiency
$\pi$	Pressure
$\delta$	Deflection angle
$\tau$	Fuel-to-air ratio
$\gamma$	Heat capacity ratio
$\lambda$	Flow drag factor
$\sigma(R)$	Stresses depended on radius
$\sigma_{dop}$	Allowable stresses
$\sigma_r$	Radial stresses
$\sigma_u$	Tangential stresses
$\sigma_w$	Stresses assumed from mass stresses
$\sigma_z$	Reduced stresses
$\sigma$	Loss coefficient
$\theta$	Peripheral component
$\omega$	Angular velocity
$\pi$	Pressure ratio
$\rho$	Density

*Suffix*

1	Intake inlet station
2	Intake exit station
3	Compressor exit station
4	Combustor exit station
alt	Altitude
amb	Ambient
av	Average
b	Burner

c	Compressor
dTamb	Delta T from ISO
dPnorm	Pressure losses
eff	Adiabatic efficiency
ec	Economical
efPoly	Polytrophic efficiency
eRam	Ram recovery
Fram	Ram drag
gamt	Ratio of specific heats
h	Hub
ht	Stagnation enthalpy
iz	Isentropic
InEng	Inlet efficiency
k	Heat capacity ratio
opt	Optimal
pwr	Power off-take
r	Radial component
rel	Relative
s	Static
t	Total
trq	Torque

#### *Abbreviations*

BSFC	Brake specified fuel consumption
CMC	Ceramic Matrix Composites
CO	Carbon Monoxide
EPA	U.S. Environmental Protection Agency
ESHP	Equivalent shaft power delivered
ESFC	Equivalent specified fuel consumption
FAR	Fuel-to-air ratio
HPC	High pressure compressor
HPT	High pressure turbine
ITTC	Power turbine inlet temperature
KTAS	Knots true aircraft speed
LHV	Lower heating value
LPC	Low pressure compressor
LPT	Low pressure turbine
MN	Mach number
NO <sub>x</sub>	Nitric Oxide
NPSS	Numerical Propulsion System Simulation
OPR	Overall pressure ratio
RFP	Request for proposal
RQL	Rich – Quench – Lean
SHP	Shaft power delivered
SLS	Sea level standard
THP	Thrust equivalent to power

TRIT	Turbine rotor inlet temperature
TR	Temperature ratio
UAV	Unmanned Aerial Vehicle
UHC	Unburned hydrocarbon
VTAS	Vehicle true aircraft speed

# 1. Introduction

The RFP is calling for candidate hybrid electric propulsion which might be used in medium altitude long endurance search and rescue UAV[1.1]. The new engine must be more efficient, lighter, fit in a similar envelop and have a low lifecycle costs.

Originally Honeywell TPE331-10 (figure 1.1) was a single-shaft turboprop driving an electric propulsion system. It contained :

- Highly consolidated boundary layer ingesting intake ;
- Two stages of centrifugal compressor;
- Reverse-flow combustion chamber;
- Three stages of axial turbine;
- Diffuser;

Overall parameters and performance are presented in table 1.1.

The first run of this engine was in 1960, this engine, after all, reliable and efficient, it has been on duty for 59 years what without changes in architecture results that in compare to modern engineering it is behind times. Nowadays materials have better thermal properties, are lighter and higher cycle pressure ratios are achievable.

Table 1.1. Honeywell TPE331-10: Basic Data and Performance [1.1]

Parameter	Unit	Value
Overall Pressure Ratio (OPR)	—	10.55
Mass flow	$\frac{\text{lb}}{\text{s}}$	7.7
Turbine Rotor Inlet Temperature ( $T_{4.1}$ )	°R	2576
Outer Casing Diameter	in	27
Engine length	in	43
Engine weight	lb	385
Brake specific fuel consumption (BSFC)	$\frac{\text{lb}}{\text{hr} * \text{hp}}$	0.534
Shaft power delivered (SHP)	hp	940

The main goal is to provide 25 % savings of fuel burn at loiter. It is expected to achieve at least 20 hours of loiter with 602 gallons of fuel capacity. The airframe gas generator propels an electrical propulsion system. The system has been designed to fit the required shaft horsepower provided by the baseline engine during its flight envelope. The customer does not want any modification to their electrical generator or system.



**Fig. 1.1. Honeywell TPE331-10 turboshaft [1.2]**

In addition, variety of other requirements were specified and presented in RFP. The proposed cycle, has to meet power requirements presented in table 1.2.

**Table 1.2 General power requirements**

Takeoff	SLS Std. Day	953 shp
Cruise	220 KTAS, 12500 ft	690 shp
Loiter	190 KTAS, 7000 ft	603 shp

Process of accurate reproduction and optimization of TPE331-10 cycle proceeded using Numerical Propulsion System Simulation (NPSS) software and self-written programs in MS Excel 2010.

## 2. Cycle analysis

This section contains the arrangements of the design engine, called PFF-63, like trade-off studies and design. The baseline design cycle and comparison of key parameters and performance will be presented in tables. In the end of this chapter a final engine design cycle is presented.

### 2.1. Parametric design concept

Engine design started with parametric cycle analysis, which assumes that all design choices are still under control and that the size of the engine has not been chosen yet. At this point in the development process the engine is just a mental image which, after deep analysis and research on needs, would become a final, polished product. Therefore, each complete set of design choices results in a component with its own geometry and operating characteristics. This stage of design is usually called in the literature as an "on-design" or "design point" cycle analysis.

Commonly it is difficult and even sometimes impossible to identify a single point that may dictate the proper way of a design. The final design of an engine is based on its performance over the entire aircraft mission. The best solution is chosen in favor of balanced behavior over the whole flight spectrum and fully matches one of the mission flight conditions. The best option is to refer to the operating point (for example loiter) at which all design quantities are known as the "reference point." There are at least three good reasons for this practice. Firstly, engine performance analysis at conditions away from the reference point, usually referred to in the literature as "off-design" cycle analysis, can not start until the reference point and the size of the engine have been chosen by some means. Secondly, parametric analysis is much less tedious and time consuming than performance analysis, often providing mathematical optima that can be directly exploited.

Thirdly and the most importantly, identifying the combinations of design choices that provide the best performance at each mission flight condition reveals trends that show the way to the best solution. A reasonable expectation after the completion of the parametric cycle analysis is that the most promising type of cycle has been identified and the possible range of each design choice has been bracketed [2.1].

### 2.1.1. Engine cycle constraints and assumptions

At the beginning it was necessary to find out the capabilities offered by modern materials. Due to research it was decided that max temperature  $T_4$  should not be greater than 2650 °R. This fact was used as a primary assumption that lead to optimal overall pressure ratio.

According to publications of Wiatrek [2.2] economical pressure ratio, which related to minimal specified fuel consumption, is higher than optimal overall pressure ratio given by equation 2.1:

$$\pi_{ek} > \pi_{opt} = \left( \sqrt{k_{av} * \tau * \eta_T * \eta_C} \right)^{\frac{k}{k-1}} = 9.9 \quad (\text{Eq. 2.1})$$

where:

$k_{av}$  – average heat capacity ratio (~1.02-1.04)

$\tau$  – engine heat ratio ( $\frac{T_4}{T_{amb}}$ )

$\eta_T$  – turbine isentropic efficiency

$\eta_C$  – compressor isentropic efficiency

The main requirement, to provide 25 % fuel burn savings at the loiter, would be achieved through lower fuel flow rate. This might be obtained via higher compressor pressure ratio and lower mass flow rate. The equations and calculations needed to show this tendency are shown in table 2.1 and figure 2.1.

**Table 2.1. Fuel-Air Ratio and fuel mass flow calculations**

Parameter	Equation	Value	Unit
$\pi_c$	$\frac{T_3^*}{T_{amb}^*}$	10.53	–
$\eta_s$	–	0.715	–
$\sigma_b$	–	0.99	–
LHV	–	18400	$\frac{\text{BTU}}{\text{lb}}$
$T_4^*$	–	1341	°R
$T_3^*$	$T_3^* = T_2 * \left( 1 + \left( \frac{(\pi_c)^{\frac{k}{k-1}} - 1}{\eta_s} \right) \right)$	1111	°R
$C_p'$	$C_p' = \left( \frac{k'}{k' - 1} \right) * R$	0.265	$\frac{\text{BTU}}{\text{lb} * ^\circ\text{R}}$
$C_p$	$C_p = \left( \frac{k}{k - 1} \right) * R$	0.297	$\frac{\text{BTU}}{\text{lb} * ^\circ\text{R}}$
FAR	$FAR = \frac{C_p' * T_4^* - C_p * T_3^*}{LHV * \sigma_b}$	0.021	–
$W_{air}$	–	7.2	$\frac{\text{lb}}{\text{s}}$
$W_{fuel}$	$W_{fuel} = W_{air} * FAR$	0.152	$\frac{\text{lb}}{\text{s}}$

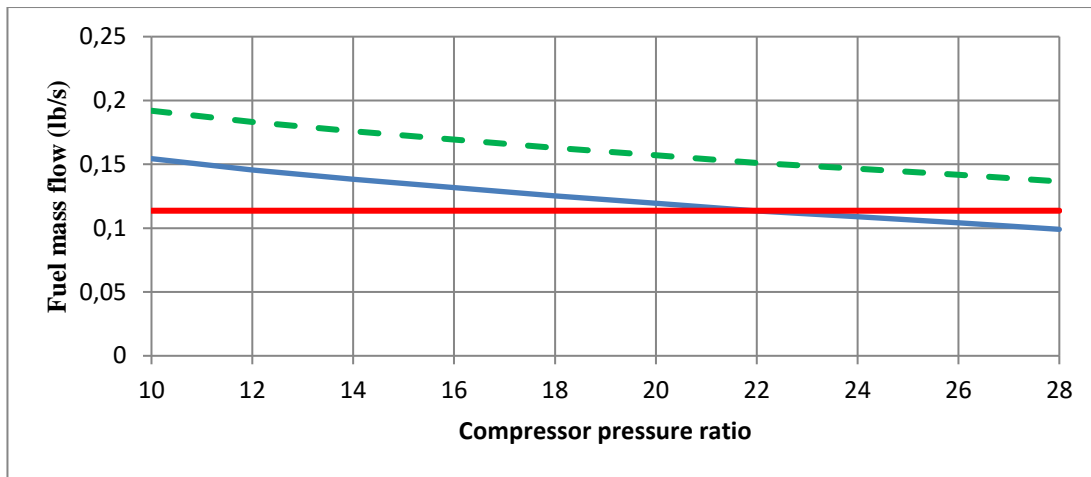


Fig. 2.1. Fuel mass flow in function of compressor pressure ratio for different turbine inlet temperatures: **blue line** – for  $T_4^* = 2414$  °R, **green line** –for  $T_4^* = 2700$  °R, **red line** – a required value

To provide sufficiently low fuel burn at loiter significantly higher compressor pressure ratio is required. Figure 2.1 shows that this parameter should be twice as high as the optimal specified for TPE331-10.

## 2.2. Engine concepts for PFF-63

In this paper, three different, promising concepts were taken into consideration:

1. Bringing the Honeywell TPE331-10 up-to-date via higher compressor stage loading, efficiency and higher turbine inlet temperature.
2. Replacing one of baseline engines centrifugal compressor with multistage (2 - 3) axial compressor, higher loading of centrifugal compressor stage and higher turbine inlet temperature.
3. Increase of turbine inlet temperature and usage of highly loaded centrifugal stage of compressor with counter-rotating diffuser to provide high pressure ratio and efficiency in compact form.

Concept number 1 is a very convenient choice. Since well known architecture with improvement of components is easy to achieve, nevertheless high pressure ratios combined with the low mass flow rate results in low values flow paths area. Consequently, the gap between outer centrifugal compressor casing and a rotor on the exit of the compressor might be too small to manufacture blades which would work correctly. On the other hand it leads to reduction of efficiency. The second and the third concepts are very similar in terms of cycle performance. Both might provide high pressure ratios and high efficiencies. The concepts mainly differ in geometry. Although concept number 2 provides similar thermal efficiency cycle performance, it might be occupied with extra mass and length.

## 2.3. Concepts analysis

As the concepts differ only in the way compression is done, in this subsection comparison of compression efficiency, compressor geometry and overall concept mass will be presented.

### 2.3.1. Compression efficiency

According to publication of Farokhi [2..3] efficiency of standard centrifugal compressor reaches up to  $\eta = 0.86$  for low pressure ratio and is equal to  $\sim 0.84$  for stages with pressure ratio of 5...8 (figure 2.2). It means that for two stages in series for pressure ratio of  $\pi = 25 \dots 30$  the isentropic compression efficiency will be approximately equal to 0.7.

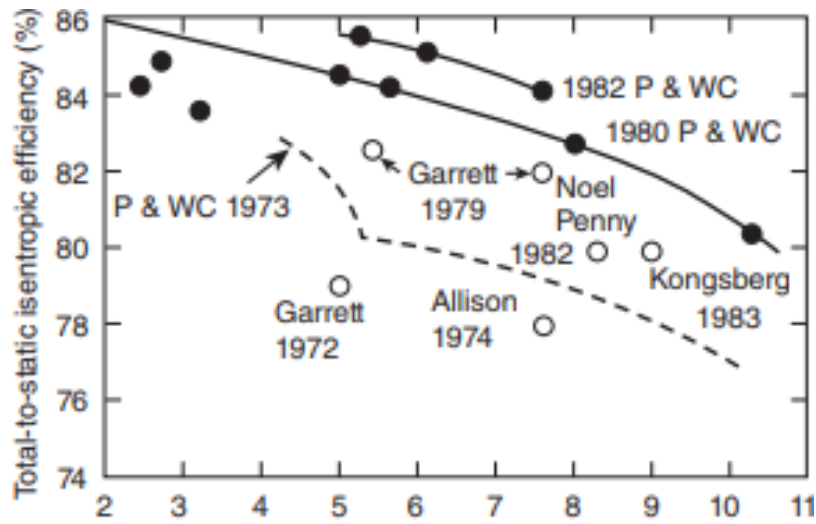


Fig. 2.2. Centrifugal compressor isentropic efficiency in function of stage loading [8]

In the figure 2.2 it is shown that any combination of two stages of centrifugal compressor would provide satisfying efficiency. Therefore replacing the first stage with two or three stages of low loaded axial stages and incensement of centrifugal stage loading might lead to a better solution. According to publication of Farokhi [2.3] single stage efficiency might obtain  $\eta_{stage} \approx 0.92$ . Taking into consideration three stages of axial compressor, which stage loading is equal to  $\pi_{stage} = 1.40$  and then one stage of centrifugal compressor with pressure ratio of  $\pi_c = 9$ , leads to compression rate of nearly  $\pi = 25$  with isentropic efficiency of  $\eta = 0.73$ .

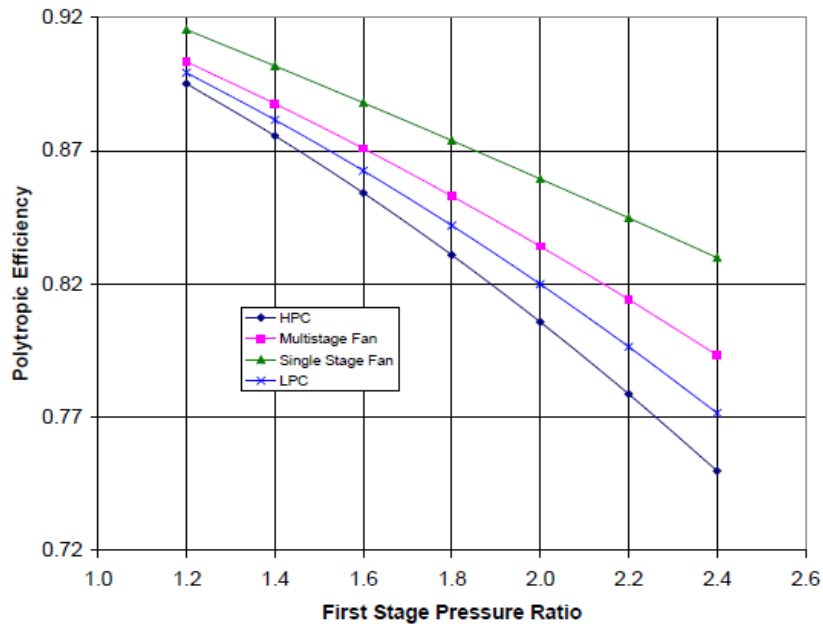


Fig. 2.3. Axial compressor stage efficiency in function of stage loading [1]

Compressor adiabatic efficiency was obtained through equation 2.2.

$$\eta_c = \frac{\pi^{\frac{k-1}{k}} - 1}{\pi_c^{\frac{k-1}{k}} - 1} \quad (\text{Eq. 2.2})$$

As it was mentioned before centrifugal compressor with counter-rotating diffuser on the top reaches compression rate equal to  $\pi = 25$  with isentropic compression efficiency of  $\eta = 0.8$ .

### 2.3.2. Compressors geometry comparison

The centrifugal compressor, due to its excellent performance in low mass flow rate environment, is a base for every concept. The comparison focused on two most significant dimensions: the impeller radius  $r_2$  as it would determine engine envelope maximum diameter and the impeller exit width  $b$ . The low value of this second parameter results in significant losses related to short blades. Following calculations consider the final compressor stage. It means that compressor inlet parameters were calculated earlier and are different for each concept.

In table 2.2 the comparison of all three concepts in terms of geometry are presented. All calculations were done based on the reference [2.3].

**Table 2.2. Impeller radius and width at the exit calculations for each concept**

Parameter	Equation	Unit	Value for concept		
			1	2	3
Imp. inlet temperature	$T_1 = T_{t1} - \frac{C1^2}{2 * c_p}$	°R	843.3	680.4	493.9
Imp. inlet sound velocity	$a = \sqrt{((k - 1) * c_p * T_2)}$	$\frac{\text{ft}}{\text{s}}$	1420.6	1279.2	1089.4
Imp. inlet Mach number	$M_1 = \frac{C_1}{a_1}$	–	0.382	0.426	0.5
Imp. exit tangential velocity	$C_{\theta 2} = U - W_{\theta 2} * \tan(\beta)$	$\frac{\text{ft}}{\text{s}}$	1765.1	1949.5	1831.2
Imp. exit absolute velocity	$C_2 = \sqrt{C_{\theta 2}^2 + C_{2r}^2}$	$\frac{\text{ft}}{\text{s}}$	1847.1	2021.8	1910.4
Imp. exit peripheral velocity	$M_{T2} = \frac{U_2}{a_1}$	–	1.46	1.76	1.96
Support constant 1	$B = \frac{a_2}{a_1} \approx \sqrt{1 + \frac{\left(\frac{y-1}{2}\right) * M_{T2}^2}{1 + \left(\frac{y-1}{2}\right) * M_1^2}}$	–	1.19	1.27	1.31
Imp. exit sound velocity	$a_2 = A * a_1$	$\frac{\text{ft}}{\text{s}}$	1692.9	1618.8	1450.0
Support constant 2	$D = \frac{T_{t2}}{T_{t1}} \approx \frac{U_2^2}{c_p * T_{t1}} * \left(\frac{C_{\theta 2}}{U_2}\right)$	–	1.69	2.04	2.26
Imp. exit total temp.	$T_{t2} = B * T_{t1}$	°R	1490.4	1440.0	1173.1
Imp. exit static temp.	$T_2 = T_{t2} - \frac{C_2^2}{2 * c_p}$	°R	1231.2	1098.3	869.2
Imp. exit tangential velocity	$M_{\theta 2} = \frac{C_{\theta 2}}{a_2}$	–	1.04	1.20	1.27
Imp. exit Mach number	$M_2 = \frac{C_2}{a_2}$	–	1.09	1.24	1.32
Imp. heat ratio	$\tau_c = \frac{T_{t2}}{T_{t1}}$	–	1.69	2.04	2.26
Imp. exit total pressure	$P_2 = P_{t1} * \pi_c$	psi	364.38	365.06	182.53

The continuation of the table is on the next page.

The continuation of the table 2.2.

Parameter	Equation	Unit	Value for concept		
			1	2	3
Imp. exit static pressure	$P_1 = \frac{P_{t1}}{\left(1 + \frac{k-1}{2} * M_1^2\right)^{\frac{k}{k-1}}}$	psi	65.08	35.70	12.27
Imp. Inlet density	$\rho_1 = \frac{P}{R * T_1}$	$\frac{\text{lb}}{\text{ft}^3}$	0.21	0.16	0.07
Imp. Inlet area	$A_1 = \frac{W}{\rho_1 * C_{1z}}$	in <sup>2</sup>	6.2	9.3	24.11
Imp. Inlet tip radius	$r_{1t} = \sqrt{\frac{A_1}{\pi} + r_{1h}^2}$	in	2.87	2.76	1.66
Rotational speed	$\omega = a_1^2 * M_{rel1}^2 - C_{z1}^2$	$\frac{\text{rad}}{\text{s}}$	6821	4975.6	6821.4
Rotational speed	$\omega_{rpm} = \omega * \frac{60}{2 * \pi}$	RPM	65139	47514	65139
Imp. exit static pressure	$P_2 = \frac{P_{t2}}{\left(1 + \frac{k-1}{2} * M_2^2\right)^{\frac{k}{k-1}}}$	psi	173.77	141.76	63.89
Imp. exit density	$\rho_2 = \frac{P_2}{R * T_{r2}}$	$\frac{\text{lb}}{\text{ft}^3}$	0.41	0.35	0.23
Imp. exit area	$A_2 = \frac{W}{\rho_2 * C_{2r}}$	in <sup>2</sup>	12.4	4.65	8.05
Imp. exit radius	$r_2 = \frac{U_2}{\omega}$	in	5.51	5.11	3.54
Imp. exit width	$b = \frac{A_2}{2 * \pi * r_2}$	in	0.03	0.14	0.32

Impeller radius is the lowest for concept number 3 and is 36 % lower than for concept number 1. Further only centrifugal compressor with rotating diffuser provides sufficient impeller exit width. In such case higher mass flow rate for the concept 1 and 2 is needed. Further analysis of this pattern is shown in figure 2.4.

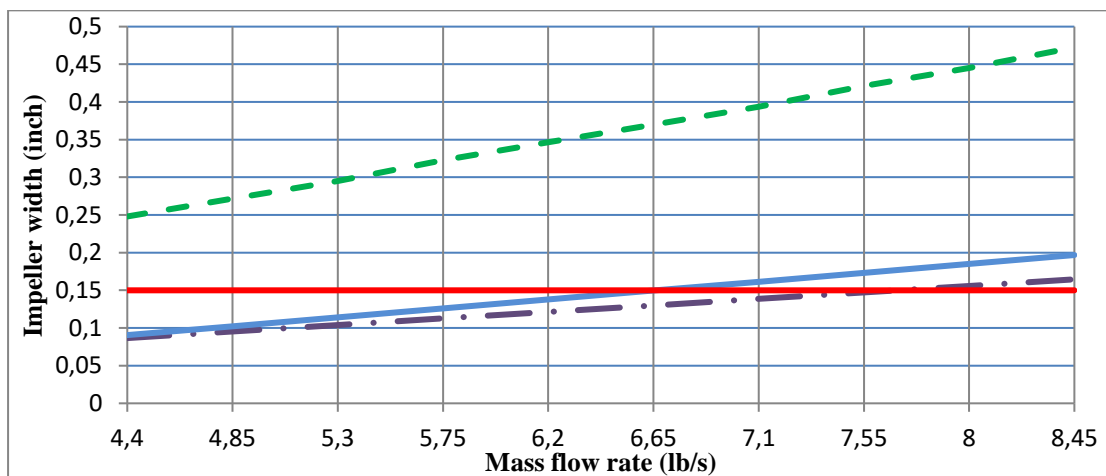


Fig. 2.4. An impeller width comparison: Violet line - concept 1, blue line - concept 2, green line - concept 3, red line - a minimal value

Calculations have shown that concept 1 requires mass flow rate of at least  $7.55 \frac{lb}{s}$  to provide sufficient impeller width. For other concepts this parameter is much lower. Mass flow rate affects overall engine mass fuel flow rate largely.

### 2.3.3. Concepts of mass comparison

Every concept requires less air mass flow to work efficiently than Honeywell TPE331-10, thus none of them has been initially rejected. All mass calculations have been done based on publication of Grigoriew [2.4]. The methodology is based on equation 2.3 and contains variety of statistical coefficients.

$$M_e = B * K_{m0} * K_{Tg} * W^{m_1} * (\pi^{0.286} - 1)^{m_2} * K_s * K_{res} \quad (\text{Eq. 2.3})$$

Where:

$B, m_1, m_2$  – coefficients that differ for engines with and without reduction gear:

- Engines with reduction gear -  $m_1 = 0.831, m_2 = 0.206, B = 56.3,$
- Engines without reduction gear -  $m_1 = 0.888, m_2 = 0.541, B = 36.9,$

$K_{rec}$  – coefficient calculated using lifecycle of engine, varies from 0.9-1 for military and acrobatic vehicles and reaches up to 1.07 for long-distance transport,

$K_{Tg}$  – coefficient dependent on turbine rotor inlet temperature and is described by equation 2.4

$$K_{Tg} = 1 + 2 * 10^{-4} * (T_{4.1}^* - 1200) \quad (\text{Eq. 2.4})$$

$K_s$  – coefficient related to technology level, dependence is shown in figure 2.5.

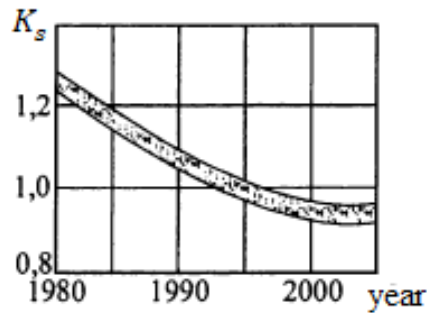


Fig. 2.5. Technology level coefficient [14]

At the beginning of engine mass analysis, validation of equation 2.3 (based on Honeywell TPE-331-10) was done. All required coefficients were chosen carefully, based on given methodology and are presented in table 2.3.

Table 2.3. Assumed values used in equation 5.4 with a result

$\pi$	10.53
$W$	7.7 lb
$B$	56.3
$K_{m0}$	1
$K_{Tg}$	1.046
$K_s$	1.2
$K_{res}$	0.9
$m_1$	0.831
$m_2$	0.206
$M_e$	393.8 lb

The result obtained is within 2.2 % of the value given by producer (385 lb). Thus, the equations can be used for further analysis.

For design concepts some changes in assumption should be done, namely:

- $\pi$  – value of compressor ratio will be set to 25 as it was assumed in section 2.4.2;
- $W$  – will be set separately for every concept (as the minimum required) based on figure 2.1;
- $K_s$  – the coefficient will be set to 0.9;
- $B, m_1, m_2$  – as a vehicle is designed for turboshaft no reduction gear is needed;

Mass values for every concept are presented in table 2.4.

**Table 2.4. Design concepts mass comparison**

	<b>Concept 1</b>	<b>Concept 2</b>	<b>Concept 3</b>
$\pi$	25	25	25
$W$	7.54 lb	6.66 lb	5.60 lb
$M_e$	124.9 lb	111.8 lb	96.0lb

## 2.4. Analysis of results

All three were compared based on their efficiency, geometry and mass. Highly loaded centrifugal stage with counter-rotating diffuser is significantly better than other concepts. It provides the highest compression efficiency, lowest maximum diameter and mass. Thus, concept 3 is the one that will be considered in further analysis. Using NPSS v2.8 a design engine was generated.

All parameters used as software inputs are listed in table 2.5.

**Table 2.5. Design inputs to NPSS v2.8 software**

<b>Ambient conditions</b>		<b>Unit</b>
Design Mach Number	0	–
Altitude	0	–
Delta T from ISO	0	–
<b>Inlet</b>		
Air mass flow	6.1	$\frac{\text{lb}}{\text{s}}$
Design Mach Number	0.5	–
<b>LPC</b>		
Design Mach Number	0.5	–
$\pi_{LPC}$	1	–
$\eta_{LPC}$	1	–
<b>HPC</b>		
Design Mach Number	0.5	–
$\pi_{HPC}$	25	–
$\eta_{HPC}$	0.8	–
<b>Bleeds</b>		
Turbine Cooling Air	0	–
Leakage Air	0	–
<b>Nozzle</b>		
Total pressure losses	0.99	–
Nozzle Thrust Coefficient	0.96	–

The continuation of the table is on the next page.

The continuation of the table 2.5.

Ambient conditions		Unit
<b>Burner</b>		
Design Mach Number	0.1	—
Total pressure losses	0.07	—
$\eta_B$	0.99	—
<b>HPT</b>		
Design Mach Number	0.3	—
$\eta_{HPT}$	0.92	—
$\pi_{HPT}$	6.826	—
<b>Inter turbines duct (D05/06)</b>		
Design Mach Number	0.3	—
Total pressure losses	0.03475	—
<b>LPT</b>		
Design Mach Number	0.35	—
$\eta_{LPT}$	0.82	—
$\pi_{LPT}$	3.853	—
Power Turbine Inlet Temp.	705.30	°C
<b>Shafts</b>		
HP Shaft rotational speed	42800	RPM
PT Shaft rotational speed	30500	RPM
PT Shaft horse power	990	hp

Input parameters listed below have been put into NPSS software. This resulted in very promising cycle. In the figure 2.6 design engine cycle is presented.

```

*****
Date:12/27/18 Time:18:52:53 Model: cdm06_tp00 mode: DESIGN converge = 1 CASE: 1
Version: NPSS_2.8 Gas Package:GasTbl iter/pass/Jacob/Broy= 13/ 18/ 1/11 Run by: karo1
*****
SUMMARY OUTPUT DATA
MN alt dTamb VTAS N1 N2 NP T41 ITTC SHP THP ESHP BSFC ESFC
0.000 0.0 0.00 0.00 42800.0 30500.0 ----- 2553.36 705.30 990.00 32.66 1022.66 0.404 0.391

FLOW STATION DATA
F010 FsEng_F1_0 W Pt Tt ht FAR Wc Ps Ts Aphy MI gant Rt
F020 InEng_F1_0 6.10 14.696 518.67 123.95 0.0000 6.10 14.696 518.67 ----- 0.0000 1.40052 0.06856
F029 Cmpl_F1_0 6.10 14.696 518.67 123.95 0.0000 6.10 12.388 493.92 23.8 0.5000 1.40052 0.06856
F030 CmpH_F1_0 6.10 367.398 1454.17 357.10 0.0000 0.41 311.169 1392.37 1.6 0.5000 1.35283 0.06856
F031 B030_F1_0 6.10 367.398 1454.17 357.10 0.0000 0.41 330.098 1414.09 1.9 0.4000 1.35283 0.06856
F040 BrnPri_F1_0 6.21 341.680 2553.36 676.72 0.0182 0.59 339.471 2549.53 10.4 0.1000 1.30016 0.06855
F045 TrbH_F1_0 6.21 60.452 1761.21 447.75 0.0182 2.78 56.973 1735.77 16.9 0.3000 1.32490 0.06855
F050 D050_F1_0 6.21 59.847 1761.21 447.75 0.0182 2.81 56.403 1735.77 17.1 0.3000 1.32490 0.06855
F060 TrbP_F1_0 6.21 15.682 1348.79 335.09 0.0182 9.39 14.452 1320.68 49.5 0.3500 1.34637 0.06855
F070 D060_F1_0 6.21 15.290 1348.79 335.09 0.0182 9.63 14.397 1328.04 58.1 0.3000 1.34637 0.06855
F090 NozPri_F1_0 6.21 15.290 1348.79 335.09 0.0182 9.63 14.696 1335.10 70.4 0.2432 1.34637 0.06855

TURBOMACHINERY PERFORMANCE DATA
CmpL Wc PR eff TR effPoly pwr SMW SMW s_Re
CmpH 6.10 1.000 1.0000 1.0000 -0.0000 0.0 13.96 19.91 1.00000
CmpH 6.10 25.000 0.8000 2.8037 0.8658 -2012.2 56.98 30.37 1.00000
TrbH 0.59 5.652 0.9200 1.4498 0.9027 2012.2
TrbP 2.81 3.816 0.8200 1.3058 0.7931 990.0

TURBOMACHINERY MAP DATA
CmpL WcMap PRmap effMap NcMap R/Param s_WcDes s_PRDes s_effDes s_NcDes
CmpL 71.45 5.397 0.8223 1.000 2.0000 0.0854 0.0000 1.2161 -----
CmpH 2.72 2.300 0.8400 1.000 2.0000 2.2426 18.4615 0.9524 -----
TrbH 10.14 6.000 0.8998 100.000 6.0000 0.0906 0.9304 1.0224 8.4701
TrbP 35.30 6.000 0.9231 100.000 6.0000 0.1234 0.5633 0.8883 7.2677

===INLETS=== PqP Afs Fram BLEEDS - output Wb/Win hscale Pscale W Tt ht Pt
InEng 1.0000 ----- 0.0 TrbH_CH B030.TCLA_CH 0.0000 1.0000 1.0000 0.0000 1454.17 357.10 367.398
TrbH_NC B030.TCLA_NC 0.0000 1.0000 1.0000 0.0000 1454.17 357.10 367.398

===DUCTS=== dPnorm MI Aphy
D050 0.0100 0.3000 16.93
D060 0.0250 0.3500 49.49

===SHAFTS=== Nmech trq in pwr in
ShH 42800.0 246.9 2012.2
ShP 30500.0 170.5 990.0

===BURNERS=== TtOut eff dPnorm Wfue1 Wfue1Hr FAR
BrnPri 2553.36 0.9900 0.0700 0.11113 400.06 0.01822

===NOZZLES=== PR Cfg CdTh Cv Ath MWth Vact Fg
NozPri 1.040 0.9900 0.9600 0.9900 73.39 0.243 423.0 81.6

```

Fig. 2.6. PFF-63 Engine cycle at SLS generated in NPSS v2.8

Nevertheless, main requirements which is 25 % lower fuel burn at loiter, are related to different ambient conditions. In figure 2.7 off-design performance at loiter is presented. Unfortunately it provides over 883 horse power to the generator. According to Request of Proposal [1.1], the shaft power delivered must be within 5 % of baseline engine which is 603 hp. The decision was taken to make another analysis that will show engine performance vs. HP shaft rotational speed. Figure 2.8 shows the results of this analysis.

```

*****
Date:12/30/18      Time:14:32:55      Model:      cdm06_tp00      mode: OFFDESIGN      converge = 1      CASE:      3
Version:           NPSS_v2.8      Gas Package:GasTb1      iter/pass/Jacb/Broy= 14/ 14/ 0/12      Run by:      karo1
*****
SUMMARY OUTPUT DATA
MW      alt      dTamb      VTAS      NI      N2      NP      T41      ITTC      SHP      THP      ESHP      BSFC      ESFC
0.300   7000.0   0.00      193.65   42800.0  30500.0  -----  2525.94  693.90   883.24  16.30   899.55   0.385   0.378

FLOW STATION DATA
F010 FsEng.F1_0      W      Pt      Tt      ht      FAR      Wc      Ps      Ts      Aphy      MW      gamt      Rt
F020 InEng.F1_0      5.22  12.071  502.61  120.10  0.0000   6.25  11.340  493.71  37.1  0.3000  1.40078  0.06856
F029 CmpL.F1_0      5.22  12.071  502.61  120.10  0.0000   6.25  10.052  476.96  23.8  0.5179  1.40078  0.06856
F030 CmpH.F1_0      5.22  312.532  1429.91  350.73  0.0000   0.41  265.136  1369.49  1.6  0.4976  1.35418  0.06856
F031 B030.F1_0      5.22  312.532  1429.91  350.73  0.0000   0.41  281.067  1390.68  1.9  0.3983  1.35418  0.06856
F040 BrnPri.F1_0    5.31  290.655  2525.94  668.49  0.0181   0.59  288.772  2522.15  10.4  0.1000  1.30085  0.06855
F045 TrbH.F1_0      5.31  51.419  1740.69  441.96  0.0181   2.78  48.464  1715.51  16.9  0.2997  1.32590  0.06855
F050 D050.F1_0     5.31  50.905  1740.69  441.96  0.0181   2.81  47.979  1715.51  17.1  0.2997  1.32590  0.06855
F060 TrbP.F1_0      5.31  12.191  1308.87  324.45  0.0181   10.17  11.046  1275.83  49.5  0.3845  1.34890  0.06855
F070 D060.F1_0     5.31  11.886  1308.87  324.45  0.0181   10.43  11.060  1284.66  58.1  0.3282  1.34890  0.06855
F090 NozPri.F1_0    5.31  11.886  1308.87  324.45  0.0181   10.43  11.340  1293.00  70.4  0.2650  1.34890  0.06855

TURBOMACHINERY PERFORMANCE DATA
CmpL      Wc      PR      eff      TR      effPoly      pwr      SMN      SMW      s_Re
6.25  1.000  0.9850  1.0000  -0.0000  0.0  18.00  24.05  1.00000
CmpH      6.25  25.891  0.7973  2.8450  0.8646  -1702.6  56.31  30.13  1.00000
TrbH      0.59  5.653  0.9204  1.4511  0.9031  1702.6
TrbP      2.81  4.176  0.8202  1.3299  0.7911  883.2

TURBOMACHINERY MAP DATA
CmpL      WcMap      PRmap      effMap      NcMap      R/Parm      s_WcDes      s_PRdes      s_effDes      s_NcDes
73.25  5.413  0.8100  1.016  2.2637  0.0854  0.0000  1.2161  -----
2.79  2.348  0.8372  1.016  2.0070  2.2426  18.4615  0.9524  -----
10.14  6.001  0.9002  100.541  6.0006  0.0906  0.9304  1.0224  8.4701
35.28  6.638  0.9233  100.588  6.6377  0.1234  0.5633  0.8883  7.2677

===INLETS===      PqP      Afs      Fnam      BLEEDS - output      Wb/Min      hscale      Pscale      W      Tt      ht      Pt
1.0000  37.08  53.0      TrbH_CH B030.TCLA_CH  0.0000  1.0000  1.0000  0.0000  1429.91  350.73  312.532
===DUCTS===      dPnorm      MW      Aphy      TrbH_NC B030.TCLA_NC  0.0000  1.0000  1.0000  0.0000  1429.91  350.73  312.532
D050      0.0100  0.2997  16.93
D060      0.0250  0.3845  49.49

===SHAFTS===      Nmech      trq in      pwr in
ShH      42800.0  208.9  1702.6
ShP      30500.0  152.1  883.2

===BURNERS===      TtOut      eff      dPnorm      Wfuel      WfuelHr      FAR
BrnPri    2525.94  0.9900  0.0700  0.09446  340.04  0.01810

===NOZZLES===      PR      Cfg      CdTh      Cv      Ath      MNth      Vact      Fg
NozPri    1.048  0.9900  0.9600  0.9900  73.39  0.265  454.0  75.0

```

Fig. 2.7. PFF-63 Engine cycle at loiter generated in NPSS v2.8

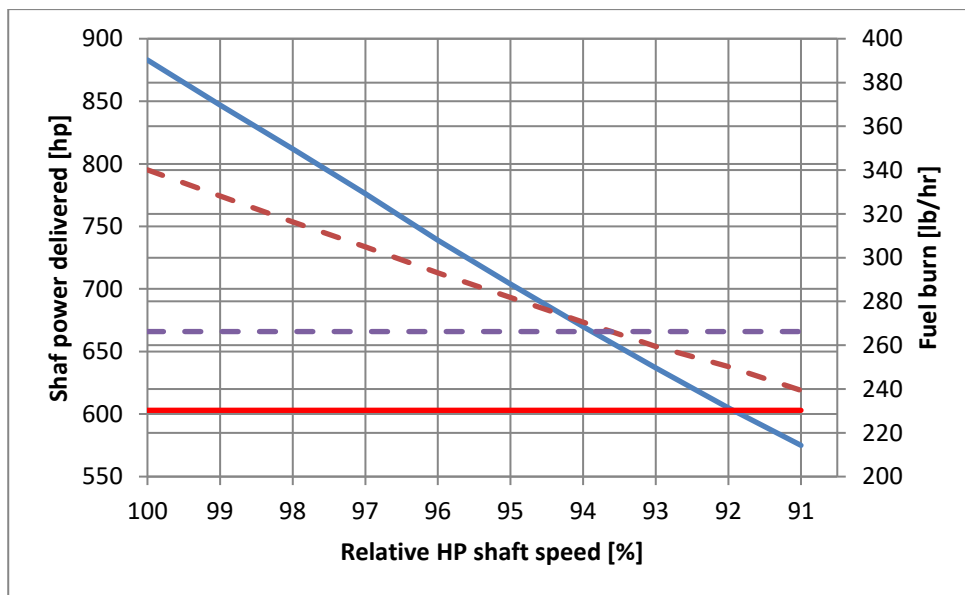


Fig. 2.8. PFF-63 shaft power delivered and Fuel burn at loiter vs. Relative HP shaft rotational speed. Solid lanes for SHP: blue - design value, red - baseline value. Dash lanes for Fuel Burn: brown - design value, purple - maximal value

This analysis allowed to choose an optimal HP shaft rotational speed. This parameter was eventually set to 39350 RPM which is equal to 92 % of maximal High Pressure Shaft rotational speed. Figure 2.9 shows the final PFF-63 thermodynamic cycle.

```

*****
Date:12/30/18   Time:14:54:17   Model:          cdm06_tp00   mode: OFFDESIGN   converge = 1   CASE:   3
Version:         NPSS_2.8     Gas Package:GasTb1   iter/pass/Jacb/Broy= 26/ 35/ 1/23   Run by:         karol
*****
                                SUMMARY OUTPUT DATA
MN      alt    dTamb    VTAS      N1      N2      NP      T41      ITTC      SHP      THP      ESHP      BSFC      ESFC
0.295   7000.0    0.00     190.42    39350.0 30500.0  ----   2303.42  604.50   604.64   4.94     609.58   0.412   0.409

                                FLOW STATION DATA
                                W      Pt      Tt      ht      FAR      Wc      Ps      Ts      Aphy      MN      gamt      Rt
F010 FsEng.F1_0  4.46  12.046  502.32  120.03  0.0000   5.36  11.340  493.71  32.3  0.2950  1.40079  0.06856
F020 InEng.F1_0  4.46  12.046  502.32  120.03  0.0000   5.36  10.660  485.05  23.8  0.4214  1.40079  0.06856
F029 CmpL.F1_0   4.46  12.046  502.32  120.03  0.0000   5.36  10.660  485.05  23.8  0.4214  1.40079  0.06856
F030 CmpH.F1_0  4.46  254.717 1342.15 327.85  0.0000   0.41  214.438 1282.23  1.6  0.5083  1.35933  0.06856
F031 B030.F1_0  4.46  254.717 1342.15 327.85  0.0000   0.41  228.069 1303.42  1.9  0.4058  1.35933  0.06856
F040 BrnPri.F1_0 4.53  236.887 2303.42 601.12  0.0155   0.59  235.353 2299.90  10.4 0.0997  1.30803  0.06855
F045 TrbH.F1_0  4.53  42.005  1579.77 396.47  0.0155   2.77  39.617  1556.68  16.9 0.2971  1.33534  0.06855
F050 D050.F1_0  4.53  41.585  1579.77 396.47  0.0155   2.80  39.220  1556.68  17.1 0.2971  1.33534  0.06855
F060 TrbP.F1_0  4.53  12.013  1227.00 302.21  0.0155   8.53  11.249  1205.98  49.5 0.3126  1.35576  0.06855
F070 D060.F1_0  4.53  11.713  1227.00 302.21  0.0155   8.75  11.155  1211.38  58.1 0.2690  1.35576  0.06855
F090 NozPri.F1_0 4.53  11.713  1227.00 302.21  0.0155   8.75  11.339  1216.62  70.4 0.2189  1.35576  0.06855

TURBOMACHINERY PERFORMANCE DATA
                                Wc      PR      eff      TR      effPoly      pwr      SMN      SMW      s_Re
CmpL   5.36  1.000  1.0216  1.0000  -0.0000     0.0  4.56  11.78  1.00000
CmpH   5.36  21.145 0.8033  2.6719  0.8658    -1312.7 56.85 30.13 1.00000
TrbH   0.59  5.639 0.9160  1.4581  0.8977     1312.7
TrbP   2.80  3.462 0.8184  1.2875  0.7926     604.6

TURBOMACHINERY MAP DATA
                                WcMap  PRmap  effMap      NcMap  R/Parm      s_WcDes  s_PRdes  s_effDes  s_NcDes
CmpL   62.78 4.739 0.8401  0.934  1.4728     0.0854  0.0000  1.2161  ----
CmpH   2.39 2.091 0.8434  0.934  1.9017     2.2426 18.4615 0.9524  ----
TrbH   10.14 5.986 0.8959  96.799 5.9864     0.0906 0.9304  1.0224  8.4701
TrbP   35.12 5.370 0.9213  105.587 5.3702     0.1234 0.5633  0.8883  7.2677

===INLETS===
InEng   PqP      Afs      Fram      BLEEDS - output      Wb/Win  hscale  Pscale      W      Tt      ht      Pt
1.0000  32.26    44.6      TrbH_CH B030.TCLA_CH  0.0000  1.0000  1.0000     0.0000 1342.15 327.85 254.717
0.0000  0.0000  0.0000  0.0000  0.0000  1.0000  1.0000     0.0000 1342.15 327.85 254.717

====DUCTS====
D050    dPnorm      MN      Aphy
0.0100  0.2971  16.93
D060    0.0250  0.3126  49.49

===SHAFTS===
Nmehc  trq in  pwr in
ShH    39350.0 175.2 1312.7
ShP    30500.0 104.1 604.6

===BURNERS===
TtOut  eff  dPnorm  Wfuel  WfuelHr  FAR
BrnPri 2303.42 0.9900 0.0700 0.06924 249.26 0.01551

===NOZZLES===
PR      Cfg      CdTh      Cv      Ath      MNth      Vact      Fg
NozPri 1.033  0.9900  0.9600  0.9900  73.39  0.219  364.6  51.4

```

**Fig. 2.9. PFF-63 Engine final cycle at loiter generated in NPSS v2.8**

In the end the performance of the engine at the cruise condition is shown in figure 2.10. Performance provide that was not determined by any requirements but the shaft power delivered. Thus, the HP spool rotational speed was chosen to provide at least ~ 690 hp of SHP.

Table 2.6 and table 2.7 contain comparison of both baseline and designed engine parameters and performance. The requirements about fuel burn savings have been achieved and exceeded to over 29 %. Cycle provides almost exact match of the shaft power delivered to the electrical generator. Moreover, the cycle thermal efficiency has been improved by 42.25 %.

```

*****
Date:01/03/19 Time:13:17:28 Model: cdm06_tp00 mode: OFFDESIGN converge = 1 CASE: 3
Version: NPSS_2.8 Gas Package:GasTb1 iter/pass/Jacb/Broy= 28/ 46/ 2/24 Run by: karo1

SUMMARY OUTPUT DATA
MN alt dTamb VTAS NI N2 NP T41 ITTC SHP THP ESHP BSFC ESFC
0.350 12500.0 0.00 221.41 41800.0 30500.0 ----- 2430.13 654.74 705.81 9.10 714.90 0.380 0.375

FLOW STATION DATA
W Pt Tt ht FAR Wc Ps Ts Aphy MN gamt Rt
F010 FsEng.F1_0 4.34 9.975 485.74 116.06 0.0000 6.18 9.164 474.09 32.0 0.3500 1.40102 0.06856
F020 InEng.F1_0 4.34 9.975 485.74 116.06 0.0000 6.18 8.355 461.71 23.8 0.5093 1.40102 0.06856
F029 CmpL.F1_0 4.34 9.975 485.74 116.06 0.0000 6.18 8.355 461.71 23.8 0.5093 1.40102 0.06856
F030 CmpH.F1_0 4.34 254.461 1378.38 337.27 0.0000 0.41 215.708 1319.52 1.6 0.4982 1.35717 0.06856
F031 B030.F1_0 4.34 254.461 1378.38 337.27 0.0000 0.41 228.740 1340.18 1.9 0.3987 1.35717 0.06856
F040 BrnPri.F1_0 4.41 236.649 2430.13 639.46 0.0172 0.59 235.116 2426.46 10.4 0.0999 1.30362 0.06855
F045 TrbH.F1_0 4.41 41.886 1670.20 421.99 0.0172 2.78 39.488 1645.93 16.9 0.2987 1.32979 0.06855
F050 D050.F1_0 4.41 41.467 1670.20 421.99 0.0172 2.80 39.004 1645.93 17.1 0.2987 1.32979 0.06855
F060 TrbP.F1_0 4.41 9.856 1250.73 308.86 0.0172 10.23 8.923 1218.62 49.5 0.3856 1.35315 0.06855
F070 D060.F1_0 4.41 9.610 1250.73 308.86 0.0172 10.47 8.936 1227.21 58.1 0.3290 1.35315 0.06855
F090 NozPri.F1_0 4.41 9.610 1250.73 308.86 0.0172 10.47 9.164 1235.31 70.4 0.2656 1.35315 0.06855

TURBOMACHINERY PERFORMANCE DATA
Wc PR eff TR effPoly pwr SMN SMW s_Re
CmpL 6.18 1.000 0.9925 1.0000 -0.0000 0.0 15.32 21.20 1.00000
CmpH 6.18 25.511 0.7986 2.8377 0.8654 -1356.8 56.41 30.12 1.00000
TrbH 0.59 5.650 0.9201 1.4550 0.9028 1356.8
TrbP 2.80 4.207 0.8206 1.3354 0.7909 705.8

TURBOMACHINERY MAP DATA
WcMap PRmap effMap NcMap R/Parm s_WcDes s_PRdes s_effDes s_NcDes
CmpL 72.40 5.445 0.8161 1.009 2.0920 0.0854 0.0000 1.2161 ---,---
CmpH 2.76 2.328 0.8386 1.009 2.0025 2.2426 18.4615 0.9524 ---,---
TrbH 10.14 5.998 0.8999 100.109 5.9976 0.0906 0.9304 1.0224 8.4701
TrbP 35.22 6.694 0.9238 102.689 6.6939 0.1234 0.5633 0.8883 7.2677

===INLETS=== PqP Afs Fram
InEng 1.0000 32.02 50.4 BLEEDS - output Wb/Win hscale Pscale W Tt ht Pt
0.0000 1378.38 337.27 254.461
===DUCTS=== dPnorm MN Aphy TrbH_CH B030.TCLA_CH Wb/Win hscale Pscale W Tt ht Pt
D050 0.0100 0.2987 16.93 0.0000 1.0000 1.0000 0.0000 1378.38 337.27 254.461
D060 0.0250 0.3856 49.49 TrbH_NC B030.TCLA_NC 0.0000 1.0000 1.0000 0.0000 1378.38 337.27 254.461

===SHAFTS=== Nmech trq in pwr in
SH 41800.0 170.5 1356.8
ShP 30500.0 121.5 705.8

===BURNERS=== TtOut eff dPnorm Wfuel WfuelHr FAR
BrnPri 2430.13 0.9900 0.0700 0.07451 268.23 0.01719

===NOZZLES=== PR Cfg CdTh Cv Ath MNth Vact Fg
NozPri 1.049 0.9900 0.9600 0.9900 73.39 0.266 445.6 61.1

```

Fig. 2.10. PFF-63 Engine final cycle at cruise condition generated in NPSS v2.8

Table 2.6. Baseline and Designed engine overall parameters

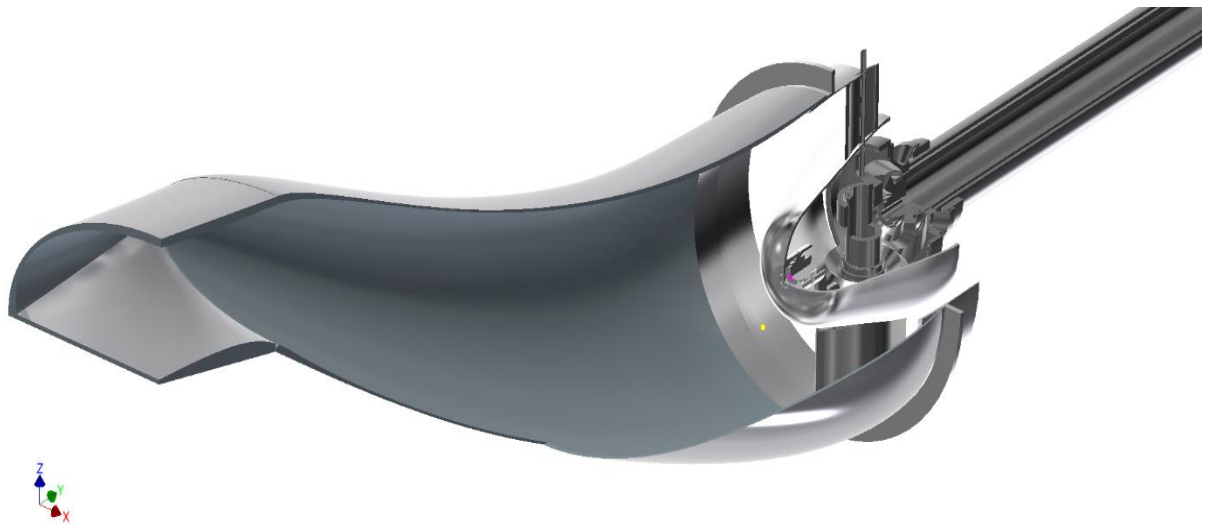
	Baseline cycle	Design cycle
Engine Type	Single Spool	Two Spool
Number of compressor stages	2 centrifugal	1 centrifugal with counter rotating diffuser
Number of HP turbine Stages	3 Axial	2 Axial
Combustor type	Reverse Annular	Reverse Annular
Maximum power at sea level	1000 hp	990 hp
Overall pressure ratio at max. Power	10.55	25
Max. Envelope diameter	27 inch	16.92 inch
Max. Envelope length	43 inch	34 inch
Dry weight	385 lb	211.64 lb

Table 2.7. Comparison of baseline and designed engine cycle performance

	Baseline cycle	Design cycle	Improvement compared to baseline
Loiter Speed	190 kts	190 kts	0%
Cruise Speed	220 kts	220 kts	0%
Loiter Fuel Burn	354.93 lb	249.26 lb	29.77%
Takeoff BSFC	0.534 $\frac{lb}{hp*hr}$	0.404 $\frac{lb}{hp*hr}$	24.34%
Loiter BSFC	0.549 $\frac{lb}{hp*hr}$	0.417 $\frac{lb}{hp*hr}$	24.04%
Thermal Efficiency	0.2329	0.3313	42.25%

### 3. Inlet design

There are a few suitable designs for the inlet. The most promising, in case of placing the engine inside the aircraft, is highly consolidated boundary layer ingesting s-duct inlet. It has many benefits in reduction of drag, weight and size by eliminating the boundary layer diverter and pruning the inlet duct. Ram drag is reduced along with the momentum of the inlet flow [3.1]; which lowers the chances of being detected in case of military usage. The application of s-duct inlets is not new, even for commercial vehicles. The Boeing 727 [3.2] and Lockheed L-1011 successfully utilized offset or s-duct inlet designs [3.3]. As indicated in references [3.3] the first curvature in a s-duct inlet causes a nonhomogeneous vertical pressure distribution that creates secondary flows along the duct wall. These secondary flows tend to migrate the wall boundary layer toward the low pressure side of the bend (lower wall for current investigation). If sufficient boundary layer is accumulated, it produces a lift-off effect or separation of the inlet core flow. Although it might be expected that the second bend in an s-duct would reverse or mitigate this effect, studies have indicated that this is not the case [3.5]. References [3.4] and [3.5] indicate that the s-duct losses penalty relative to a straight duct is about 2 %. In the reference [3.2] it is suggested that the s-duct may decrease TPR at 0.25 Mach number, where duct curvature and boundary layer ingesting effects are very small, pressure recovery decreases slightly with increasing airflow while at  $M > 0.25$ , pressure recovery increases with increasing airflow. At low Mach numbers and low throttle of airflow settings, the inlet is able to meet airflow requirements with very small losses (basically friction) and thus pressure recovery is high. However, at high throttle settings, the inlet throat area is too small and the inlet must suck air into the duct from the surrounding flow field. This can not only create larger lip losses (internal lip separation can occur in the extreme case) but also ingest additional boundary layer into the duct and thus lower pressure recovery [3.5]. The calculations included in table 3.1 show the inlet dimensions are small. It is the consequence of low air mass flow  $m = 4.46$  lbs, which is a positive aspect in relation to the drag.



**Fig. 3.1. Model 3D of inlet**

In comparison to s-duct inlet, axial bilateral would extend the duct more because of the ducts connecting area. Moreover, the application of single s-duct inlet would ensure more homogenous distribution of velocity and pressure at the engine face. Further, down the inlet surface there would be installed the radial particle separator, which is essential element while operating in dusty or desert regions. The size of dust separator is determined by the size of the smallest particles. Due to this fact it is not included in drawings.

**Table 3.1. Calculations of the inlet flow**

Parameter	Equation	Value	Unit
Reynold's number	$Re = \frac{V_1 * d_2}{\eta}$	566670	–
Nikuradase's equation – a flow drag factor for the Range	$\lambda = 0.0032 + \left(\frac{0.221}{Re^{0,237}}\right)$ $4 * 10^3 < Re < 3,2 * 10^6$	0.0127	–
Local drag factor	$1 - InEng = 1 - \lambda * \frac{L}{d_2}$	0.02	–
Pressure loss	$\Delta p = 1 - (1 - InEng) * \rho_0 * \frac{V_1^2}{2}$	1.01	psi
Inlet area	$Aphy_1 = \frac{m}{V_1 * \rho_1}$	32.3	in <sup>2</sup>

According to the structure, the inlet would be made with Aluminum 6061-T6 sheet components, stiffen by frames and printed (or embossed) ribbed mesh. The front frame may be used as the oil tank, with about 61 in<sup>3</sup> capacity. The integrated nose - cap allows to connect the inlet with the compressor. Through the nose-cap rib, the oil would be supplied to engine-generator oblique gear. It would be the first speed reduction. Moreover, inside the bottom rib would be a shaft passing the power to generator. Nevertheless, continuity of the duct is provided by the convergent walls. The drawing of inlet is attached as an appendix 1. Due to very promising development of three dimensional printing it is possible that, by year 2025, it would be possible to print whole component as a one part.

### 3.1. Inlet construction technical description

An appendix 1 - the drawing of the UAV inlet (IN) presents main inlet dimensions and assemblies. The inlet cover consists of a few parts. The first is a metal sheet (39) which starts at the first stage of the inlet. It is weighted by a front frame (37). The frame is also used as an oil tank. The mentioned metal cover may be made as separate segments connected by rivets (38) or as one integrated part. The description of this montage should be in the another assembly drawing. The next flange, is an integrated tip rib (3) and integrated hub rib (35). These two segments are connected by bolts (32). It is designed as two parts because of the complicity of the airfoil bearing montage (43, 44, 45). These elements are connected by bolts (31) and they support the airfoil bearing. The third flange is a compressor cover (5). The montage should starts from the setting the airfoil bearing in the integrated ribs, then the toothed wheel (17) should be set and locked (15, 16). In the same time, a passive shaft have to be passed throughout the hub rib and in meantime the second toothed wheel have to be set on it when it is exerted for few inches above the hub rib. Further, the bearings (28), which had to be placed in the holder - the part of the integrated tip rib. Then the ball bearing holder (29) two has to be montage and connected to the first holder by the bolt (32). It also has to be connected with the nose cap (26) which should be montage (23, 24) at the end.

## 4. Compressor

Many concepts of the compressor design may be distinguished. Considering a few variations, presented in the chapters 2.4.1 and 2.4.2, the most promising option is the birotational compressor. While providing required high pressure ratio and efficiency it is characterized by lower mass. The idea of such counter-rotating system appeared during the WWII, however, there were no possibilities to manufacture such component. Nevertheless, nowadays a few working prototypes were made what leads to conclusion that this solutions might be a promising replacement for a classical approach.

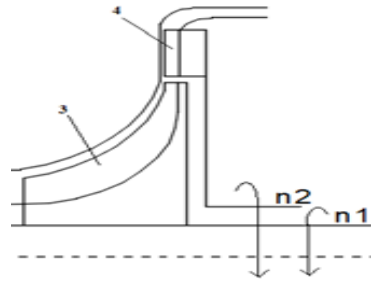


Fig. 4.1. Scheme of compressor: 3 - radial stage impeller, 4 - radial stage diffuser

### 4.1. Gas-dynamic analysis

The engine cycle was received by optimal selection of basic parameters like: pressure ratio, temperature at the exit of combustion chamber and air flow. Based on generated engine cycle the parameters of the compressor inlet were given.

#### 4.1.2. The centrifugal compressor

Calculations for this component are based on reference [4.2] Main parameters are presented below in table 4.1.

Table 4. 1. Basic parameter of centrifugal compressor

Parameter	Equation	Value	Unit
Inlet temperature	$T_3 = T^*_3$	493.96	°R
Inlet total pressure	$p^*_3$	15.05	psi
Inlet static pressure	$p_3 = \frac{p^*_3}{(1 + 0.2 * M_3^2)^{3.5}}$	12.69	psi
Inlet tip radius	$r_{3t}$	3.26	in
Inlet density	$\rho_3$	0.067	$\frac{\text{lb}}{\text{ft}^3}$
Inlet area	$A_3 = \frac{\dot{m}}{\rho_3 * C_3}$	24.8	in <sup>2</sup>
Exit total temperature	$T^*_4 = T^*_3 * [1 + \left(\frac{U^2}{C_p * T^*_3}\right) * \left(\frac{C_{4u}}{U}\right)]$	1173.11	°R
Efficiency	$\eta_c$	0.84	—
Pressure ratio	$\pi_c = [1 + \eta_c * \left(\frac{M_{r4}}{T^*_3} - 1\right)]^{3.5}$	12.5	—

The continuation of the table is on the next page.

The continuation of the table 4.1.

Parameter	Equation	Value	Unit
Exit total pressure	$p_4^* = p_3^* * \pi_c$	188.76	psi
Exit static pressure	$p_4 = \frac{p_4^*}{\left(\frac{T_4^*}{T_4}\right)^{3.5}}$	61.67	psi
Exit tip radius	$r_{4t}$	3.77	in
Exit density	$\rho_4 = \frac{p_4}{R * T_4}$	0.197	$\frac{\text{lb}}{\text{ft}^3}$
Impeller exit width	$b = \frac{\dot{m}}{c_{4r} * \rho_4}$	0.197	in

In contrast to axial compressor the calculations for centrifugal stage are for one radius. The calculated velocities are shown in table 4.2.

**Table 4.2. The velocity triangles of centrifugal compressor**

Parameter	Symbol	Value	Unit
Peripheral velocity	U	2145.1	$\frac{\text{ft}}{\text{s}}$
Absolute inlet velocity	$C_3$	544.4	$\frac{\text{ft}}{\text{s}}$
Relative inlet velocity	$W_3$	943.3	$\frac{\text{ft}}{\text{s}}$
Inlet Mach number	$M_3$	0.49	—
Absolute exit velocity	$C_4$	1831.2	$\frac{\text{ft}}{\text{s}}$
Relative exit velocity	$W_4$	628.7	$\frac{\text{ft}}{\text{s}}$
Exit Mach number	$M_4$	1.33	—

The graphical interpretations of above parameters are drawn the velocity triangles in figure 2.5.

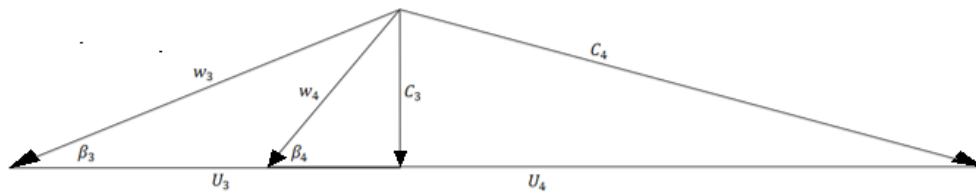


**Figure 2.5. The velocity triangles**

The rotor length is 3.83 inch and entire component is 4.93 in.

### 4.1.3. The centrifugal compressors diffuser

Calculations for this component were based on PhD Kawalec's thesis [4.3]. The basic inlet parameters like static or total temperature and pressure, density, surface and rotor velocity are the parameters of exit from the centrifugal compressor. The basic parameters are presented in table 4.3. Next, the calculations of the diffuser velocity triangles are in table 4.4.

**Table 4. 3. Basic parameter of diffuser**

Parameter	Equation	Value	Unit
Inlet static temperature	$T_5 = T_4$	869.13	°R
Inlet static pressure	$p_5 = p_4$	61.67	psi
Inlet tip radius	$r_5 = r_{4t}$	3.77	in
Exit total temperature	$T^*_6 = T_{5w} + \frac{U_5 * C_{4u}}{C_p}$	1449.82	°R
Pressure ratio	$\pi_d = \frac{p_{5w}}{p_5}$	2	-
Exit static pressure	$p_6 = p_5 * \pi_d$	123.34	psi
Exit tip diameter	$d_6 = 2 * r_5 + 2.36$	4.96	in

**Table 4. 4. The velocity triangles of diffuser**

Parameter	Symbol	Value	Unit
Rotational velocity	n	14000	RPM
Inlet peripheral velocity	$U_5$	461.03	$\frac{\text{ft}}{\text{s}}$
Inlet relative velocity	$w_5$	2343.98	$\frac{\text{ft}}{\text{s}}$
Inlet absolute velocity	$C_5$	1831.29	$\frac{\text{ft}}{\text{s}}$
Inlet Mach number	$M_5$	1.63	—
Exit peripheral velocity	$U_6$	605.3	$\frac{\text{ft}}{\text{s}}$
Exit relative velocity	$w_6$	1538.44	$\frac{\text{ft}}{\text{s}}$
Exit absolute velocity	$C_6$	986.58	$\frac{\text{ft}}{\text{s}}$
Exit Mach number	$M_6$	1.06	—

The graphical interpretation of above parameters is a drawing of the velocity triangles in figure 4.6.

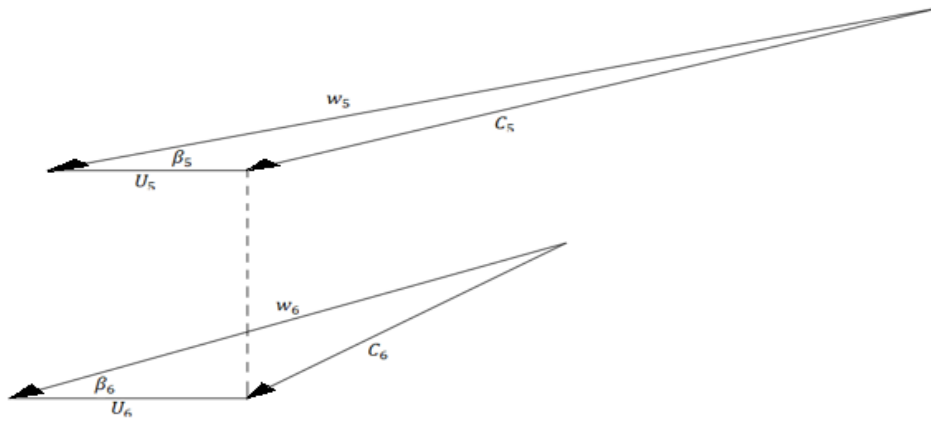


**Fig. 4.6. The velocity triangles**

The compression process in rotating diffuser is a result of decelerating supersonic velocity in relative movement with simultaneous supply of additional energy to the stream. Adequate shape profiling of supersonic rotating airfoil cascade allows for receiving higher aerodynamic efficiency than in supersonic diffuser, which does not move. It is important that the stream decelerating in supersonic movement takes place in forced air compression, oblique shock and one closing normal wave, which arise as a result of proper selection of flow path shape in inlet part of rotating diffuser cascade.

In reality, in viscous gas, because of unfavorable influence increasing boundary layer in diffuser, only a finite number of oblique shocks (one to three) can be implemented. One of conditions is that oblique shock or reflected wave from the diffuser walls cannot penetrate to blades of compressor rotor. The problem is with intensity optimization of adopted oblique shock system, for actual supersonic diffuser, where after the closing normal wave occurs polytropic deceleration of stream to acceptable Mach number. The Mach number  $M \leq 0.3$  is restricted by combustion chamber. It is necessary to choose such wave intensity to obtain maximal value of total pressure in outlet diffuser section.

For non-viscous ideal gas the selection of optimal oblique shock and normal wave intensity, which provide the maximal value of total pressure coefficient are elaborated by Oswaticz [4.4]. Based on that the maximal value of total pressure coefficient in system of aero compression waves is received, when the intensity of all waves is the same and perpendicular wave intensity is smaller than the intensity of oblique shock wave elements. To obtain a higher total pressure improvement than a normal shock inlet, we have to design an inlet construction, which contains multiple shocks. The supersonic diffusion process efficiency is defined by the total pressure recovery of the shock system. To hold the shock system external to the inlet it is important to designed its throat at the cowl lip.

The two-dimensional external compression inlets have got external ramps to create oblique shocks, where axisymmetric inlets use multiple cones to create conical shocks. The normal one is depended on the inlet backpressure and its optimal location is at the throat, because the flow Mach number is the least there. When the terminal shock is at the cowl lip, then it is achieved the intended effect. The calculations are as follows below.

The shock total pressure recovery as a function of Mach number  $M$  and the wave angle  $\beta$  is:

$$\frac{p_{t2}}{p_{t1}} = \frac{\left(\frac{\frac{\gamma+1}{2} * M^2 * \sin^2 \beta}{1 + \frac{\gamma-1}{2} * M^2 * \sin^2 \beta}\right)^{\frac{\gamma}{\gamma-1}}}{\left(\frac{2}{\gamma+1} * M^2 * \sin^2 \beta - \frac{\gamma-1}{\gamma+1}\right)^{\frac{1}{\gamma-1}}} \quad (\text{Eq.2.1})$$

Next, we need to establish the wave and the local Mach numbers upstream of every shock by using an oblique shock chart for  $\gamma=1.4$ . The figure 2.7 let us to know one of  $\beta$ ,  $\delta$  or  $Ma$  parameter when we have got two of them. For the first oblique shock is known the Mach number and the flow turning angle.

$$M_0 = M_5 = 1.63 \quad (\text{Eq.2.2})$$

$$\delta_1 = 5^\circ \quad (\text{Eq.2.3})$$

Based on oblique chart:

$$\beta_1 = 44^\circ \quad (\text{Eq.2.4})$$

$$M_{n1} = M_0 * \sin \beta_1 = 0.9 \quad (\text{Eq.2.5})$$

It follows that:

$$\frac{p_{t1}}{p_{t0}} = 0.9926 \quad (\text{Eq.2.6})$$

Also following equation it is given  $M_n$  downstream of the first shock.

$$M_{n2}^2 = \frac{2 + (\gamma-1) * M_{n1}^2}{2 * \gamma * M_{n1}^2 - (\gamma-1)} = 0.89 \quad (\text{Eq.2.7})$$

$$M_2 = \frac{M_{n2}}{\sin(\beta_2 - \delta_2)} = 1.26 \quad (\text{Eq.2.8})$$

The next step is the oblique shock 2.

$$M_2 = 1.26 \quad (\text{Eq.2.9})$$

$$\delta_2 = 5.5^\circ \quad (\text{Eq.2.10})$$

Based on oblique chart:

$$\beta_2 = 50.4^\circ \quad (\text{Eq.2.11})$$

$$M_{n3} = M_2 * \sin \beta_2 = 0.88 \quad (\text{Eq.2.12})$$

It follows that:

$$\frac{p_{t2}}{p_{t1}} = 0.9927 \quad (\text{Eq.2.13})$$

$$M_3 = M_6 = \frac{M_{n3}}{\sin(\beta_3 - \delta_3)} = 1.06 \quad (\text{Eq.2.14})$$

For the normal shock it is calculated the local Mach number downstream of the second oblique shock as  $M_3 = 1.06$ . Since the flow is normal, it means  $\beta=90^\circ$ , which may be substituted in the above equation for  $\frac{p_{t3}}{p_{t2}}$ .

$$\frac{p_{t3}}{p_{t2}} = 0.9929 \quad (\text{Eq.2.15})$$

Overall shock total pressure recovery

$$\left(\frac{p_{t2}}{p_{t1}}\right)_{overall} = \frac{p_{t1}}{p_{t0}} * \frac{p_{t2}}{p_{t1}} * \frac{p_{t3}}{p_{t2}} = 0.978 \quad (\text{Eq.2.16})$$

Comparison to a normal shock inlet

$$\left(\frac{p_{t2}}{p_{t1}}\right)_{Normal\ shock} = 0.89 \quad (\text{Eq.2.17})$$

Described with above calculations is a method, which shows that the wave angle helps to establish the value of oblique shock system. It depends on the flow to the shock ( $M_n = M * \sin\beta$ ). As long as the local Mach number is supersonic, it is needed to begin with the first oblique shock and continue downstream through multiple ramps and shocks. Analyzing the above calculations there is a huge improvement in total pressure recovery where multiple ramps are used. The compression process of air stream through rotating diffuser is a result of deceleration of supersonic flow in the shock system. Thermodynamic results are a function of number and intensity of shocks inside the diffuser. Calculations for chosen rotating velocity  $n=14000$  RPM are listed below in table 4.5.



Fig. 4.7. Model 3D of compressor diffuser

Table 4.5. Calculations for chosen rotating velocity  $n=14000$

Parameter	Symbol	Equation	Value	Unit
Coefficient of conservation of total pressure by Oswaticz	$\sigma_T$	—	0.978	—
Predicted value of Coefficient of conservation of total pressure with losses through real flow	$\sigma^*$	—	0.905	—
Pressure ratio through relative flow in inlet	$\pi_{c3T}$	$\pi_{c3T} = \frac{p_{3w}}{(p_3 * (1 + 0.2 * M_3^2))^{3.5}}$	2.16	—
Summary pressure ratio behind normal shock through diffuser	$\pi_{c3p}$	$\pi_{c3p} = \pi_{c3T} * \sigma^*$	1.95	—
Static temp. behind normal shock	$T_p$	$T_p = T_{3w} * (1 + 0.2 * M_3^2)$	959	K
Static pressure ratio behind normal shock	$\pi_{stp}$	$\pi_{stp} = \frac{p_{3w} * \sqrt{(1 + 0.2 * M_3^2)}}{p_3 * (1 + 0.2 * M_3^2)^{3.5}} * \pi_{c3p}$	3.44	—
Static pressure behind normal shock	$p_6$	$p_6 = \pi_{stp} * p_{3w}$	286	psi
Total pressure behind normal shock	$p_6^*$	$p_6^* = p_6 * (1 + 0.2 * M_3^2)^{3.5}$	438	psi
Pressure ratio	$\pi$	$\pi = \frac{p_6^*}{p_1^*}$	30	—

#### 4.1.4. Planetary gear

As it was mentioned before, in birotational compressor it is necessary to change diffuser direction of rotation. To make it happen it was decided to use a planetary gear. Hitherto, the most common are gears, in which wheel axis are permanently established vis-à-vis casing and the wheels make rotating movement in regard to its axis. Even if one of the wheel axis is mobile then such kind of gear is called the planetary or epicyclical gear. Described construction solution is necessary in birotational compressor to ensure counter rotating diffuser. The planetary gear is embedded on different shaft than axial and centrifugal compressor. Its rotational speed is 14000 RPM and to obtain that value the planetary gear is essential.

More of parameters characteristic for epicyclical gear like: transmission ratio, ratio of diameters, addendum modification coefficient and number of teeth or ratio of wheel's width to its diameter can be moved from one construction to the second one, regardless of the module pitch or distance spacing of axles change. Design of planetary gear is not so simple, because of fact that not every one of parameters can be simultaneously chosen. Some of them are selected based on preliminary calculations. In the table 4.6. basic parameters are listed.

**Table 4.6. Basic parameters of gear**

Parameter	Symbol	Value	Unit
Rotational speed of shaft	$n_1$	42800	RPM
Rotational speed of gear	$n_2$	14000	RPM
Module pitch	$M$	0.07	in
Power	$P$	831.43	hp

Based on above table and Muller [4.5] and Czerni [4.6] there was a possibility to continue calculations, which were necessary to obtain all gear parameters. All of them are listed in table 4.7.

**Table 4.7. Geometric of gear**

Parameter	Equation	Value	Unit
The transmission ratio	$i = \frac{n_1}{n_2} * (-1)$	-3.05	—
The number of teeth on first wheel	$z_1$	34	—
The number of teeth on third wheel	$z_3 = z_1 * (-i)$	104	—
The number of teeth on second wheel	$z_2 = \frac{z_3 - z_1}{2}$	35	—
The height of teeth head	$h_h = M$	0.07	in
The height of teeth feet	$h_f = 1.25 * M$	0.086	in
The height of teeth	$h = 2.25 * M$	0.155	in
The tip clearance	$c = 0.25 * M$	0.017	in
The side shake	$j = 0.04 * M$	0.003	in
The diameter of first gear	$d_1 = 69 + \frac{h}{2}$	2.77	in
The diameter of second gear	$d_2 = M * z_2$	3.86	in
The diameter of third gear	$d_3 = M * z_3$	10.06	in

The last important parameter is  $p$  – the wheel width. To obtain it the necessary was some additional calculations.

**Table 4.8. The additional parameter of gear**

Parameter	Equation	Value	Unit
Velocity	$v_1 = \frac{\Pi * n_1 * 0.001 * d_1}{60}$	521.65	$\frac{\text{ft}}{\text{s}}$
Force	$F_1 = \frac{1000 * P}{v_1}$	876.08	lbf
Momentum	$M_1 = F_1 * d_1 * 0.001$	204.00	ft * lb
The wheel width	$p = \frac{2 * M_1}{(d_1 * 0.001)^2 * 16000000}$	0.28	in

Because of way the planetary gear works there was a need to take into consideration the oil system. To compute necessary mass flow of oil through the bearings, which support the engine rotor, it is used the calculations of heat stream. The necessary oil mass flow is between several dozen to several hundred pounds per hour and it depends on rotational speed of shaft and dimension of bearings. The most important condition to use oil is its scope of temperature, in which oil save its physical and chemical properties. The lower yield temperature states the cold starting. Important is the oil temperature has to be higher than its congeal point. In turn on the upper yield temperature fundamental impact has got the air speed.

#### 4.1.5. Compressor construction technical description

The compressor (see appendix 2) is a centrifugal flow and one centrifugal stage with a birotational diffuser.

From the left there is centrifugal compressor-impeller (4). The impeller has three rows of blades. The torque from the power shaft to the impeller was transmitted via the multispline ring (41). Next the flow drifts into rotating diffuser (33). This component consists the rotating ring with internal canals (the internal constructions is presented on a side view), on which is the change of duct angle. Such solution was necessary to decelerating Mach number of air flow. Each of changes are calculated and selected to obtain appropriate parameters, which are shown above.

Because of the fact that in this case the diffuser is counter rotating, there was a necessity to design a gear, which enable to counter rotating with another rotating velocity. The best choice was the planetary gear. It contains one gear (34) on the shaft (10), one gear with internal teeth (38) and three satellite gears (19) with bearing (20) under them. The places where diffuser and planetary gear are connected between themselves are elements (30) with bolt (15). There is also predicted the air pipe (42), which is for feeding the air to the bearing's air chamber. To plug planetary gear they are used drawing sheet (30, 31, 36) with labyrinth seal integrated with lead rings. Both of them 30 and 31 are divided to make easier the montage and are amalgamated with rivets (18).

All bolts (6, 13, 16, 28) have got the nuts (7, 14, 17, 29) and washers (8, 15, 18, 30) to protect them against to unscrew. What is more the ending of the power shaft (10) and carriers (23) have got the nuts (11, 24) with washers (32, 9) too, because of the same reasons as bolts.

Important was to assure a lack of free space between elements and that is way there are used some elements like protective tube (22), lock washer (26) and expanding rings (39).

## 5. Combustion system

In this section all detailed information about the combustion chamber and the integrated features would be shown. PFF-63 uses an annular combustor chamber preceded with dump diffuser and additional fuel nozzle to pre-mix the air-fuel flow. Mentioned in section 2, trade studies led to set  $T_4 = 2525 \text{ }^\circ R$  and  $Pt_4 = 290.65 \text{ psi}$ . Moreover, low emission and high efficiency design is preferred.

### 5.1. Combustor Inlet Analysis

Airflow exits the PFF-63 compressor with Mach number of 0.4. Velocity inside the combustor liner has to be 4-5 times lower [5.3]. At the end of the compressor a short with constant area section is applied. It minimizes the appearance of aerodynamic wakes leaving compressor exit - nozzle.

The next section is a faired diffuser. The optimal opening angle (with minimal pressure losses) is between  $7^\circ$  and  $12^\circ$  [5.3]. In this section, airflow velocity is decreased to 60% of the primal value and then it is dumped to the chamber with the high cross-section area. Such a solution allows to obtain the correct Mach number inside the combustor liner as well as significantly lower the length and mass of the whole chamber [5.3].

### 5.2. Combustor flow analysis

Airflow leaving the dump diffuser is partitioned into 4 sub-flows: primary zone, secondary zone, dilution zone, cooling airflows. Division of mass flow between zones is shown along with cooling effectiveness are shown in table 5.1.

**Table 5. 8 Air mass flow values in each zone**

Parameter	Value	Unit	Air to fuel ratio
Air mass flow in primary zone	1.66	$\frac{\text{lb}}{\text{s}}$	1.25
Air mass flow in secondary zone	0	$\frac{\text{lb}}{\text{s}}$	—
Air mass flow in dilution zone	2.49	$\frac{\text{lb}}{\text{s}}$	1.8
Air mass flow of cooling airflows	1.05	$\frac{\text{lb}}{\text{s}}$	—
Fuel mass flow	0.09445	$\frac{\text{lb}}{\text{s}}$	—

One of the common solutions is air mass flow equal to  $0 \frac{\text{lb}}{\text{s}}$  in the Secondary Zone. This purposeful action leads to decreasing as much temperature as possible in single row of dilution holes. This leads to significant reduction of  $\text{NO}_x$  and CO due to shorter time in higher temperatures [5.2].

### 5.3. Combustion efficiency

The PFF-63 combustor has a transpiration cooling applied. It was provided with  $1.05 \frac{\text{lb}}{\text{s}}$  of air mass flow which is equal to nearly 20 % of the total mass flow of primary flow. It means that both convection/film cooling and transpiration cooling will provide sufficient efficiency. According to Figure 5.3 PFF-63 combustion equivalence ratio is equal to 1.163.

Combustion efficiency is the most important parameter that describes its quality. To meet EPA requirements, the efficiency has to be at 99%. All calculation was done using Methods in “Aircraft Propulsion” by Farokhi. Using the reaction rate parameter,  $b$ , we managed to plot Lefebvre combustor loading parameter (CLP).

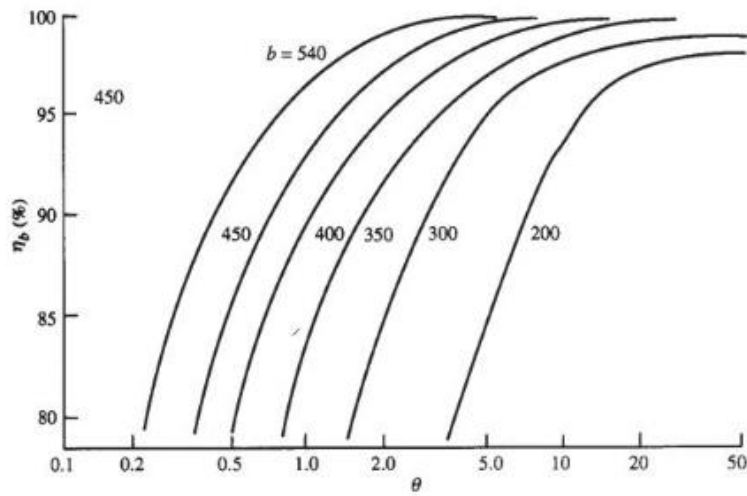


Fig. 5.1. Combustion efficiency in function of CLP

$$b = 382 * \left( \sqrt{2} \pm \left( \frac{\varphi}{1.03} \right) \right) = 535.63 \tag{Eq.5.1}$$

- + for  $\varphi > 1.03$
- - for  $\varphi < 1.03$

$$CLP = \theta = \left( (p_3^{1.75}) * A_{ref} * h * e^{\frac{T_3}{300}} \right) = 30 * 10^5 \tag{Eq.5.2}$$

This results in combination with figure 5.4 gives information of nearly 100% combustion efficiency, which is satisfying to the authors.

### 5.4. Temperature profile

Spikes in temperature are very dangerous for combustor chambers and turbines, especially in the first stage. Therefore, the authors decided to set down the temperature profile. Based on the methodology of Farokhi, a pattern factor (PF) of 0.2 was selected, as well as a profile factor (Pf) of 1.04.

$$PF = \frac{T_{tmax} - T_{tavg}}{T_{tavg} - T_{tin}} \tag{Eq.5.3}$$

$$Pf = \frac{T_{tmaxavg} - T_{tin}}{T_{tavg} - T_{tin}} \tag{Eq.5.4}$$

$$\text{Assumed PF and Pf lead to } T_{tmax}=2495^\circ\text{R and } T_{Tmax-avg}=2341^\circ\text{R.} \tag{Eq.5.5}$$

## 5.5. Used materials

It was decided to apply ceramic matrix composites (CMC) as the layer for the combustor liner protection. For the liner itself, the super alloys with refractory metals such as tungsten, molybdenum, niobium and tantalum can be used. CMC properties remain unchanged to temperatures of nearly 2800 °R. Mentioned in section 5.2, 20%-utilization of total mass flow as cooling airflows and applying extra protection using silicon carbide CMC's provides satisfying safety. According to NASA/TM—2002-211509 this material has over 260 hours of promising tests [5.1].

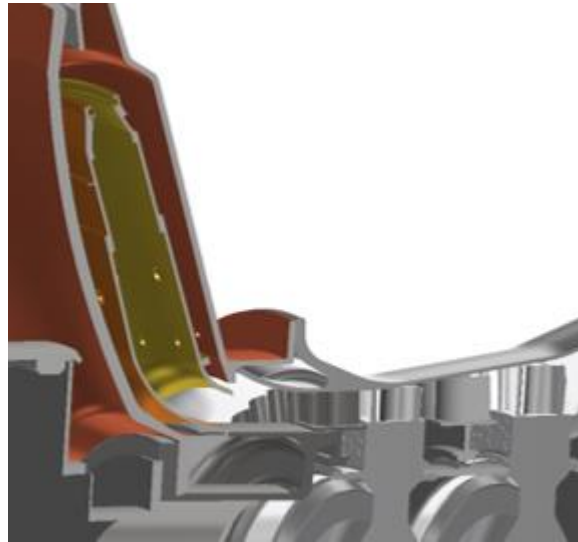


Fig. 5.2. Cross-section of combustor chamber 3D model

## 6. Turbine design

This part of report includes: cycle analysis, material selection, blade and disk design and cooling. Projecting engine contains a high pressure (HPT) and power turbine (PT), the first one supplies power to the compressor and the PT provides power to the electric generator.

### 6.1. Projecting assumptions

Due to requirements given by organizers about weight, diameters and power output, after early research about engines with similar performance it was decided to change baseline engine from single-spool into two-spool system with 1 stage of HPT and 1 nozzle-less stage of PT. The HPT was calculated as with constant inner radius. The PT, to decrease mass and complexity of construction, as a vaneless system[6.1]. First analyses were prepared using NPSS and from that software were taken intake parameters and basic parameters for this project (table 6.1).

Table. 6.1. Inlet parameters

Parameter	Value	Unit
Pressure $P_4$	236.887	psi
Temperature $T_4$	2303.42	°R
HPT rotational speed $\omega_{HPT}$	39350	RPM
PT rotational speed $\omega_{PT}$	30500	RPM
Mass flow $\dot{m}$	4.53	$\frac{lb}{s}$

## 6.2. Gas-dynamic analysis of HPT

At the beginning of project it was necessary to find out what power must be provided to compressor in such architecture. It was assumed that work of turbine is approximately equal to work of compressor, however, some losses and energy for additional systems must be included [6.2]. All calculations were made using equations shown in table 6.2. In the figures 6.2-6.3 are presented velocity triangles.

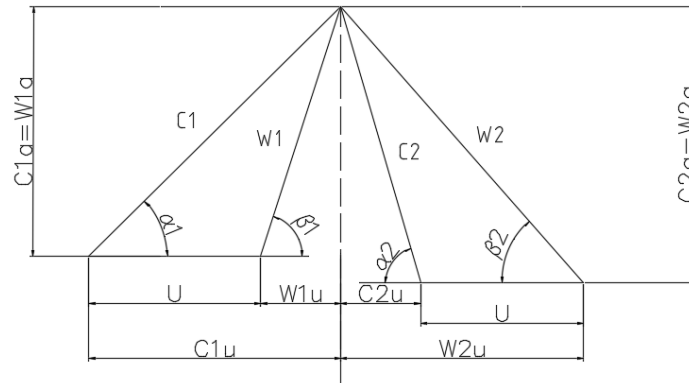


Fig. 6.2. General scheme of velocity triangles [6.3]

Table 6.2. Gas-dynamic equations

Parameter	Equation	Unit
Absolute speed	$c_1 = \varphi \sqrt{2l_t(1 - \rho)}$	$\frac{\text{ft}}{\text{s}}$
Absolute axial speed	$c_{1a} = c_1 \sin \alpha_1$	$\frac{\text{ft}}{\text{s}}$
Absolute circumferential speed	$c_{1u} = c_1 \cos \alpha_1$	$\frac{\text{ft}}{\text{s}}$
Nozzle relative angle	$\beta_1 = \arctg \frac{c_{1a}}{c_{1u} - U}$	°
Relative speed	$w_1 = \frac{c_1}{\sin \beta_1}$	$\frac{\text{ft}}{\text{s}}$
Relative circumferential speed	$w_{1u} = c_{1u} - U$	$\frac{\text{ft}}{\text{s}}$
Relative rotor circumferential speed	$w_{2u} = \frac{l_{st}}{u} - w_1 \cos \beta_1$	$\frac{\text{ft}}{\text{s}}$
Relative rotor axial speed	$w_{2a} = Ma_2 \sqrt{k'R'T_2}$	$\frac{\text{ft}}{\text{s}}$
Relative rotor angle	$\beta_2 = \arctg \frac{w_{2a}}{w_{2u}}$	°
Absolute rotor circumferential speed	$c_{2u} = w_{2u} - U$	$\frac{\text{ft}}{\text{s}}$
Absolute rotor angle	$\alpha_2 = \arctg \frac{c_{2a}}{c_{2u}}$	°

These are all basic velocities on a turbine stage on pitch-line. Similar way of counting was used for other radiuses (inner and tip) and other stages. Results are presented in table 6.3. In the table 6.4 are presented measurements of angles and degree of reaction.

**Table 6.3. Velocities on three radiuses. Indexes: 1- the first nozzle 2- the first rotor, 3- the second nozzle, 4- the second rotor**

Symbol	Hub	Pitch	Tip	Unit	Mach no.		
					Hub	Pitch	Tip
$u_1$	1175.591	1243.143	1310.728	$\frac{\text{ft}}{\text{s}}$	0.54	0.57	0.60
$c_1$	1674.672	1764.829	1855.249	$\frac{\text{ft}}{\text{s}}$	0.77	0.81	0.85
$c_{1a}$	426.957	426.357	426.357	$\frac{\text{ft}}{\text{s}}$	0.20	0.20	0.20
$c_{1u}$	1619.324	1712.402	1805.446	$\frac{\text{ft}}{\text{s}}$	0.74	0.79	0.83
$w_1$	615.808	634.416	653.777	$\frac{\text{ft}}{\text{s}}$	0.28	0.29	0.30
$w_{1u}$	443.336	469.257	494.507	$\frac{\text{ft}}{\text{s}}$	0.20	0.22	0.23
$u_2$	1175.591	1246.522	1317.487	$\frac{\text{ft}}{\text{s}}$	0.56	0.60	0.63
$c_{2a}$	627.654	627.654	627.654	$\frac{\text{ft}}{\text{s}}$	0.30	0.30	0.30
$c_{2u}$	389.748	411.173	433.927	$\frac{\text{ft}}{\text{s}}$	0.19	0.20	0.21
$w_{2u}$	1564.665	1657.972	1751.28	$\frac{\text{ft}}{\text{s}}$	0.75	0.79	0.84
$w_2$	1685.663	1772.605	1860.171	$\frac{\text{ft}}{\text{s}}$	0.81	0.85	0.89
$c_2$	738.577	750.656	762.656	$\frac{\text{ft}}{\text{s}}$	0.35	0.36	0.36
$u_3$	1175.591	1249.902	1324.245	$\frac{\text{ft}}{\text{s}}$	0.59	0.63	0.66
$c_3$	1911.549	2015.978	2121.227	$\frac{\text{ft}}{\text{s}}$	0.92	0.94	0.96
$c_{3a}$	713.874	713.874	713.874	$\frac{\text{ft}}{\text{s}}$	0.36	0.36	0.36
$c_{3u}$	1773.491	1885.597	1997.703	$\frac{\text{ft}}{\text{s}}$	0.89	0.95	0.97
$w_3$	930.7087	955.462	980.711	$\frac{\text{ft}}{\text{s}}$	0.47	0.48	0.49
$w_{3u}$	597.8675	635.627	673.458	$\frac{\text{ft}}{\text{s}}$	0.30	0.32	0.34
$u_4$	1175.591	1331.562	1487.566	$\frac{\text{ft}}{\text{s}}$	0.62	0.70	0.79
$c_{4a}$	875.853	875.853	875.853	$\frac{\text{ft}}{\text{s}}$	0.46	0.46	0.46
$c_{4u}$	65.906	61.766	57.278	$\frac{\text{ft}}{\text{s}}$	0.03	0.03	0.03
$w_{4u}$	1240.65	1392.749	1545.308	$\frac{\text{ft}}{\text{s}}$	0.66	0.74	0.82
$w_4$	1518.668	1645.276	1776.247	$\frac{\text{ft}}{\text{s}}$	0.80	0.87	0.94
$c_4$	878.2808	877.856	877.559	$\frac{\text{ft}}{\text{s}}$	0.46	0.46	0.46

**Table 6.4. Angles and degree of reaction on each stage of HPT (N – Nozzle, R - Rotor)**

Symbol	$\alpha$			$\beta$			Unit	Degree of reaction		
	hub	pitchline	tip	hub	pitchline	tip		hub	pitchline	tip
N1	14.39	14.00	13.63	38.32	37.57	36.77	°	—	—	—
R1	54.70	53.93	53.18	21.46	20.74	20.07	°	0.33	0.35	0.37
N2	21.77	20.74	19.80	49.84	48.33	46.89	°	—	—	—
R2	76.26	76.95	77.57	32.66	30.23	28.09	°	0.33	0.36	0.38

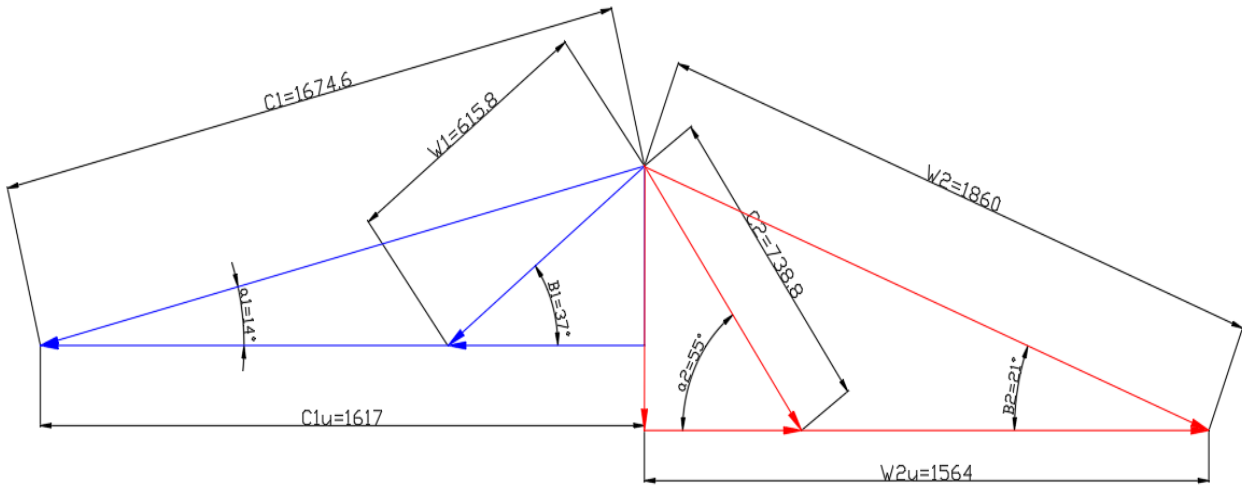


**Fig. 6.3. Scheme of hub velocity triangle of the first stage**

Gas-dynamic calculations consists also distribution of temperature and pressure on different radiuses and each stage. All results are presented in tables 6.5.-6.6. and in figures 6.4.-6.5[6.3].

**Table 6.5. Temperature distribution**

Stage	Temperature			Unit
	hub	pitch	tip	
0	2302	2302	2302	°R
N1	2132	2090	2059	°R
R1	1988	1949	1890	°R
N2	1816	1772	1751	°R
R2	1645	1596	1561	°R

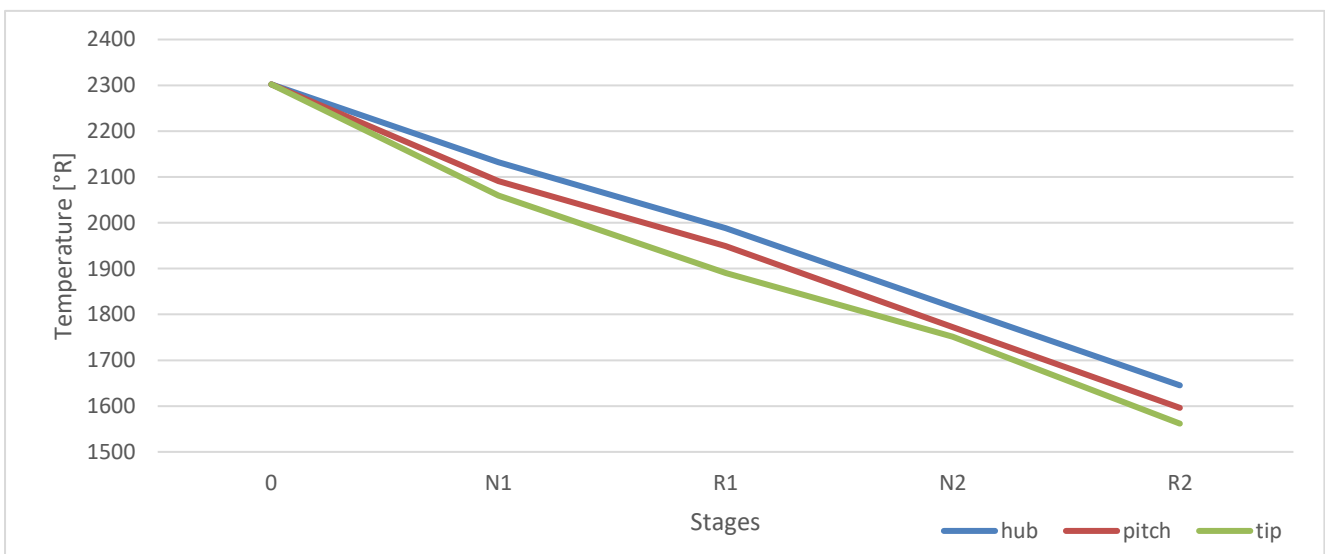


**Fig. 6.4. Temperature distribution**

**Table 6.6. Pressure distribution**

	Pressure			Unit
	Hub	Pitch	Tip	
0	236.525	236.525	236.525	psi
N1	140.83	138.068	135.307	psi
R1	111.486	109.300	107.114	psi
N1	65.078	63.802	62.526	psi
R2	41.795	40.975	40.156	psi

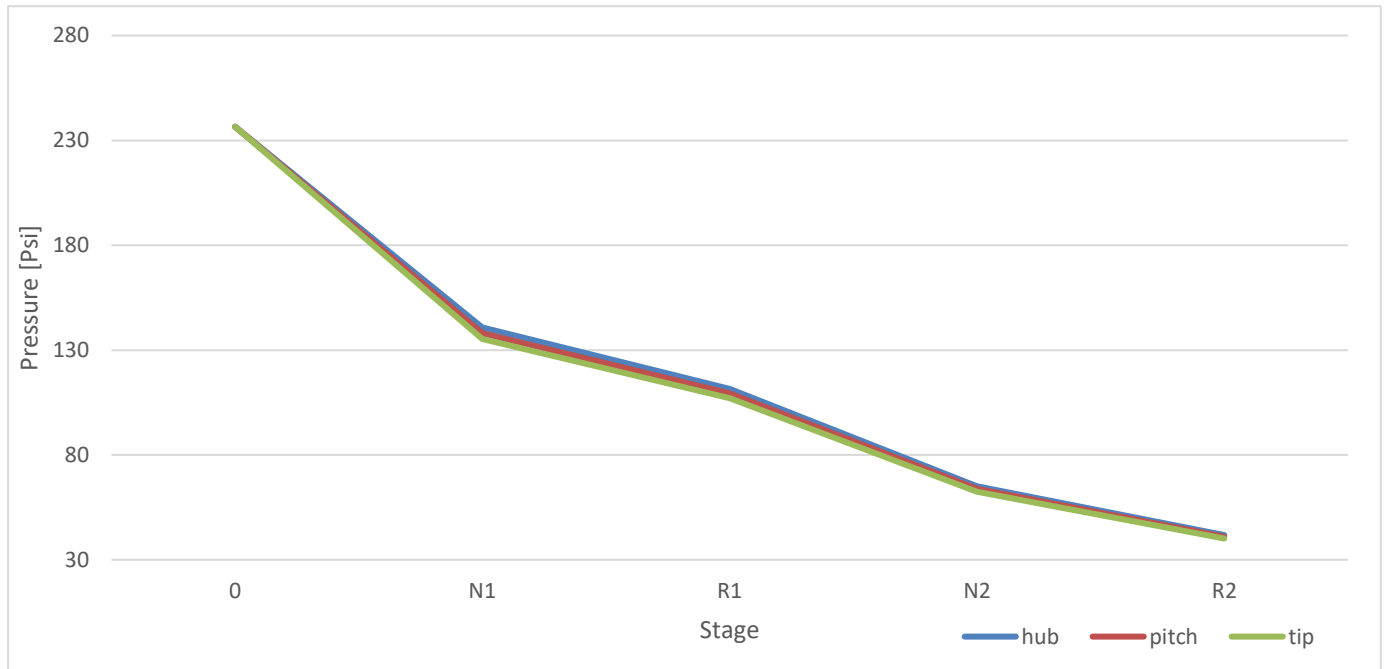


**Fig. 6.5. Pressure distribution**

At this point of work it is worth to admit that values of parameters from *NPSS* and from step-by-step calculations are close to each other up to 1% (look table 6.7). That proves correctness of calculations and allows to move to next step of the project

**Table 6.7. Comparison of outlet parameters from step-by-step calculation to Gasturb**

Parameter	<i>NPSS</i>	Step-by-step	Unit	Difference of results
Pressure $P_{r2}$	41,585	40,975	psi	1%
Temperature $T_{r2}$	1579	1596	°R	1%

**Table 6.8. Basic geometry of flow-path**

Stage:	Diameter			Unit
	hub	pitch	Tip	
N1	0.571	0.604	0.636	ft
R1	0.571	0.607	0.650	ft
N2	0.571	0.607	0.656	ft
R2	0.571	0.646	0.722	ft
R3	0.722	0.837	0.951	ft

### 6.3. Gas-dynamic analysis of PT

In the classical approach toward projecting turbines it is necessary to use nozzle and rotor. However, in multi-rotor system, when machinery is rotating in opposite directions, there is a possibility to remove nozzle part of a stage. This solution decreases efficiency of a stage, nevertheless, it is compensated by lower mass, complication and shorter engine in general [6.3].

Whole procedure of counting is similar to the common solution. Intake parameters to that *half-stage* were taken from previous stage normally. However, it was important to find proper rotor speed to eliminate a swirl which appeared after rotor of HPT. In tables 6.9-6.11 are shown general, counted parameters of that stage (value of velocity U is negative since turbomachinery is rotating in opposite way than HPT stages).

**Table 6.9. Velocities on PT turbine**

Symbol	Hub	Pitch	Tip	Unit	Mach no.		
					Hub	Pitch	Tip
$u_1$	-1036.88	-1167.8	-1298.72	$\frac{\text{ft}}{\text{s}}$	0.54	0.61	0.67
$c_1$	875.86	875.8599	875.85	$\frac{\text{ft}}{\text{s}}$	0.45	0.45	0.45
$c_{1a}$	373.05	381.4792	389.91	$\frac{\text{ft}}{\text{s}}$	0.19	0.20	0.20
$c_{1u}$	1409.93	1549.278	1688,63	$\frac{\text{ft}}{\text{s}}$	0.73	0.80	0.88
$w_1$	1659.83	1779.71	1902.26	$\frac{\text{ft}}{\text{s}}$	0.86	0.92	0.99
$w_{1u}$	951.99	955.33	958.729	$\frac{\text{ft}}{\text{s}}$	0.49	0.50	0.50

**Table 6.10. Angles and degree of reaction of PT stage**

	$\alpha$			$\beta$			Unit	Degree of reaction		
	hub	pitchline	tip	Hub	pitchline	tip		hub	pitchline	tip
Rotor(out)	89.18	89.14	89.10	35.92	32.23	28.83	°	1	1	1

**Table 6.11. Comparing results from NPSS and step-by-step**

Parameter	NPSS		Step-by-step		Unit	Difference of results
Pressure $P_r$	hub	—	hub	12.19	psi	2%
	pitch	12.03	pitch	11.84	psi	
	tip	—	tip	11.48	psi	
Temperature $T_r$	hub	—	hub	1256	°R	2%
	pitch	1227	pitch	1208	°R	
	tip	—	tip	1184	°R	

Due to used solution it might be seen that calculations made step-by-step and computer analysis are not matching. It is a result of used solution – eliminating nozzle. In traditional approach nozzle blades are responsible for decompressing and function of rotors is to exchange kinetic energy into power usable

for something else. In nozzleless system rotors are responsible for both. Because of that they are not perfect in any of them. However reduction of mass and shortening of an engine is profitable enough.

## 6.4. Blade-profile design

Intake parameters for blade design are: velocities triangles on proper radius, radiuses of leading edge and trailing edge and width of disk. For nozzle blade on pitch-line was assumed density of blades on a level equal to 1 and length of blade to chord as 1.5 due to relative low inner radius. In HPT on each stage 47 blades and 51 in PT were calculated.

With these and previously designed parameters it was possible to draw blade profiles and check fluency of flow-paths. According to theory designed blades should form convergent flow-path since there would be continuous decompression, which is desirable. In the figures 6.6 and 6.7 is shown property of those assumptions.

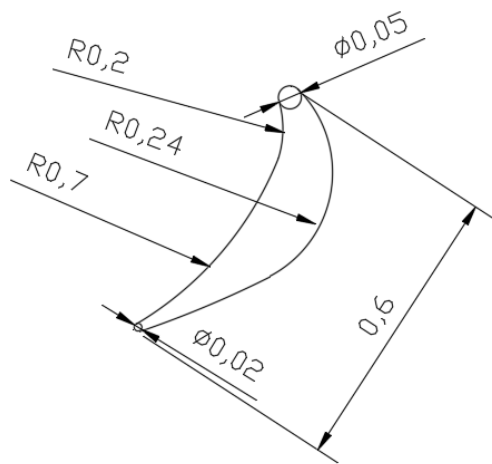


Fig. 6.6. Designed blade profile (HPT)

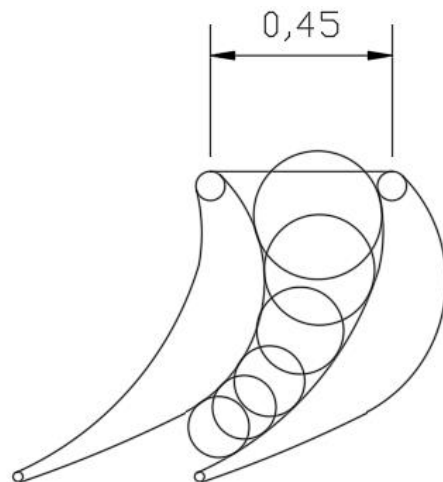


Fig. 6.7. Check of fluency of a flow-path

## 6.5. Material selection

From the beginning of aeronautics there was a trend to maximize efficiency and performance of planes and engines. Such feats require modern materials which are tough and immune to high temperatures. Presently nickel-based super-alloys are in use. However, as engines work in higher temperatures, these alloys became inadequate and because of that fact more complicated and advanced cooling systems are required[6.4]. Due to that fact in this project research about modern materials has been done. Currently the best choice for a new turbine materials appear to be ceramic composites. They require not so much or even no cooling at all and are 60% lighter than nickel alloys [6.5]. These materials consist of fibres cured in a matrix, usually carbon or silicon carbide.[6.5] Since the maximum inlet temperature in turbine equals  $2303\text{ }^{\circ}\text{R}$  the most suitable candidate for this project is A-N720 Oxide Ceramic Matrix Composite [6.6]. Oxide ceramic matrix composites products are based upon sol-gel derived matrices and 3M Corporation's Nextel™ fibre products.

These materials can be used up to  $2652\text{ }^{\circ}\text{R}$  in air environments and are primarily used in both aerospace and gas turbine applications. Density of the material is comparable to aluminium what provides much decrease in mass of component, moreover, it is worth to admit that increase of temperature does not lead to significant decrease in durability. In table 6.11 are presented general parameters of an A-N720 Oxide Ceramic Matrix Composite.

## 6.6. Cooling system

Mostly, due to requirement of maximum efficiency, in modern engines there is observed a tendency to increase temperature before turbine. One of the consequences of high temperatures is heat exchange with blades and later with disks which results in: decreasing material strength and properties. Because of that fact, especially on the first stages of turbine, there is a need of using cooling system. This allows blades to survive in such extreme environment. Nevertheless, as it was mentioned before the A-N720 has great thermal properties. Maximum temperature before turbine equals 2303°R and maximum service temperature to A-N720 is 2652°R (look table 6.11). Due to that fact it was decided not to use any cooling system (apart from passive). However, as it is commonly known thermal strikes, which may be around maximum service temperature, might occur in combustion chamber. Because of that it was decided` to use a coating protection. Selected material is the Al<sub>2</sub>O<sub>3</sub>-Y<sub>2</sub>O<sub>3</sub>. Thermal barrier made of this would increase maximum service temperature for another 180 °R [6.7]

**Table 6.11. Main material properties[6.6]**

Material property	Value	Unit
Density	168.55	$\frac{lb}{ft^3}$
Tensile strength (in 518°R)	24.51	Psi
Tensile strength (in 2651°R)	20.45	Psi
Creep strength (in 100 Psi)	360000	s
Young modulus	10.15	Msi
Maximum Service Temperature	2651	°R
Thermal conductivity	$3.3 \cdot 10^{-6}$	$\frac{1}{°R}$

## 6.7. Tensile calculations

Primary task of disks in turbomachinery is to take from rotor blades loads, which are from forces and moments of inertia, and transmit it via spool to compressor. Mentioned loads are results of thermo-gas-dynamic processes which allow creating thrust of power for propeller.

In turbine disks main loads are created by forces of inertia from their own mass, however, significant part of tensions are from gradient of temperature which might be up to 300 K [6.10] since a disk is some kind of cooler for blades on it.

To judge properly importance and influence of each load in a disk it is important to separate them because in early stage of projecting there is a way of impact on each type of loads for example there is an option use material with different density or form disks along radius in proper way.

At the beginning of counting it was assumed that a disk was with constant width which is easier to describe by mathematic functions. Whole calculations were made on the basis of work “J.Lipka Wytrzymałość maszyn wirnikowych” (WNT,1967)[6.8]. Equations in table 6.12 were used to find all loads. On inner and outer radius it assumed that radial loads are equal 0.

**Table 6.12. Equations used for load calculations**

Parameter	Equation	Unit
Radial thermal loads	$\sigma_{tr} = \frac{\alpha ET}{4} \left[ \left(1 + \frac{R_o}{R}\right)^2 \left[ 1 - \left(\frac{R_o}{r}\right)^2 \right] - \frac{r^4 - R_o^4}{r^2 R^2} \right]$	psi
Circumferential thermal loads	$\sigma_{tu} = \frac{\alpha ET}{4} \left[ \left(1 + \frac{R_o}{R}\right)^2 \left[ 1 + \left(\frac{R_o}{r}\right)^2 \right] - \frac{r^4 - R_o^4}{r^2 R^2} - 4\left(\frac{r}{R}\right)^2 \right]$	psi
Radial from inertial forces loads	$\sigma_{mr} = \frac{3 + \nu}{8} \rho U^2 \left[ \left(1 + \frac{R_o}{R}\right)^2 - \left(\frac{R_o}{r}\right)^2 - \left(\frac{r}{R}\right)^2 \right]$	psi
Circumferential from inertial forces loads	$\sigma_{mu} = \frac{3 + \nu}{8} \rho U^2 \left[ \left(1 + \frac{R_o}{R}\right)^2 + \left(\frac{R_o}{r}\right)^2 - \frac{1 + 3\nu}{3 + \nu} \left(\frac{r}{R}\right)^2 \right]$	psi
Radial from blades loads	$\sigma_r = \frac{\sigma}{1 - \left(\frac{R_o}{R}\right)^2} \left[ 1 - \left(\frac{R_o}{r}\right)^2 \right]$	psi
Circumferential blades loads	$\sigma_u = \frac{\sigma}{1 - \left(\frac{R_o}{R}\right)^2} \left[ 1 + \left(\frac{R_o}{r}\right)^2 \right]$	psi
Total radial loads	$\sum \sigma_r = \sigma_{mr} + \sigma_{br} + \sigma_{tr}$	psi
Total circumferential loads	$\sum \sigma_u = \sigma_{mu} + \sigma_{bu} + \sigma_{tu}$	psi
Total loads	$\sigma_{total} = \sqrt{\sigma_r^2 + \sigma_u^2 - \sigma_r \sigma_u}$	psi

In the figures 6.8-6.9 are presented results of tension calculations of the first disk and theoretical width of disks. It is worth to admit that total tensions are lower than circumferential ones since in a disk exists distribution of temperature which creates significant compressing forces inside a disk what results in decrease of total loads.

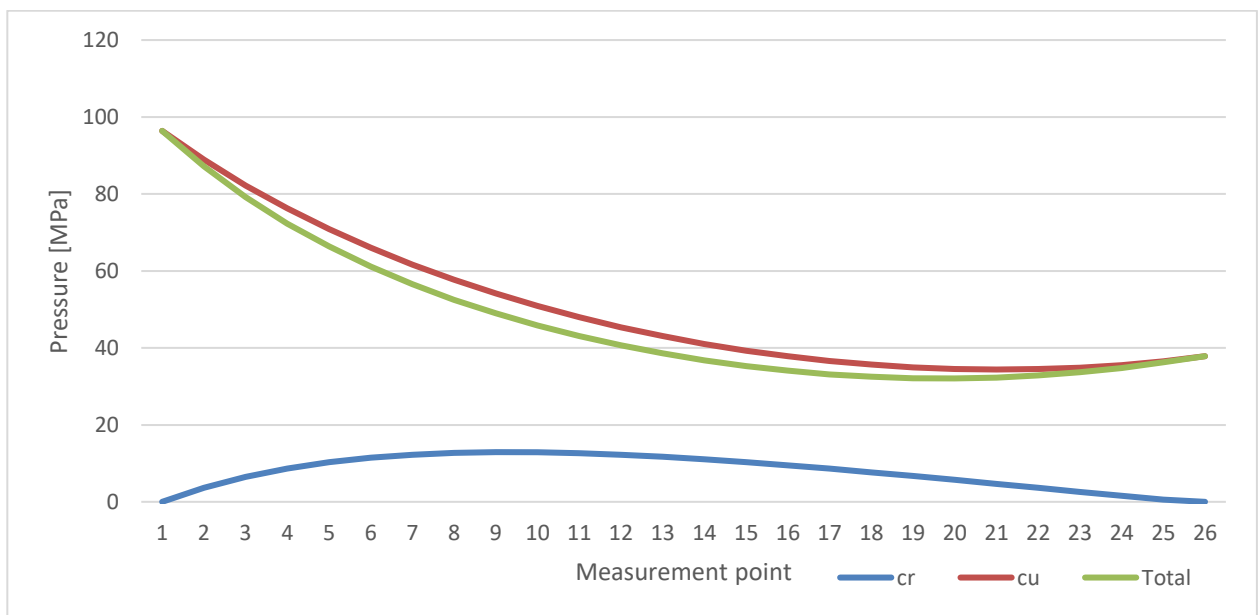


**Fig. 6.8. Tensions in the first disk**

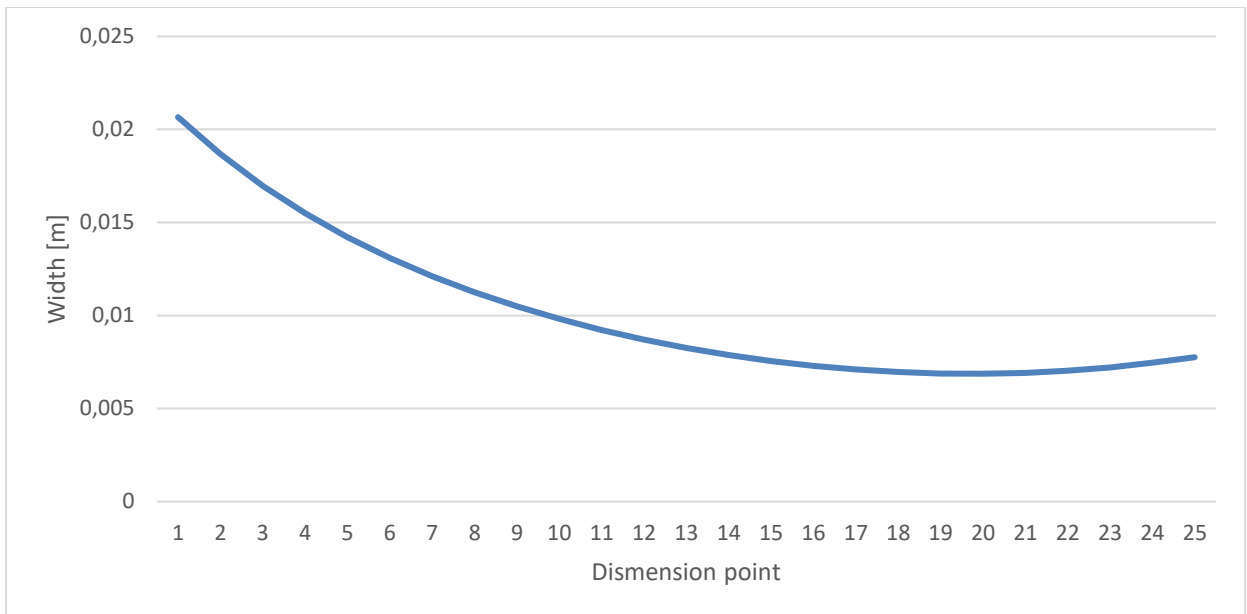


**Fig. 6.9. Theoretical width of the first disk**

Calculated shape of a disk is just theoretical since a disk need to have predicted places for montage, seals, holes for screws, locking pieces. Due to that shape of a final disk is just a little bit similar to that theoretical.

Also 3D models has been done since that fact it was possible to find out about volume of a disks and count their mass (table 6.13). In figures 6.10.-6.11 and in appendix 4 is presented final form of a disk.

**Table 6.13. Mass of each disk**

	<b>Mass</b>	<b>Unit</b>
Disk 1	1.62	lb
Disk 2	1.62	lb
Disk 3	2.05	lb

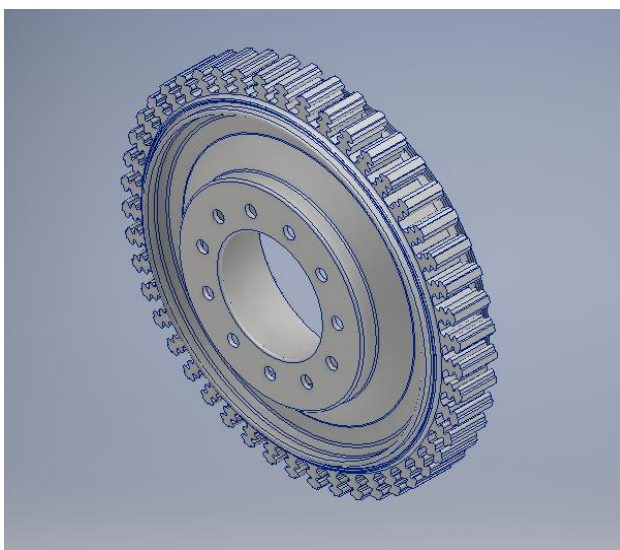


**Fig. 6.19. 3D model of a disk**

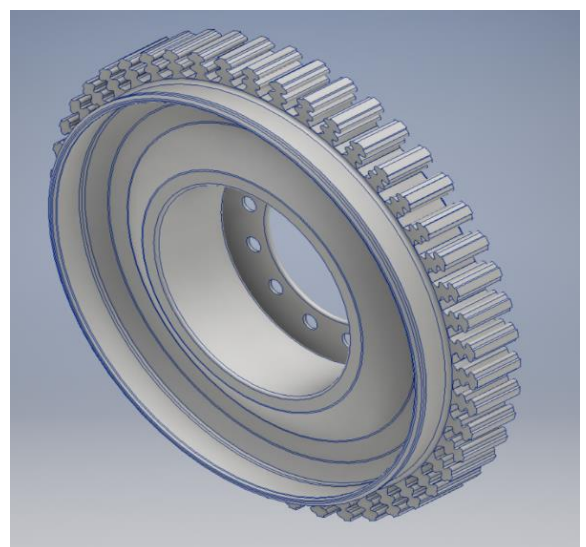


**Fig. 6.20. 3D model of backside of a disk**

## 6.8. Locking piece design

At the early stage of project, since dimensions of the engine and the turbine are relatively small, it was considered to use mono-structural disk plus blade. However, due to high rotational speed, which results in huge loads, that solution would be inefficient and non-durable [6.9]. Due to that it was chosen to use classical approach and design locking piece.

Calculations of locking pieces relies on checking value of surface pressure and stretch stress. Also it is assumed that centrifugal force is evenly spread on each ledge with assumed constant width of piece. Precision of adhesion determines efficiency of heat exchange between a blade and a disk and at the same passive cooling of a blade.

Pressure on surface and stretch stress were calculated using equations in table 6.14.

**Table 6.14.** Equations used in calculations of locking piece.

Parameter	Equation	Unit
Surface pressure	$P_s = \frac{F_r}{el}$	psi
Stretch tension	$F_r = \frac{1}{2k \cos\alpha + \mu \sin\alpha} F$	lbf
Radial force	$F = \frac{mu^2}{r}$	lbf
Length	$e = \frac{F}{P_s l}$	in
Stretching stress in waist	$\sigma_r = \frac{F}{bl}$	psi

Tensions in a locking piece are smaller than maximum tensions (with safety coefficient equal 2 included) what means that this locking piece is acceptable. In the figure 6.25. is presented scheme of locking piece and in 6.24. is shown model 3D.

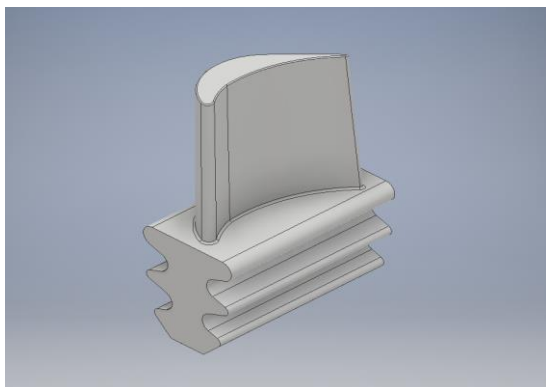


**Fig. 6.24.** Model 3D of a blade

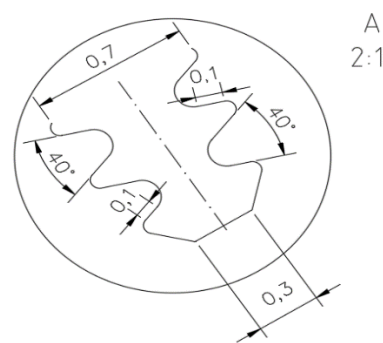


**Fig.6.25.** Scheme of locking piece

## 6.9. Tensile calculation of blades

In turbine, in traditional approach, blades are divided into two types: nozzle – static blades and rotors – – moving, rotating blades.

In nozzles decompression, decrease of temperature and increase of velocity is done. Also a flow is directed before achieving rotors to increase efficiency. Nevertheless, in rotors decompression is continued, however, main purpose of rotors is to take kinetic energy of flow, not decompressing a flow.

Main loads which occur on nozzle blades are these form aerodynamic forces and difference of pressure before and after blades. Circumferential and axial loads were counted separately and then they were summed up geometrically. Calculations have been done using equations in table 6.15.

**Table 6.15. Equations used in calculations of a blade**

Parameter	Equation	Unit
Circumferential loads	$q_u = \frac{\dot{m}}{LZ} (c_{u2} - c_{u1})$	lbf
Axial loads	$q_w = \frac{1}{LZ} [\pi(R_z^2 - R_w^2)(p_2 - p_1) + \dot{m}(c_{w2} - c_{w1})]$	lbf
Summed loads	$q = \sqrt{q_u^2 + q_w^2}$	lbf
Bending moment	$M_{max} = \frac{1}{8} qL^2$	lbf*in
Total tensions	$\sigma = \frac{M_{max}}{W}$	psi

**Table 6.16. Results of nozzle blades tensile calculations.**

Stage	$q_u$ [lbf]	$q_w$ [lbf]	$q$ [lbf]	$M_{max}$ [lbf*in]	$\sigma$ [Psi]
1	517.3	-2086.9	2150.4	0.088	53.18
2	161.8	-1925.7	1932.4	0.419	165.86

Rotor blades, apart from loads which are on nozzles are also loaded by circumferential forces from rotational movement.

Due to the fact that projected blades are extremely short and thin it was decided to project blades as with constant area of cross section. That solution will increase mass slightly, however, due to usage of the new material that would not be problem since density of material is very low. A profit of that is much easier crafting of a blade. For blades with unchangeable cross section area equation for tensions looks:

Parameter	Equation	Unit
Tensions in blade with unchangeable cross section area	$\sigma(R) = \rho\omega^2 \frac{R_z^2 - R^2}{2}$	Psi

Results for each stage are presented in table 6.17. In figure 3.31 model 3D.

**Table 6.17. Results of tensions on blades of each rotor**

Radius [in]	$\sigma$ (Stage 1) [Psi]	$\sigma$ (Stage 2) [Psi]	$\sigma$ (Stage 3) [Psi]
3.42	96.779	107.032	—
3.47	58.435	72.204	—
3.50	31.537	44.073	—
3.54	14.971	24.042	—
3.59	6.125	11.535	—
3.62	2.099	4.769	—
3.66	0.578	1.651	—

3.70	0.120	0.460	—
3.74	0.017	0.097	—
3.78	0.001	0.014	—
3.82	0	0.001	—
3.86	—	0	—
3.94	—	—	519.222
4.02	—	—	480.209
4.09	—	—	440.413
4.18	—	—	399.848
4.25	—	—	358.514
4.33	—	—	316.397
4.40	—	—	273.527
4.49	—	—	229.873
4.57	—	—	185.435
4.64	—	—	140.244
4.73	—	—	94.270
4.80	—	—	47.512
4.88	—	—	0

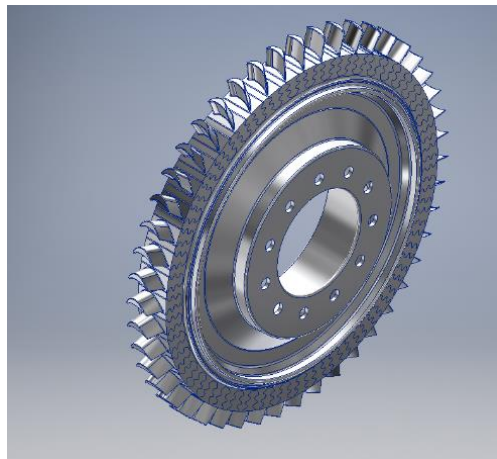


**Fig. 6.26. Final model 3D**

## **6.10. Turbine construction technical description**

The appendix 4 presents a construction of the whole turbine. Component is divided into two main parts – two-stages HPT and counter rotating nozzle less stage of PT. HPT disks are joined to a shaft using 11 bolts M6. Between those disks is placed a sealing ring, this ring is held by holdfast from one disk to another. Disks and rings are made of A-N720 CMC.

Nozzles are assembled with the cover by threaded (M4) pins which protrude from the top shelf of the nozzle through cover. Due to that cover is divided circumferentially into 6 parts since those parts are holding nozzle blades. At the bottom of the lower shelf of each nozzle is placed graphite sealing which works with sealing rings. Same solution is on every flow-path connected with the ribs rotor blades are montaged to a disk by locking pieces and locked by the washer. There are 47 blades in HPT and 51 in PT. Blades, rotor and nozzle, are made of A-N720 CMC.

PT disk is mounted to shaft by spline and blocked from one side with a usage of a nut. Behind PT there are 3 ribs which connect cover with flow patch and a nozzle.

Between turbines there are 3 ribs connected to a cover with the same solution as nozzles. Those ribs are assembled with airfoil bearings. In this component there is one bearing between two shafts. Construction of a bearing includes single truck and one top foil for each shaft.

## 7. Diffuser design

The purpose of implementing diffuser is to discharge pressure. It leads to decrease of velocity. It allows together more enthalpy on turbine what is main target when it comes to designing power plant for electricity generator.

This issue do not require doing advanced analysis at this step because of the relatively simply construction. Shape of diffuser in a major part depends on the aircraft design, which is not provided in request for proposal. Nevertheless, the geometry of diffuser is partly determined by gas - dynamic calculation. The literature shows that the key is an angle of diffuser divergence. The larger it is the higher possibility to sub - viscous layer separation [7.1]. Due to simplicity of diffuser construction in preliminary project only the areas ratio has been calculated and presented in the table 7.1. A brief calculation shows that the exit area of diffuser should be 1.25 times bigger than turbine exit area to discharge the flow. The higher expand in diffuser is demanded, the areas ratio is higher. One threaten may occur, when scaling off the ambient pressure. Then a reverse flow chokes the diffuser and brings unsteady turbine work or even engine cuts down. According to the construction, a few of reliable designs were taken under consideration, thus two of them have been tested by CFD program simulation. The diffusers are commonly done with heat - resisted and steeliness steel alloys, for example H25N20S - 2 or X15CrNiSi - 25 - 21. The flange with ribs may be made with Ti - Al - 2.5 Sn. The structure has to sustain temperature, pressure tensile and be resistant to the vibrations. Consequently, the structure would be scattered with embossed mesh to stiffen the construction.

**Table 7.1. Calculations of the diffuser area**

Parameter	Equation	Value	Unit
Diffuser outer area	$\frac{A_1}{A_2} = \frac{\rho_1 * V_1}{\rho_2 * V_2}$	0.8	—

### 7.1 Diffuser construction technical description

The assembly drawing of the UAV diffuser (DI) is attached as the appendix 2.

A montage of the s - duct diffuser should be started from connecting the cone holder (8) by the bolts (12, 13, 14) to the integrated rib (3), then the cone (9) may be screw (10). Then, using the bolts (1, 5, 6) it have to be connected to the turbine cover (2) and to the diffuser segment

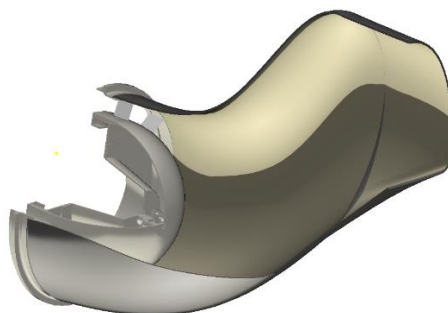


**Fig. 7.1. Three dimensional model of the diffuser**

## 8. Additional systems

This chapter includes a brief description of secondary systems like: fuel system, lubrications system, bearings, FADEC, anti-icing system, fire detection and extinguishing system.

### 8.1. Control system

Full Authority Digital Engine Controller (FADEC) is used to increase control over the aircraft and to decrease a workload of a crew during a flight. Because of the fact that engine PFF-63 is projected to UAV it is advised to use the best possible quality system. There would be no direct connection from ground crew to engine, due to that fact the engine controller must have full authority to change all parameters during a flight, even if the situation would require shutting down an engine. In the figure 8.1 is presented block diagram of a FADEC.

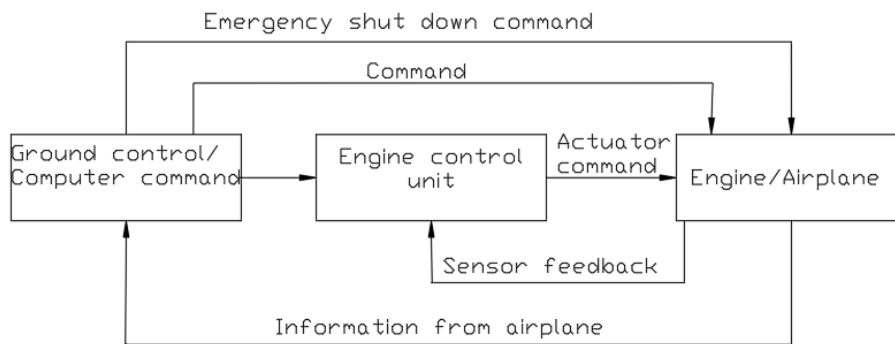


**Fig. 8.1. Block diagram of the FADEC**

Work of FADEC starts with engine startup. System accelerates the engine to a stable operational speed. From this point a control loop starts. As the first are checked all engine parameters to see if they are within operational limits. If everything is correct then airplane parameters must be checked. After that, computer or ground control makes a decision to start a flight.

### 8.2. Fuel system

In PFF-63 is proposed an electronically controlled fuel system with signals from FADEC. This system replaces all of the hydro-mechanical engine controls which were used in the baseline engine.

Firstly the fuel would be pumped the fuel from tanks and transferred, through filters to protect engine from foreign matter which might be in a fuel, to the high pressure system, then to fuel injectors which are responsible for preparing fuel-air mix.

Also engine is equipped in fuel-oil heat exchanger, to preheat the fuel and in consequences increase combustion efficiency [8.1].

### 8.3. Bearings

Classical, ball and roller, bearings are easy to manufacture, well-known and reliable, however in their efficiency is not the highest possible to achieve. Due to that fact it was decided to equip PFF-63 in a singular between shaft airfoil bearings.

Such solution increases efficiency and simplify construction of lubrication system what in consequence leads to decrease of mass. These bearings were designed specifically for high speed and high temperature applications and were successfully tested on aircrafts like Boeing 737 during the early 1960s.

Other advantages include a quieter operation, a high environmental durability and no scheduled maintenance [8.2]. In the figure 8.2 is presented scheme of the bearing system.

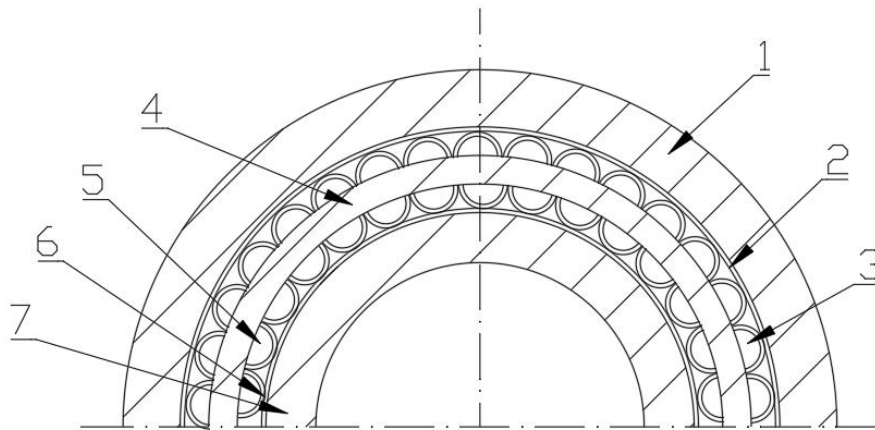


**Fig. 8.2. Scheme of bearing system.**1-HPT shaft, 2 -HPT top foil, 3-HPT bump foil, 4-bearing sleeve, 5-PT bump foil, 6-PT top foil, 7- PT shaft

Foil bearing is lubricated with PS304, a plasma sprayed composite solid lubricant. This lubricant acts as a thin foil coating layer during high temperature operations thereby enhancing its life to about 100000 start/stop cycles at around 1662°R [8.3]

#### 8.4. Lubrication system

Every rotating machinery needs some lubrication system, to decrease friction. Nevertheless, since in PFF-63 are used foil bearings, oil has to be provided only to three gearboxes in the figure 8.3 is presented block diagram of this system.

Oil is storage in the tank, which is placed in the front part of an inlet. Then is pumped with a usage of high pressure pump and then filtered before oil it would get to main components.

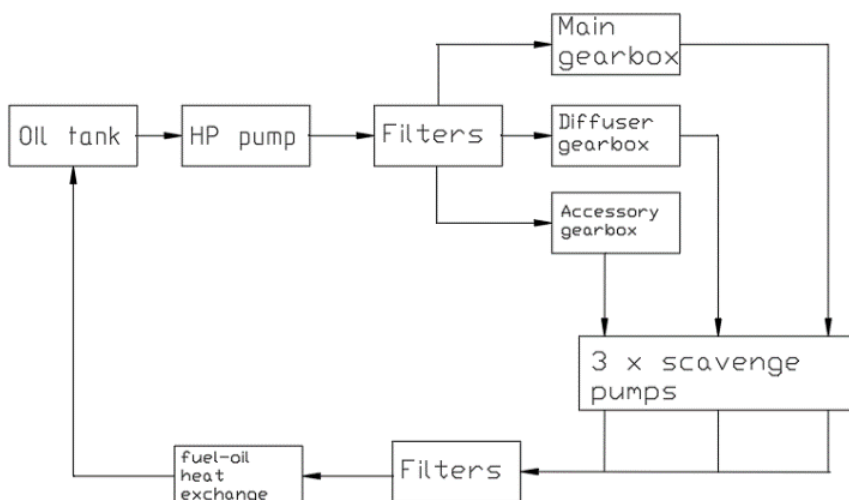


**Fig. 8.3. Block diagram of lubrication system**

The first place where this substance must be delivered is the main gearbox of an engine which is placed in the inlet cone. Oil is provided there using injections and taken away using pipes (for details look appendix 1) The second important point is gearbox of the diffuser, there is a planetary gear where oil is transported using pipes and injectors (appendix 2).

The oil tank is monitored by a thermostatic sensor and after scavenge pumps is placed filter and magnetic plug to protect system. Also there is a fuel-oil heat exchange system which takes heat from oil and preheats fuel to eventual de-icing.

Due to MIL-PRF-23699G norm, as the most suitable oil for this project was chosen oil with code: O-154. This oil was designed as product with high thermal stability, what would be the best option here [8.4].

### 8.5. Anti-icing system

Consequence of ice in inlet is disturbed flow which may lead to unsteady work of compressor or detached ice formation may even damage blades. However, due to relative low possibility of icing in this aircraft, there were predicted two ways of protecting engine from icing.

The first is oil tank in the front part of the inlet, heat from it would melt ice which may appear there, nevertheless when this system would be not be effective for same reason, for example, high humidity and low temperature, there was predicted usage of electrical heating pads.

### 8.6. Fire detection and extinguishing system

Engine is made with materials with high temperature resistance, however, in every fluid line is transported flammable substance and if any leak would occurs then it might be highly dangerous to structure of the whole aircraft.

Due to that in PFF-63 is proposed to montage fire, smoke and fuel detectors around main components of an engine. Also if this solutions would not be effective enough there should be placed thermocouples which monitors temperature around combustion chamber and when there would be increase of that parameter there would be launched extinguishing system which includes halon, and automatically engine would turn off.

## 9. Summary

World of the newest technology is the world of ecology. That is why developed solutions in industry must take care of present and future generations. This is not an easy task, however, necessary. Due to those assumptions every new aerospace construction must be adapted to those restricted requirements.

Projected engine not only matches those requirements but is also above them. In the traditional approach to the task presented solutions were: wider, heavier, longer and less efficient than in conceptional engine PFF-63. In comparison to baseline engine the differences were as follows (table 9.1. and table 9.2):

**Table 9.1. Comparing main differences between baseline engine and PFF-63**

	<b>Baseline engine</b>	<b>PFF-63</b>
Engine Type	Single Spool	Two Spool
Number of compressor stages	2 centrifugal	1 centrifugal with counter rotating diffuser
Number of turbine stages	3 Axial	2.5 Axial
Combustor type	Reverse Annular	Reverse Annular
Maximum power at sea level	1000 hp	990 hp

The continuation of the table is on the next page.

The continuation of the table 9.1.

	<b>Baseline engine</b>	<b>PFF-63</b>
Overall pressure ratio at max. Power	10.55	25
Max. Envelope diameter	27 inch	16.92 inch
Max. Envelope length	43 inch	34 inch
Dry weight	385 lb	211.64 lb

**Table 9.2 Comparison of baseline and designed engine cycle performance**

	<b>Baseline cycle</b>	<b>Design cycle</b>	<b>Improvement compared to baseline</b>
Loiter Speed	190 kts	190 kts	0%
Cruise Speed	220 kts	220 kts	0%
Loiter Fuel Burn	354.93 lb	249.26 lb	29.77%
Takeoff BSFC	$0.534 \frac{lb}{hp*hr}$	$0.404 \frac{lb}{hp*hr}$	24.34%
Loiter BSFC	$0.549 \frac{lb}{hp*hr}$	$0.417 \frac{lb}{hp*hr}$	24.04%
Thermal Efficiency	0.2329	0.3313	42.25%

During work on the project following tasks have been completed:

- Overview of modern constructions;
- Choice of the most profitable solution;
- Design of proper inlet in the shape of s-duct;
- Thermo-gas-dynamic calculations of compressor;
- Successful design of birotational compressor;
- Design of highly efficient combustion chamber;
- Thermo-gas-dynamic calculations of HPT;
- Thermo-gas-dynamic calculations of PT;
- Eliminated nozzle of PT;
- Blade profiles ;
- Chosen proper, modern highly resistant for temperatures material;
- Cooling has been eliminated due to material properties;
- Thermal barrier coating has been chosen;
- Tensile calculations have been done;
- Theoretical profiles of a disks have been counted;
- Mass of disks has been calculated;
- Locking pieces has been designed ;
- Final forms of disks have been projected;
- Designed efficient proper diffuser;
- Secondary;
- 3D models have been created;
- 2D drawings have been done.

Objectives of this work, which were savings and improvement of performance, were achieved. It was possible thanks to modern technology. Projected engine is 45% lighter, matches baseline power output, has greater maximum temperature. With aforementioned and other improvements it would be possible to achieve more efficiency and in consequences more environmental friendly engine.

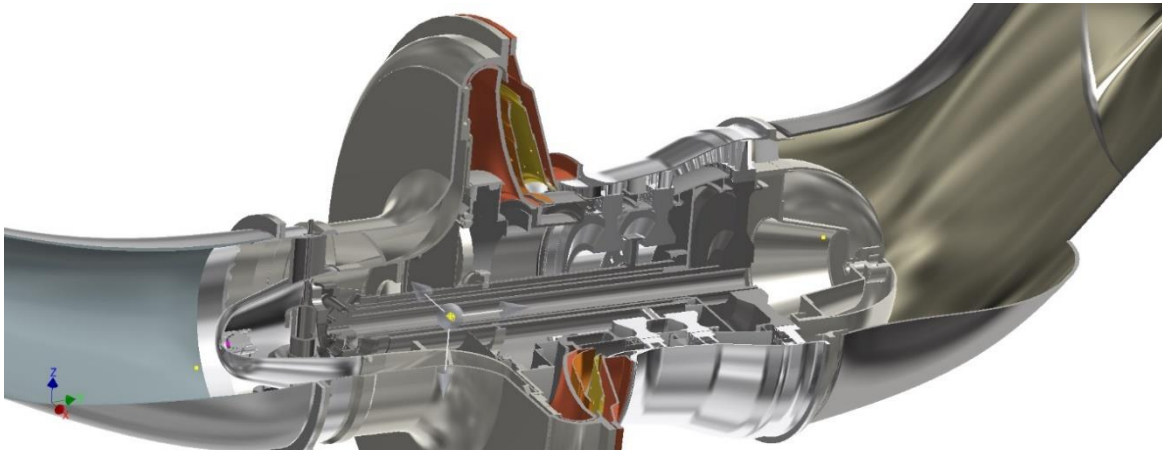


**Fig. 9.1. Three dimensional PFF-63 engine model**

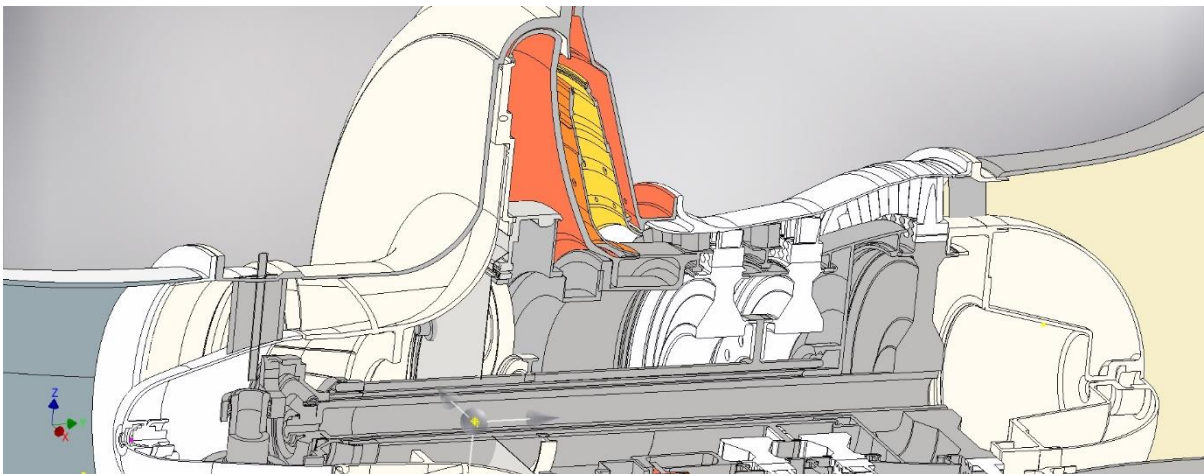
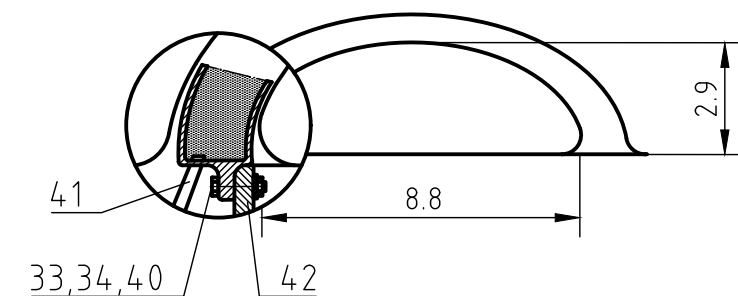
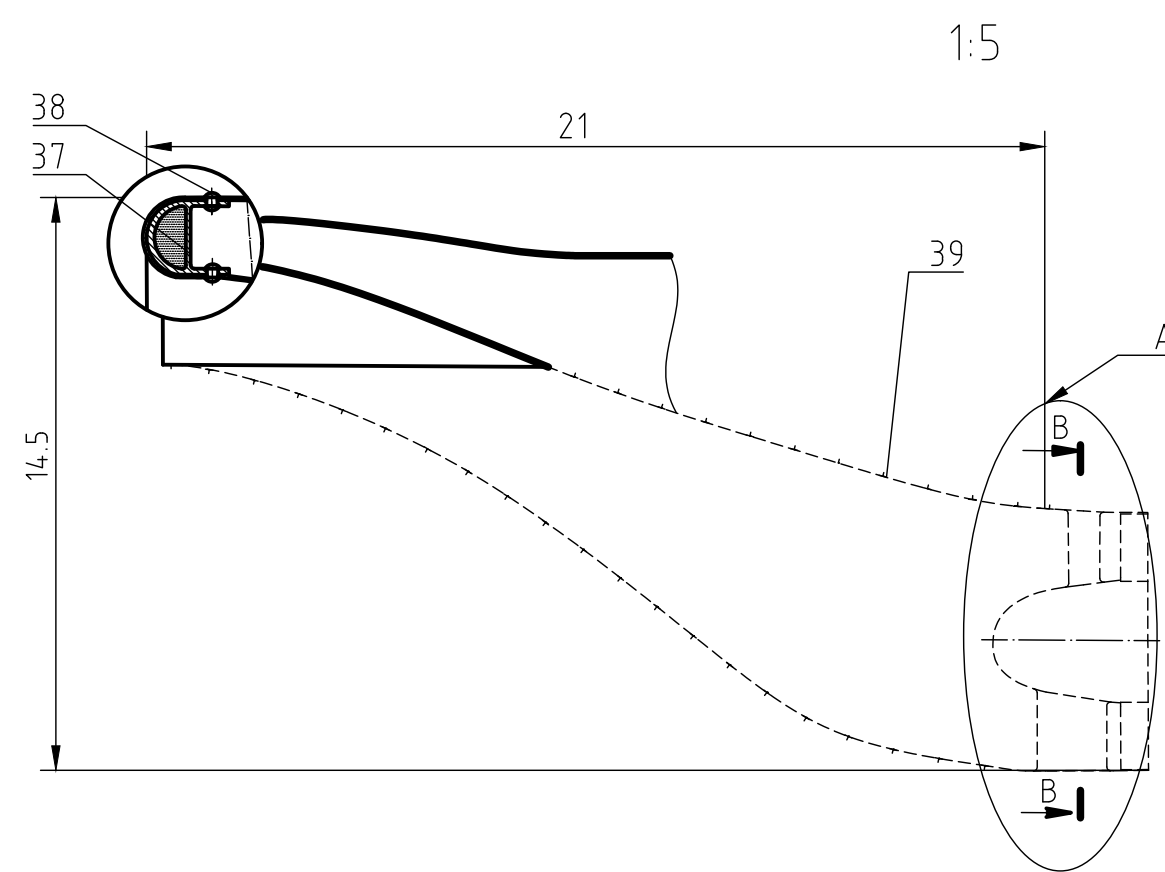
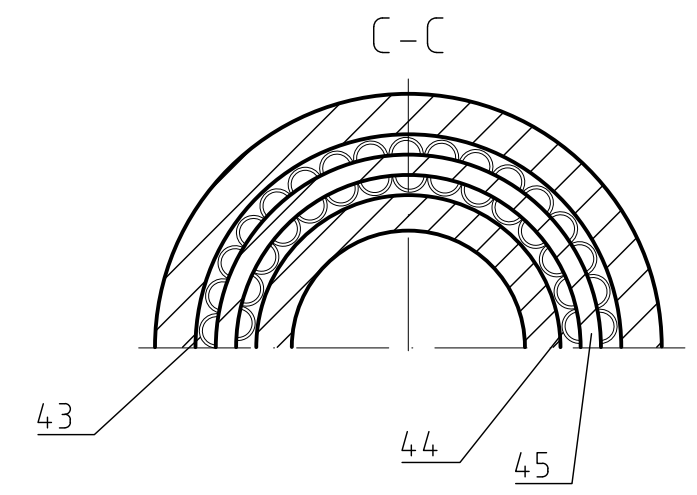
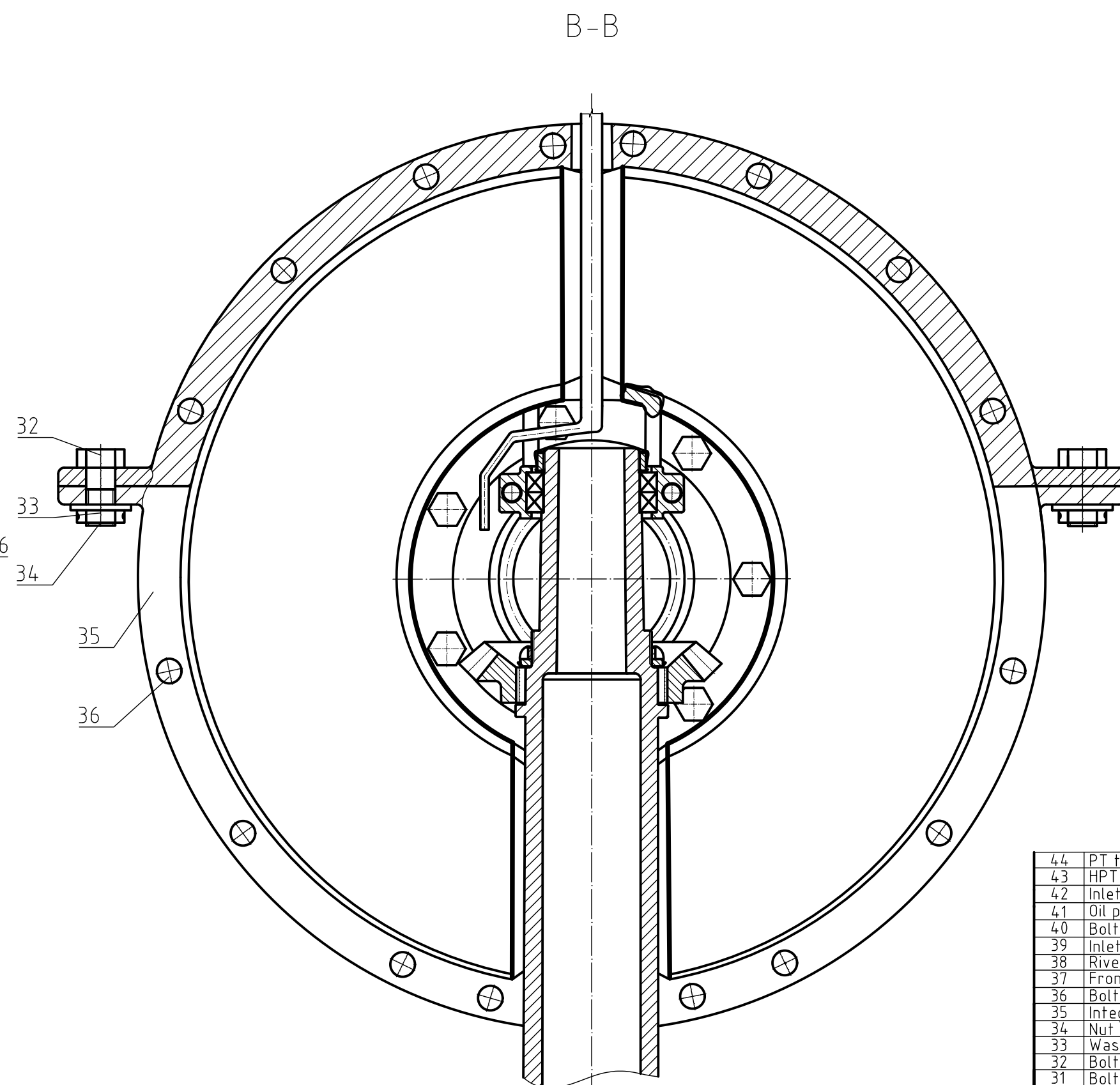
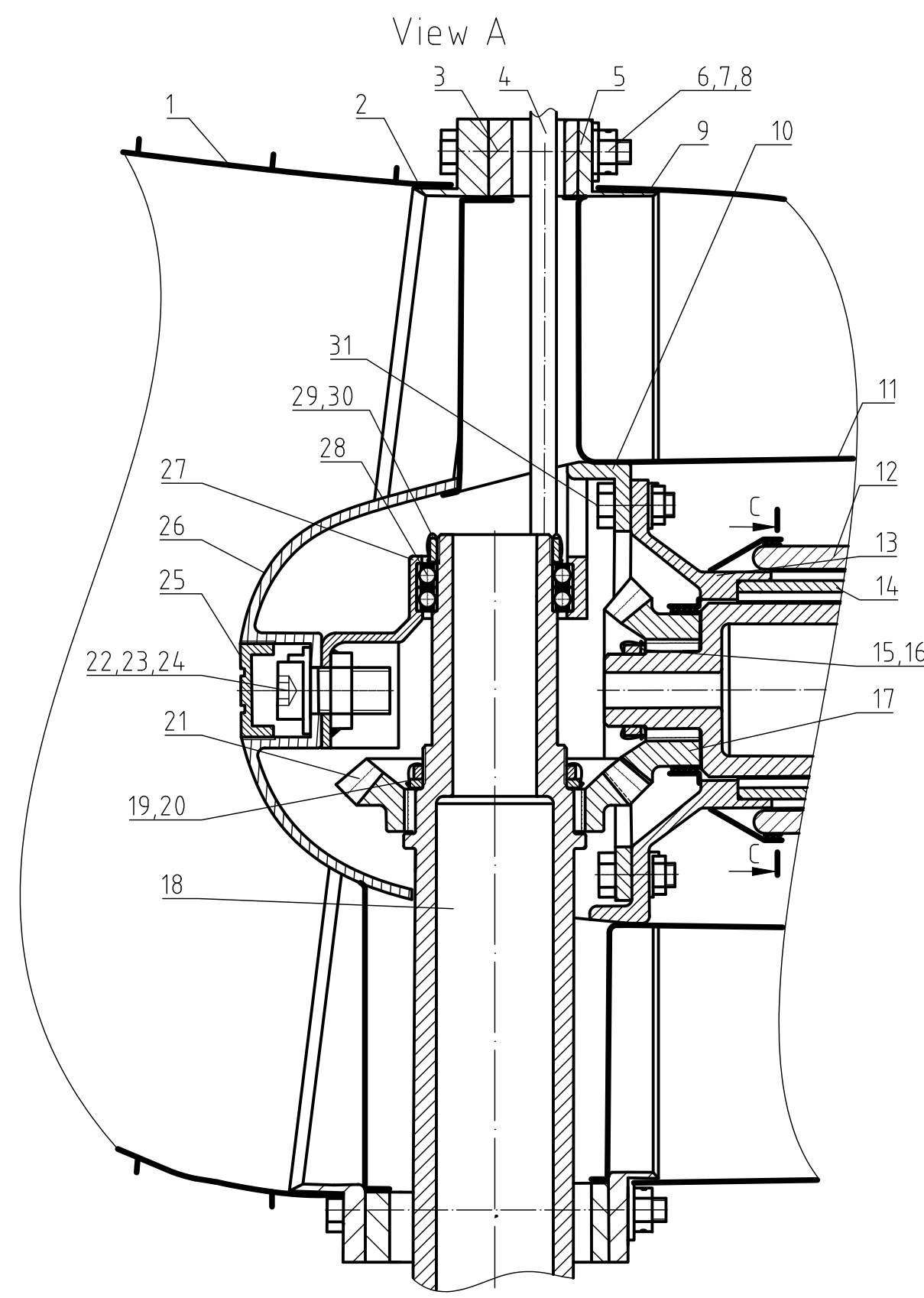


**Fig. 9.2. Three dimensional PFF-62 engine model (“technical illustration”)**

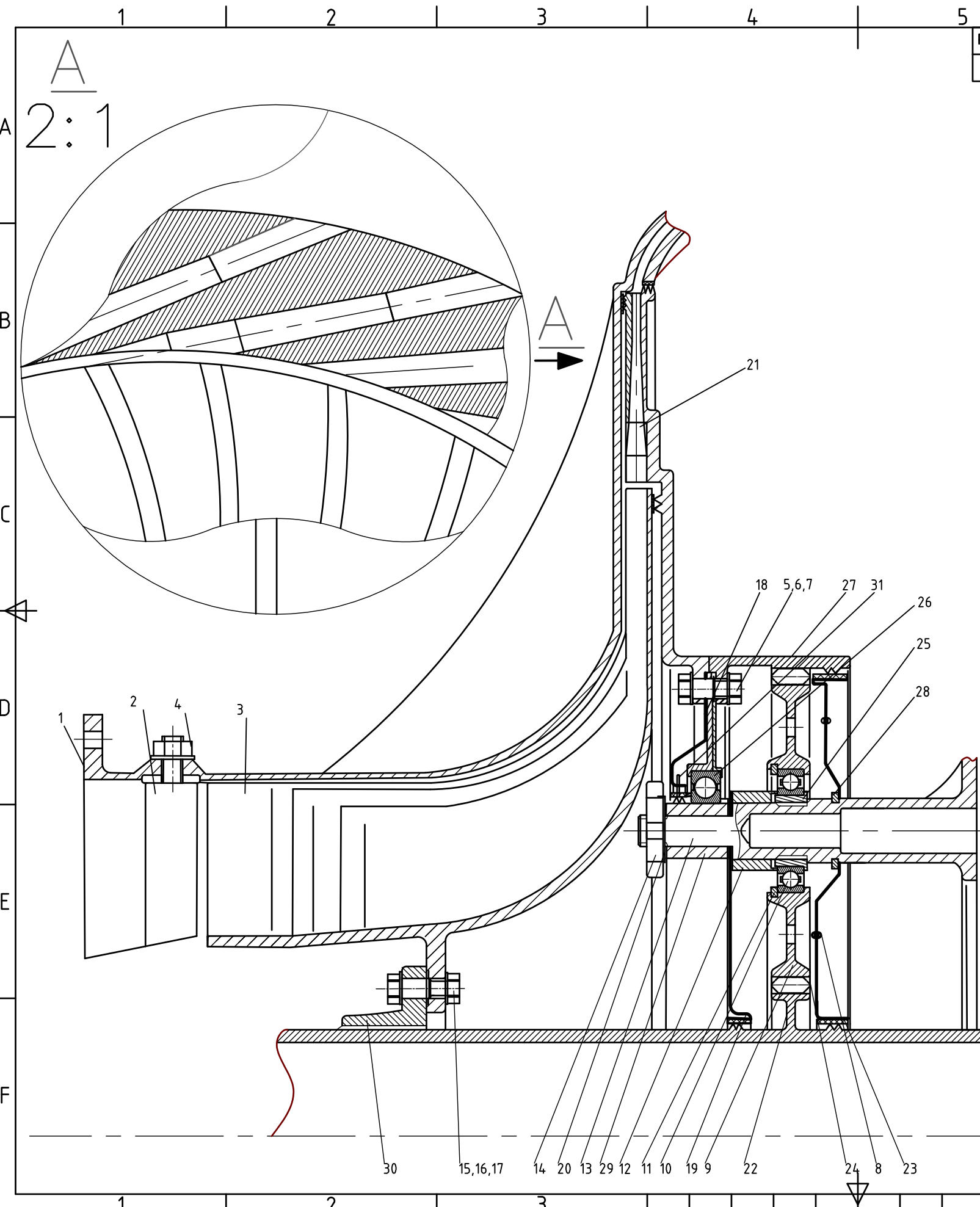
## 11. References

- 1.1. Yatskoo A.J.: *Candidate Engines for a Hybrid Electric Medium Altitude Long Endurance Search and Rescue UAV*, Request to Proposal, AIAA Foundation Student Design, Competition, Undergraduate Team – Engine 2018/19.
- 1.2. Honeywell:TPE 331-10 Turboprop engine, <https://aerospace.honeywell.com/en/~media/aerospace/files/brochures/n61-1491-000-000-tpe331-10turbopropengine-bro.pdf>, [accessed 20<sup>th</sup> of December 2018].
- 2.1. Mattingly J. D.: *Aircraft Engine Design, Second Edition*, AIAA Education Series, Virginia Polytechnic Institute and State University Blacksburg, Virginia, 2002, ISBN 1-56347-538-3
- 2.2. Wiatrek R.: *Teoria Silników Lotniczych*, WAT, Warszawa 1983
- 2.3. Farokhi S.: *Aircraft Propulsion*, 2014 John Wiley & Sons Ltd Second Edition, 2014
- 2.4. Григорьев В.А.: *Вертолётные газотурбинные двигатели* *Машиностроение*, 2007.
- 3.1. Smith D., Leroy H., *Wake Ingestion Propulsion Benefit. Journal of Aircraft and Power*. Vol. 9, No.1, Jan.Feb., 1993
- 3.2. Ting C.T. and others, *Inlet and S-Duct for B727 Airplane With Refanned JT8D Engines*, AIAA Paper 75-0059, Jan, 1975.
- 3.3. Wellborn S.R., Reichert B.A. and Okiishi T.H., *An Experimental Investigation of the Flow in a Diffusing S-Duct*, AIAA-92-3622, 1992.
- 3.4. Anabtawi A.J. and other, *An Experimental Investigation of Boundary Layer Ingestion in a Diffusing S-Duct With and Without Passive Flow Control*, AIAA 99-0739, 1999.
- 3.5. Raymer D.P., *Aircraft Design: A Conceptual Approach. Third Edition*, AIAA Education Series, American Institute of Aeronautics and Astronautics, 1999.
- 4.1. Balicki W., Chachurski R., Głowacki P., Kozakiewicz A., Szczeciński J., Szczeciński S., *Lotnicze zespoły napędowe 1*, Warszawa 2009.
- 4.2. Farokhi S., *Aircraft Propulsion second edition*, India, 2014
- 4.3. Kawalec K., *Optymalizacja energetyczna przepływowych kształtów lotniczej sprężarki promieniowej o wysokim sprężu, rozprawa doktorska*, Warszawa, 1997.
- 4.4. Hermann R., *Swierchzwukowyje wchodnyje diffuzory (Supersonic Inlet Diffusers and Introduction to Internal Aerodynamics)*, Fizmatgiz, Moskwa 1960.
- 4.5. Muller L., *Przekładnie obiegowe*, Warszawa 1983.
- 4.6. Czerni S., *Słownik lotniczo-kosmonautyczny*, Warszawa 1984.
- 5.1. Michael J. Verrilli, Lisa C. Martin Glenn, Research Center, Cleveland, Ohio, David N. Brewer, U.S. Army Research Laboratory, Glenn Research Center, Cleveland, Ohio, NASA/TM—2002-211509, "RQL Sector Rig Testing of SiC/SiC Combustor Liners"
- 5.2. Lefebvre H. A. and Ballal R. D., "Gas Turbine Combustion", 2nd ed., CRC Press, Florida, 2010
- 5.3. Łapucha R., "Komory spalania silników turbinowo-odrzutowych" - procesy, obliczenia, badania, 21, Bibliotek Naukowa Instytutu Lotnictwa, Warszawa 2004
- 6.1. Gary D., Vaneless counterrotating turbine, EUROPEAN PATENT: EP 3 372 782 A1, London 2018
- 6.2. Dzierżanowski P. *Konstrukcja silników lotniczych. Projektowanie przejściowe i dyplomowe*. Warszawa 1972.
- 6.3. Dźygałło Z., *Zespoły wirnikowe silników turbinowych* wydawnictwo komunikacji i łączności, Warszawa 1982
- 6.4. Schmid, *Manufacturing Processes for Engineering Materials*, 5th Ed., University of Notre Dame
- 6.5. Nageswara R., *Materials for Gas Turbines – An Overview*, Advances in Gas Turbine Technology. VIT University 2011
- 6.6. <http://www.matweb.com/search/datasheet.aspx?MatGUID=f186e5036c5b4a648229f9cd72b175a1> [accessed 6<sup>th</sup> of December 2018]
- 6.7. <https://www.sciencedirect.com/science/article/pii/S0169433213017169>, [accessed 7<sup>th</sup> of Dec. 2018]
- 6.8. Lipka J., *Wytrzymałość maszyn wirnikowych*, WNT 1967
- 6.9. Farokhi S., *Aircraft Propulsion 2nd Ed.*, Wiley 2014
- 6.10. Mattingly J., Heiser, W., *Aircraft Engine Design. 2nd Ed.*, AIAA, 2002.
- 7.1. Dzierżanowski P. and others, *Konstrukcja silników lotniczych*, WAT, Warszawa, 1972.



44	PT top foil	1	18Cr9Mi	AS-AB1	
43	HPT top foil	1	18Cr9Mi	AS-AB1	
42	Inlet montage rib	1	Al-6061-T6	In-mr1	
41	Oil pipe 2	1	St-AISI-321	In-op1	
40	Bolt 1/6 x 13/16	4	Carbon Steel	ASME B18.6.3	
39	Inlet skin structure	1	Al-6061-T6	In-skin	
38	Rivet 1/8 15/64	26	Carbon Steel	ASME B18.11.1	
37	Front frame	1	Carbon Steel	In-ffof	
36	Bolt 5/32 x 2 11/64	8	Carbon Steel	ASME B18.6.3	
35	Integrated hub rib	1	Al-6061-T6	In-r2	
34	Nut 1/4	16	Carbon Steel	ASME B18.2.1	For all 1/4
33	Washer φ1/4	16	Carbon Steel	ASME B18.2.1.1	For all φ1/4
32	Bolt 1/4 x 15/32	12	Carbon Steel	ASME B18.6.3	
31	Bolt 5/32 x 25/64	9	Carbon Steel	ASME B18.6.3	All undescribed
30	Washer passive wheel	1	Carbon Steel	In-wpawh	
29	Nut passive wheel	1	Carbon Steel	In-pwh	
28	Ball bearing	2		W617042ZS	
27	Bearing holder 2	1	Ti-5Al-2.5Sn	In-bhol2	
26	Nose cap	1	Carbon Steel	In-nc	
25	Cover	1	Carbon Steel	In-cov	
24	Washer φ5/16	1	Carbon Steel	ASME B18.2.1.1	
23	Nut 5/16	1	Carbon Steel	ASME B18.2.1	
22	Bolt 5/16 x 25/64	1	Carbon Steel	ASME B18.6.3	
21	Passive wheel	1	Carbon steel		
20	Washer	1	Carbon steel	In-wp1	
19	Nut	1	Carbon steel	In-mp1	
18	Shaft 1	1	Carbon	In-wsp	
17	Active wheel	1	Carbon steel	In-wha	
16	Washer active wheel	1	Carbon steel	In-wf1	
15	Nut active wheel	1	Carbon steel	In-mf1	
14	Airfoil bearing	1	Carbon	AS-AB1	
13	Airfoil bearing holder	1	Ti-5Al-2.5Sn		
12	HPT shaft	1	Carbon	ASS-2	
11	Panel 3	1	Al-6061-T6	In-p3	
10	Bearing holder	1	Ti-5Al-2.5Sn	In-bhol1	
9	Panel 2	1	Al-6061-T6	In-p2	
8	Washer φ5/32	25	Carbon steel	ASME B18.2.1.1	For all φ5/32
7	Nut 5/32	25	Carbon steel	ASME B18.2.1	For all 5/32
6	Bolt 5/32 x 13/16	8	Carbon steel	IASME B18.6.3	
5	2-nd flange	1	Al-6061-T6	In-f2	
4	Oil pipe 1	1	St-AISI 321	In-op1	
3	Integrated tip rib	1	Al-6061-T6	In-r1	
2	1-st flange	1	Al-6061-T6	In-f1	
1	Panel 1	1	Al-6061-T6	In-p1	

No.	Name of part	Quan.	Material	Standard	Coment
Scale	Author	Signs	Sheet A2	Name of drawing	
1:1	Checked by			Appendix 1 Assembly drawing of the UAV inlet	
Company name			Material	Drawing number	Pap. /No. Pap
Military University of Technology			Ti-10V-2Fe-3Al Al 6061-T6	PFF-63-IN	1/5

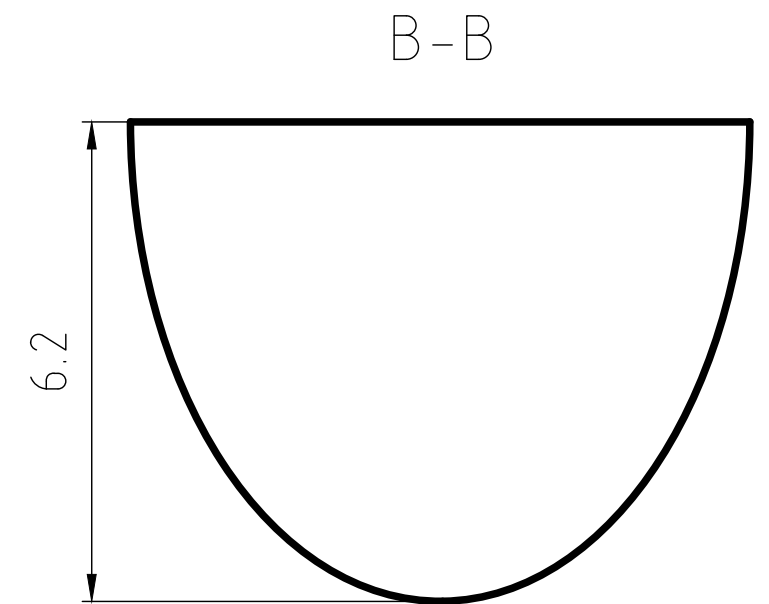
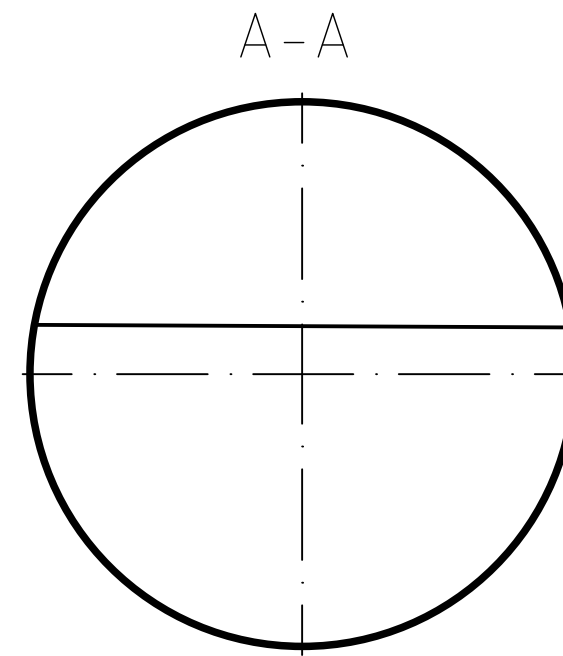
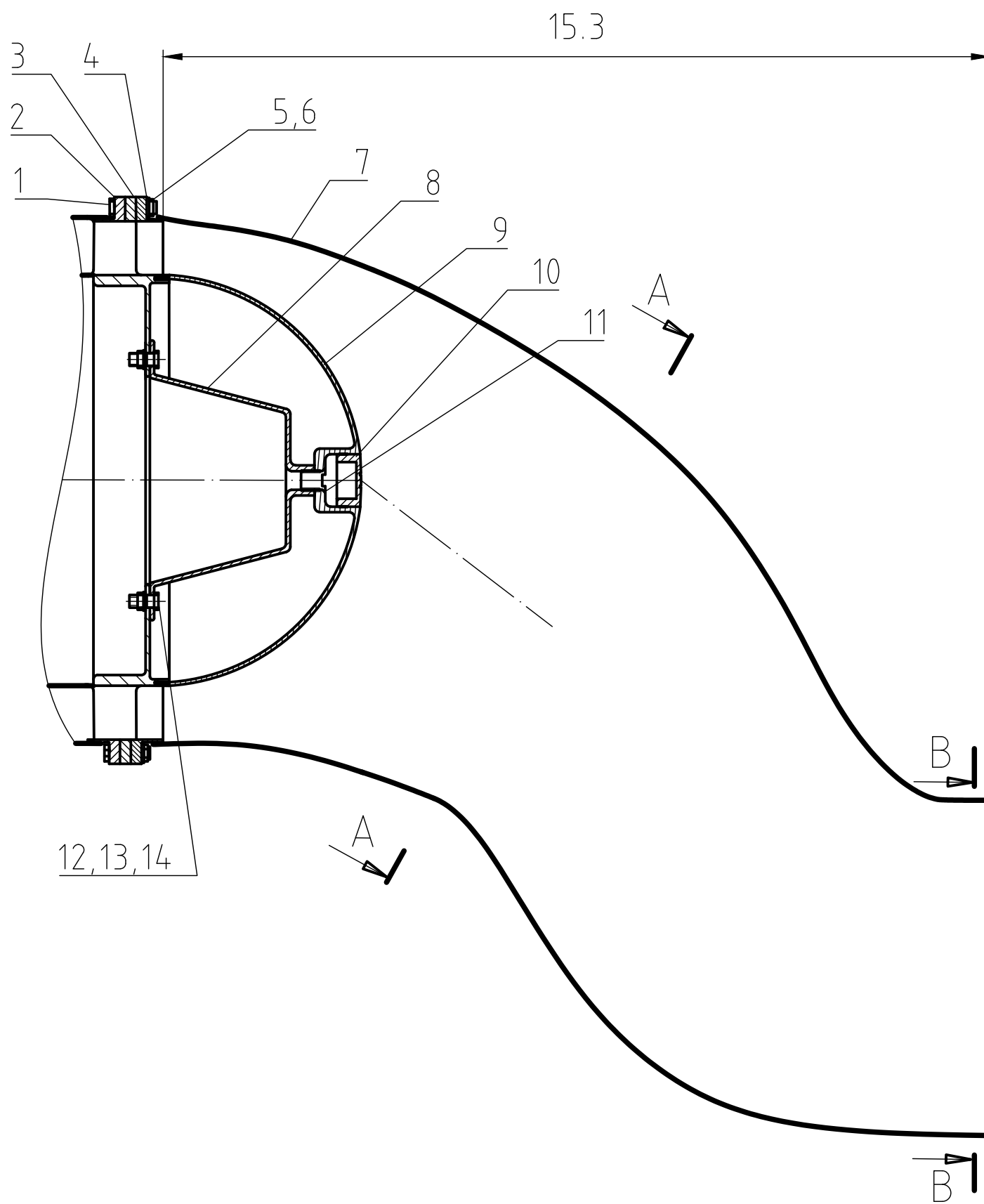


RevNo	Revision note	Date	Signature	Checked

32	Washer $\phi 0.99$	1	EB 88494		To convey a drive
31	Air pipe	1	No. PFF-63-C1-09	Carbon- steel	
29	Satelit pivot	1	No. PFF-63-C1-08	Carbon- steel	
28	Ring	3	DIN 471		
27	Gear	1	No.PFF-63-C1-G06	Carbon- steel	
26	Bearing	1	634		
25	Lead ring	7	No.PFF-63-C1-G02	Lead	
24	Gear d70	1	No. PFF-63-C1-G01	Carbon-steel	
23	Bearing	2	635		
22	Shaft	1	No. PFF-63-C1-06	H25N20S2	
21	Diffuser	1	No. PFF-63-C1-05	Ti6Al4V	
20	Washer $\phi=0.6$	3	EB 88494		
19	Drawing sheet	1	No.PFF-63-C1-G08	Steel	
18	Drawing sheet	1	No.PFF-63-C1-G07	Steel	
17	Washer $\phi=0.2$	16	DIN 125		
16	Bolt 5/ 32"-32 UNC	16	ISO 4017		
15	Nut 5/ 32"-32 UNC	16	ISO 4017		
14	Nut 9/ 16"-12 UNC	1	ISO 4017		
13	Carrier	3	No.PFF-63-C1-G05	Carbon- steel	
12	Protective tube	1	31125184.0050		
11	Expanding ring	2	DIN 471		
10	Bearing	3	634		
9	Safellite gear	3	No.PFF-63-C1-G04	Carbon-steel	
8	Rivet	2	BN-70/1121-06		
7	Washer $\phi=0.2$	16	DIN 125		
6	Bolt 5/ 32"-32 UNC	16	ISO 4017		
5	Nut 5/ 32"-32 UNC	16	ISO 4017		
4	Nut 3/ 16"-24 UNC	24	ISO 4017		
3	Impeller	1	No. PFF-63-C1-04	Ti6Al4V	
2	Guide vanes	24	No. PFF-63-C1-03	Ti6Al4V	
1	Compressor cover	1	No. PFF-63-C1-01	Ti6Al4V	
No.	Name of a part	Quantity	Norm/ No of draw	Material	Comments

FILE NAME	Appendix 2	FSCM NO	SHEET	A3	SCALE	1:1
SIZE						
DRAWN						
CHECK						
APPR.						
ISSUED						
REV						
CONTRACT NO	DWG NO PFF-63 - C0					



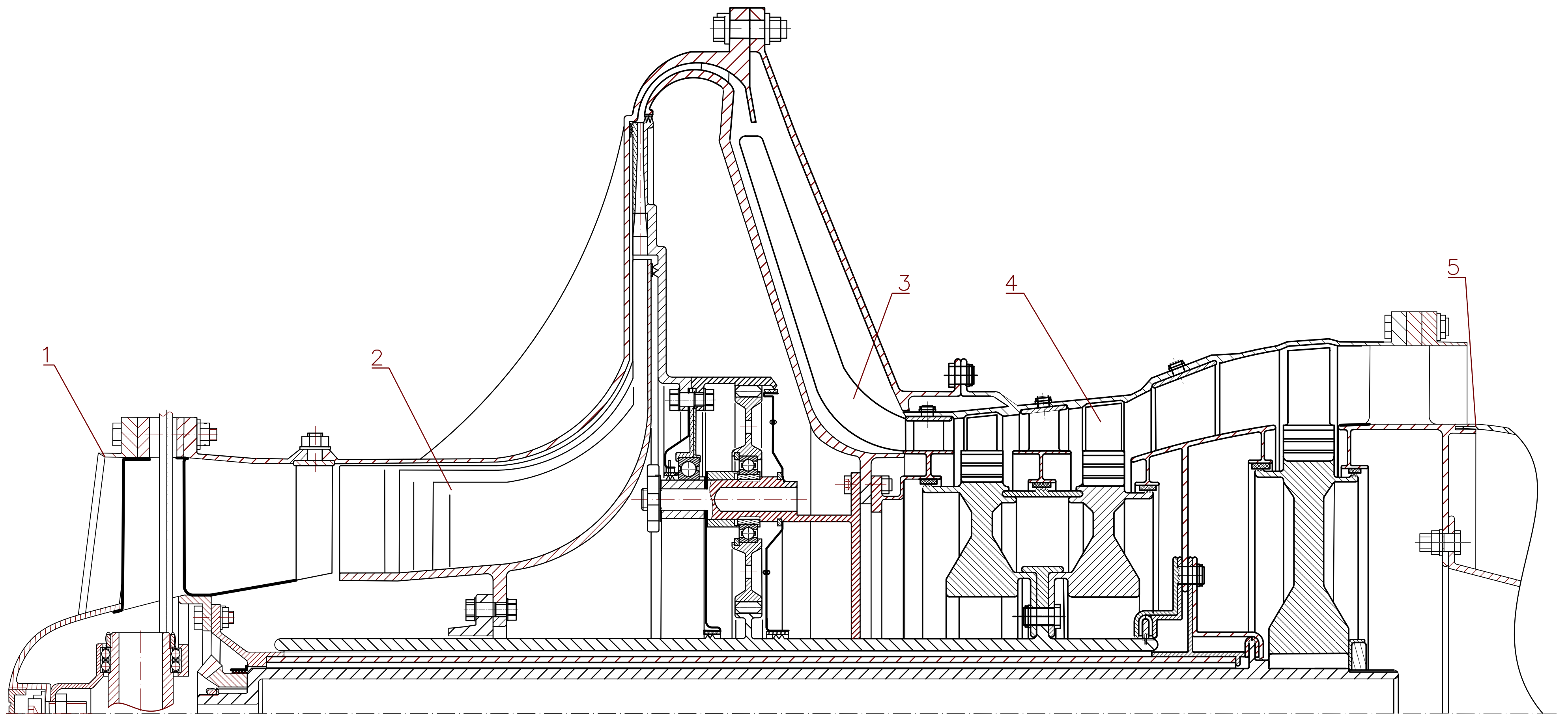


14	Bolt 5/16 x 5/32	11	Carbon steel	ASME B18.2.1	
13	Washer 5/16	11	Carbon steel	ASME B18.21.1	
12	Nut 5/16	11	Carbon steel	ASME B18.6.3	
11	Screw	1	Carbon steel	DI-SC1	
10	Plug	1	H25N20S2	DI-P	
9	Cone	1	H25N20S2	DI-C	
8	Cone strut	1	Ti-10V-2Fe-3Al	DI-CS	
7	Diffusor skin	1	H25N20S2	DI-S	
6	Washer $\phi$ 1/4	20	Carbon steel	ASME B18.21.1	
5	Nut 1/4	20	Carbon steel	ASME B18.6.3	
4	Diffusor flange	1	Carbon steel	DI-DF	
3	Integrated rib ring	1	Carbon steel	DI-IRR	
2	Turbine cover flange	1	Carbon steel	DI-TCF	
1	Bolt 1/4 x 25/32	20	Carbon steel	ASME B18.2.1	

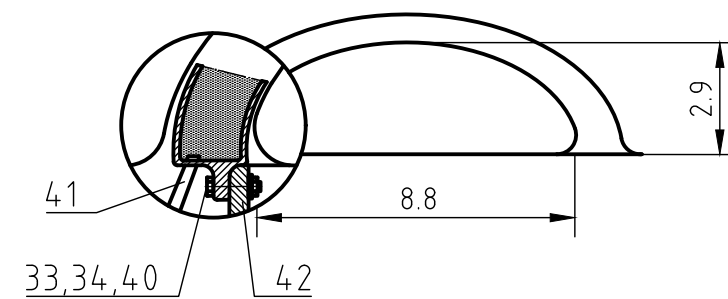
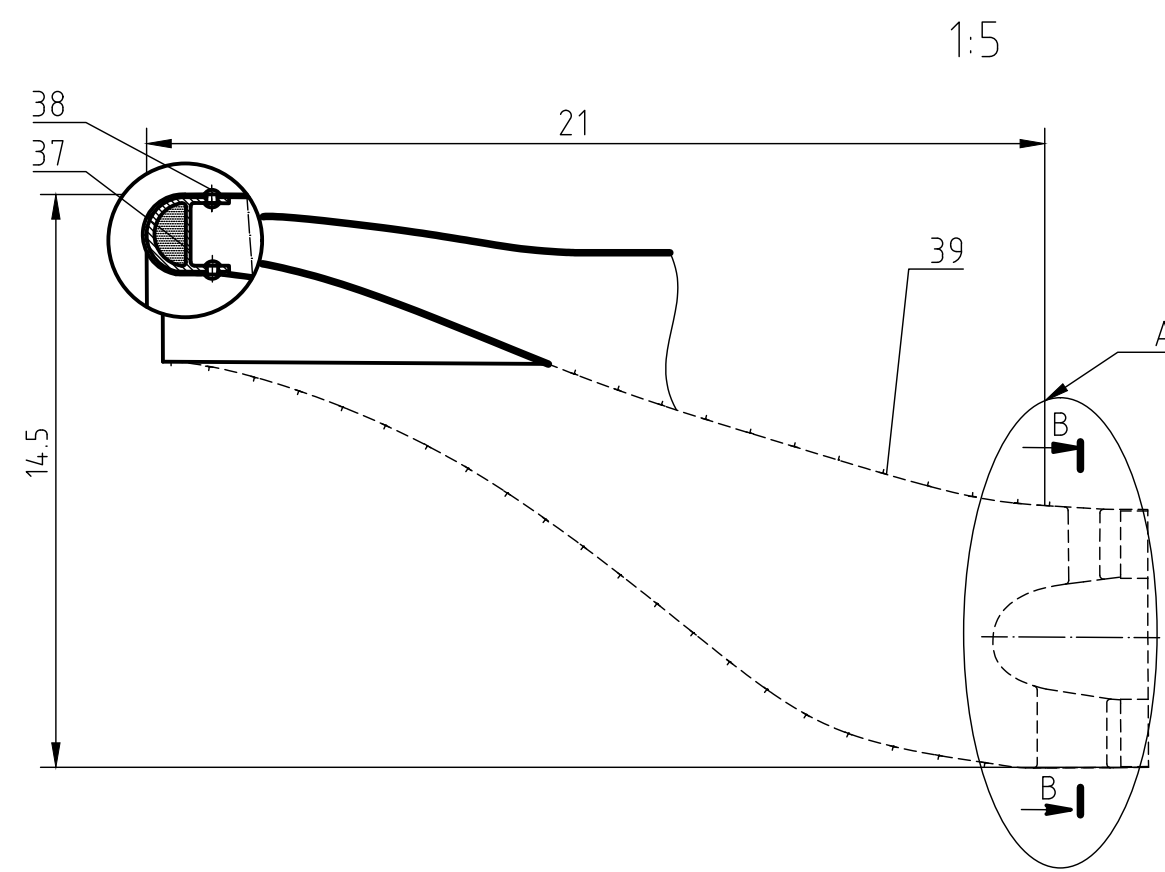
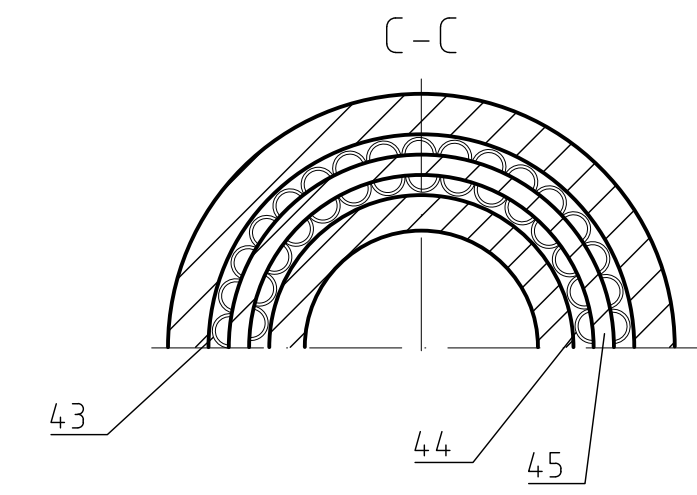
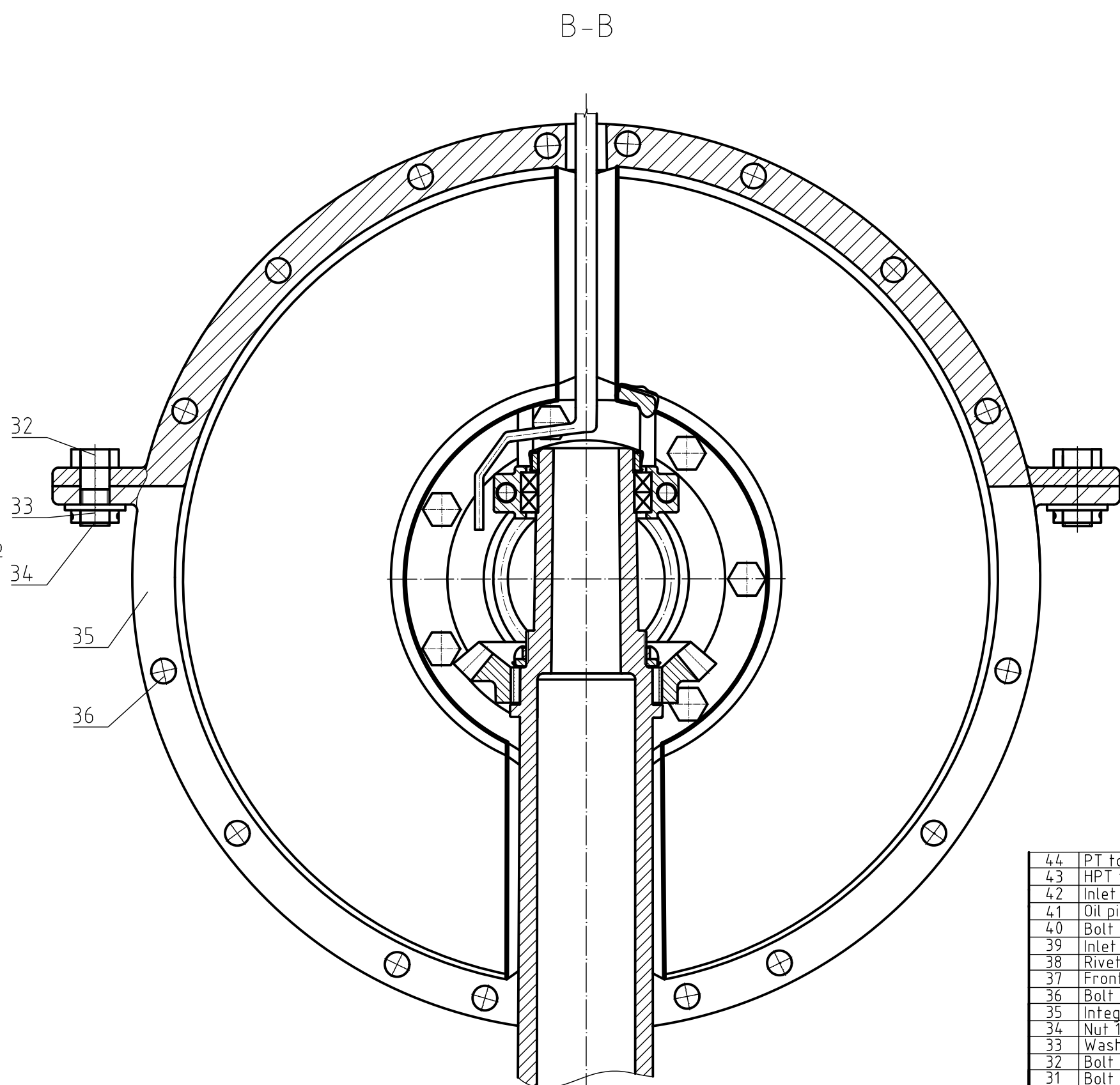
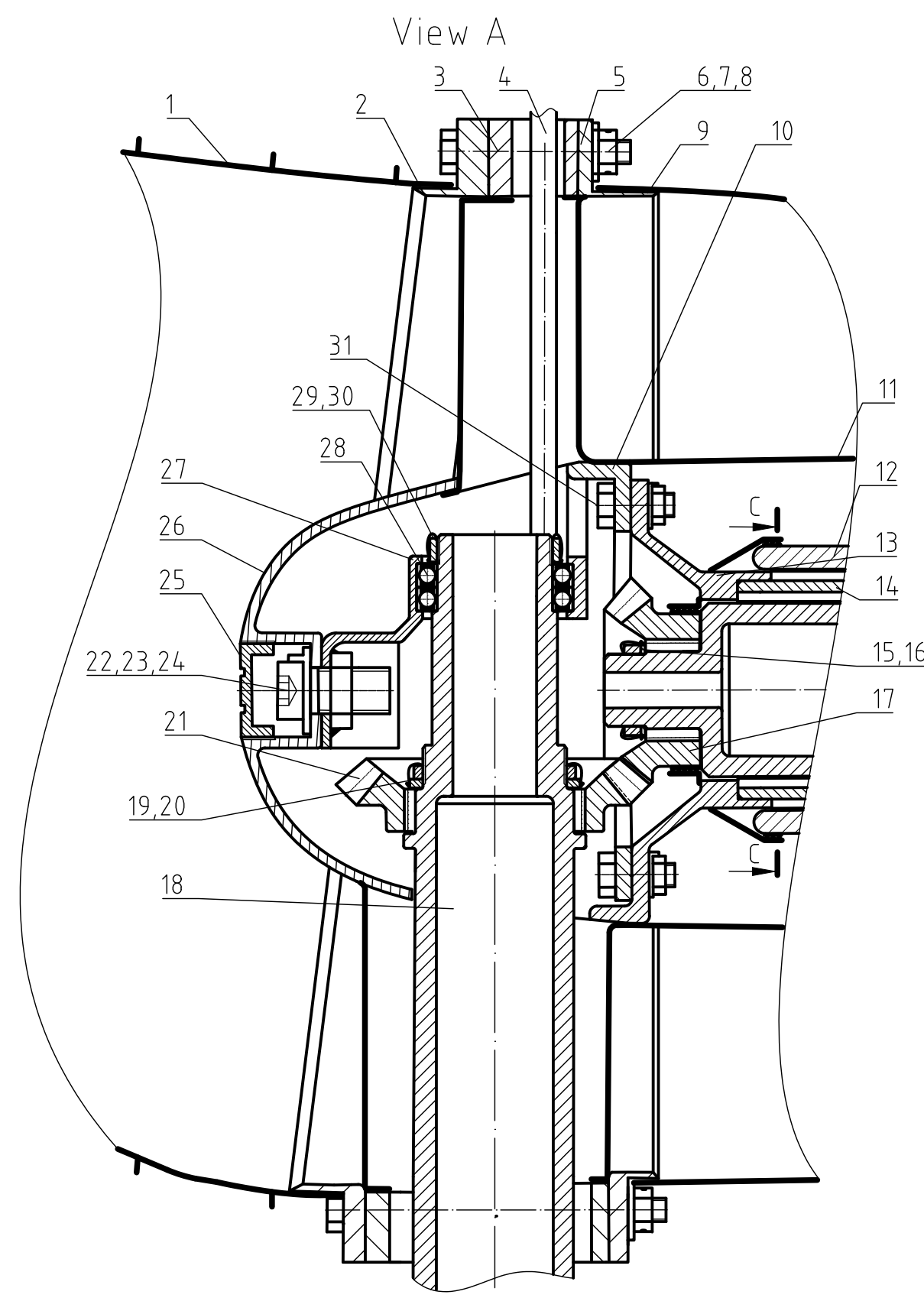
No.	Name of part	Quan.	Material	Standard	Coment
-----	--------------	-------	----------	----------	--------

Scale	Author	Surnames	Signs	Sheet A3	Name of drawing Appendix 4 Assembly drawing of the UAV diffuser
1:2.5	Checked by				

Company name	Material	Drawing number	Pap. /No. Pap
Military University of Technology	H25N20S2	PFF-63-DI	4/5

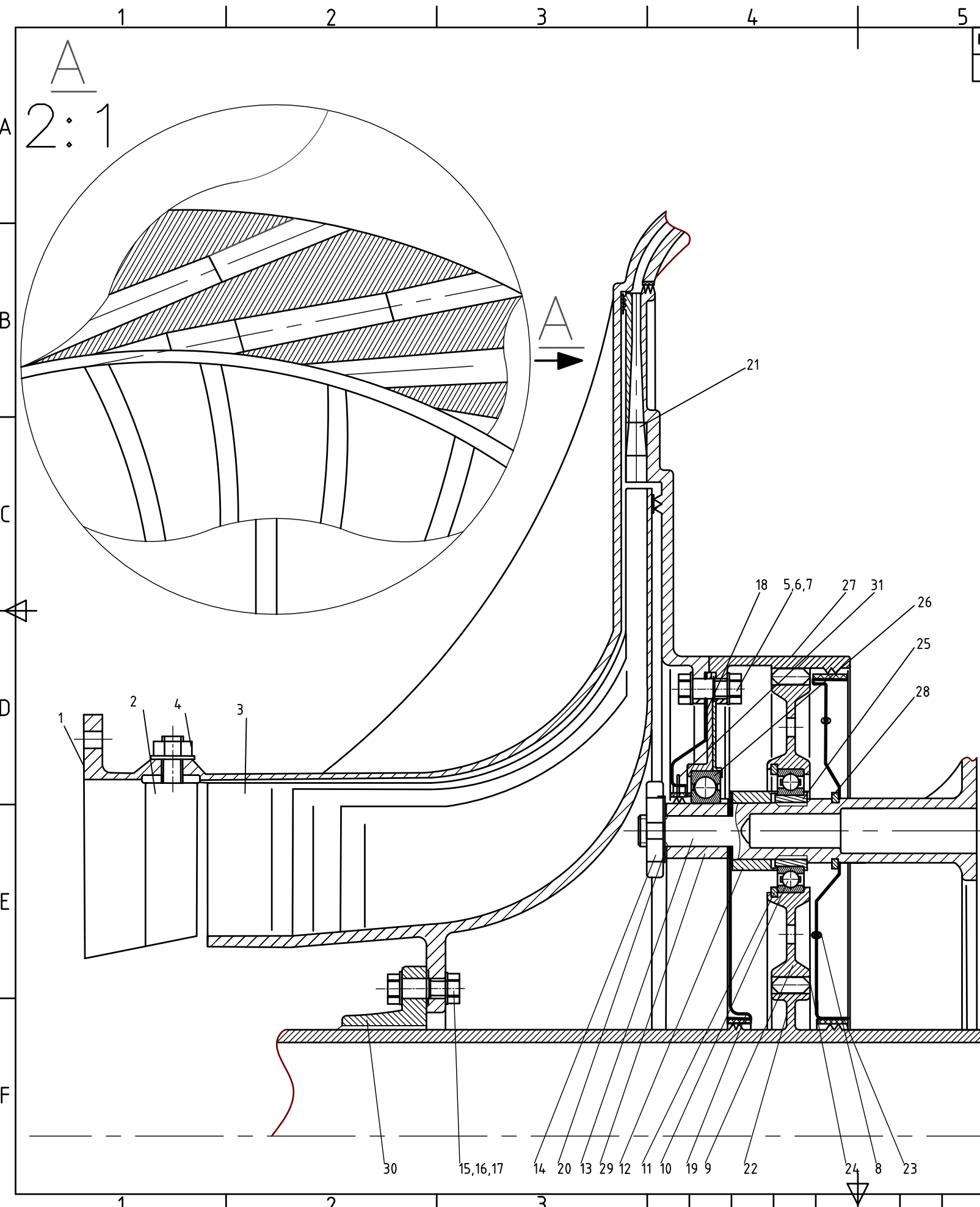


4	Diffusor	1		D.No. 4, DI	
3	Turbine	1		D.No. 3, ASS-1	
2	Compressor	1		D.No. 2, CO	
1	Inlet	1		D.No. 1, IN	
No.	Name of part	Quan.	Material	Standard	Coment
Scale	Author	Signs	Sheet	Name of drawing	
1:1	Checked by				
Company name			Material	Drawing number	Pap. /No. Pap.
Military University of Technology					5/5



44	PT top foil	1	18Cr9Mi	AS-AB1	
43	HPT top foil	1	18Cr9Mi	AS-AB1	
42	Inlet montage rib	1	Al-6061-T6	In-mr1	
41	Oil pipe 2	1	St-AISI-321	In-op1	
40	Bolt 1/6 x 13/16	4	Carbon Steel	ASME B18.6.3	
39	Inlet skin structure	1	Al-6061-T6	In-skin	
38	Rivet 1/8 15/64	26	Carbon Steel	ASME B18.11.1	
37	Front frame	1	Carbon Steel	In-ffof	
36	Bolt 5/32 x 2 11/64	8	Carbon Steel	ASME B18.6.3	
35	Integrated hub rib	1	Al-6061-T6	In-r2	
34	Nut 1/4	16	Carbon Steel	ASME B18.2.1	For all 1/4
33	Washer φ1/4	16	Carbon Steel	ASME B18.2.1.1	For all φ1/4
32	Bolt 1/4 x 15/32	12	Carbon Steel	ASME B18.6.3	
31	Bolt 5/32 x 25/64	9	Carbon Steel	ASME B18.6.3	All undescribed
30	Washer passive wheel	1	Carbon Steel	In-wpawh	
29	Nut passive wheel	1	Carbon Steel	In-pwh	
28	Ball bearing	2		W617042ZS	
27	Bearing holder 2	1	Ti-5Al-2.5Sn	In-bhol2	
26	Nose cap	1	Carbon Steel	In-nc	
25	Cover	1	Carbon Steel	In-cov	
24	Washer φ5/16	1	Carbon Steel	ASME B18.2.1.1	
23	Nut 5/16	1	Carbon Steel	ASME B18.2.1	
22	Bolt 5/16 x 25/64	1	Carbon Steel	ASME B18.6.3	
21	Passive wheel	1	Carbon steel		
20	Washer	1	Carbon steel	In-wp1	
19	Nut	1	Carbon steel	In-mp1	
18	Shaft 1	1	Carbon	In-wsp	
17	Active wheel	1	Carbon steel	In-wha	
16	Washer active wheel	1	Carbon steel	In-wf1	
15	Nut active wheel	1	Carbon steel	In-mf1	
14	Airfoil bearing	1	Carbon	AS-AB1	
13	Airfoil bearing holder	1	Ti-5Al-2.5Sn		
12	HPT shaft	1	Carbon	ASS-2	
11	Panel 3	1	Al-6061-T6	In-p3	
10	Bearing holder	1	Ti-5Al-2.5Sn	In-bhol1	
9	Panel 2	1	Al-6061-T6	In-p2	
8	Washer φ5/32	25	Carbon steel	ASME B18.2.1.1	For all φ5/32
7	Nut 5/32	25	Carbon steel	ASME B18.2.1	For all 5/32
6	Bolt 5/32 x 13/16	8	Carbon steel	IASME B18.6.3	
5	2-nd flange	1	Al-6061-T6	In-f2	
4	Oil pipe 1	1	St-AISI 321	In-op1	
3	Integrated tip rib	1	Al-6061-T6	In-r1	
2	1-st flange	1	Al-6061-T6	In-f1	
1	Panel 1	1	Al-6061-T6	In-p1	

No.	Name of part	Quan.	Material	Standard	Coment
Scale	Author	Signs	Sheet A2	Name of drawing	
1:1	Checked by			Appendix 1 Assembly drawing of the UAV inlet	
Company name			Material	Drawing number	Pap. /No. Pap
Military University of Technology			Ti-10V-2Fe-3Al Al 6061-T6	PFF-63-IN	1/5

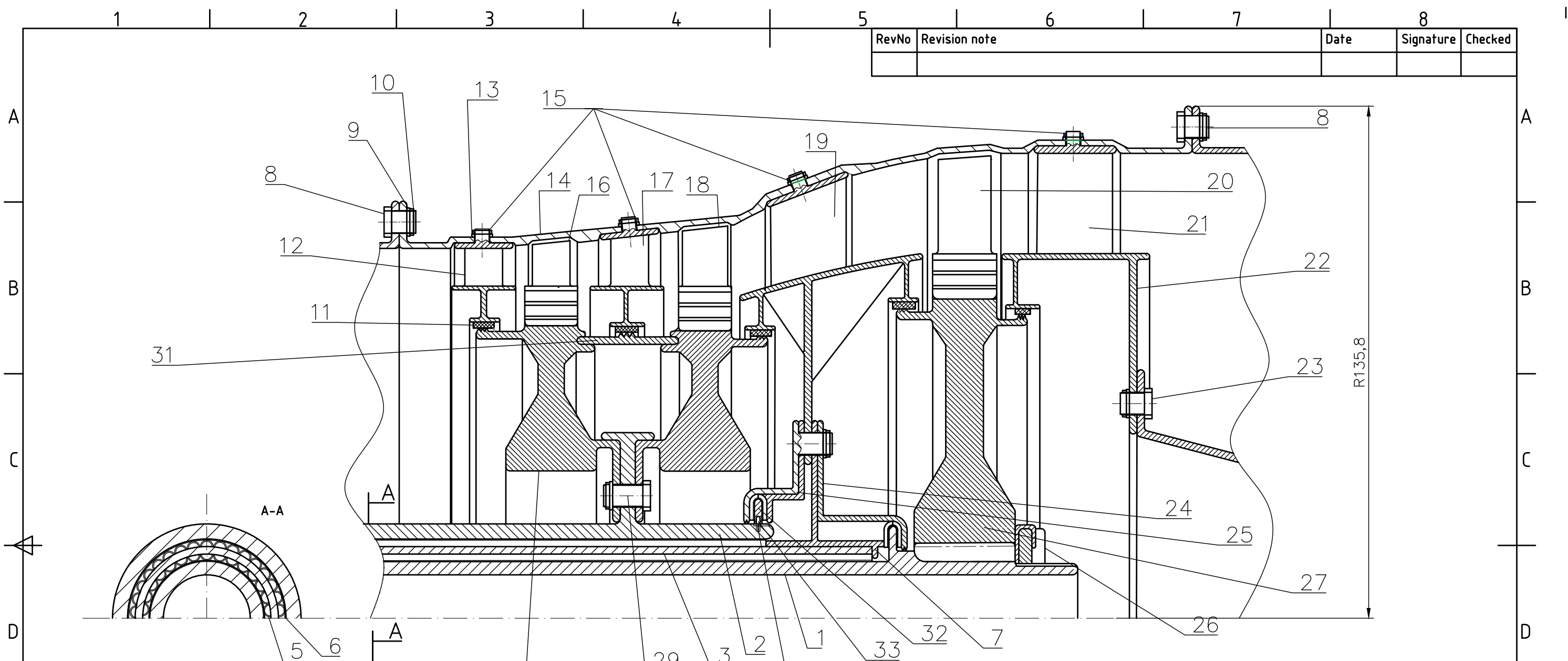


RevNo	Revision note	Date	Signature	Checked

32	Washer $\phi 0.99$	1	EB 88494		To convey a drive
31	Air pipe	1	No. PFF-63-C1-09	Carbon- steel	
29	Satelit pivot	1	No. PFF-63-C1-08	Carbon- steel	
28	Ring	3	DIN 471		
27	Gear	1	No.PFF-63-C1-G06	Carbon- steel	
26	Bearing	1	634		
25	Lead ring	7	No.PFF-63-C1-G02	Lead	
24	Gear d70	1	No. PFF-63-C1-G01	Carbon-steel	
23	Bearing	2	635		
22	Shaft	1	No. PFF-63-C1-06	H25N20S2	
21	Diffuser	1	No. PFF-63-C1-05	Ti6Al4V	
20	Washer $\phi=0.6$	3	EB 88494		
19	Drawing sheet	1	No.PFF-63-C1-G08	Steel	
18	Drawing sheet	1	No.PFF-63-C1-G07	Steel	
17	Washer $\phi=0.2$	16	DIN 125		
16	Bolt 5/ 32"-32 UNC	16	ISO 4017		
15	Nut 5/ 32"-32 UNC	16	ISO 4017		
14	Nut 9/ 16"-12 UNC	1	ISO 4017		
13	Carrier	3	No.PFF-63-C1-G05	Carbon- steel	
12	Protective tube	1	31125184.0050		
11	Expanding ring	2	DIN 471		
10	Bearing	3	634		
9	Safellite gear	3	No.PFF-63-C1-G04	Carbon-steel	
8	Rivet	2	BN-70/1121-06		
7	Washer $\phi=0.2$	16	DIN 125		
6	Bolt 5/ 32"-32 UNC	16	ISO 4017		
5	Nut 5/ 32"-32 UNC	16	ISO 4017		
4	Nut 3/ 16"-24 UNC	24	ISO 4017		
3	Impeller	1	No. PFF-63-C1-04	Ti6Al4V	
2	Guide vanes	24	No. PFF-63-C1-03	Ti6Al4V	
1	Compressor cover	1	No. PFF-63-C1-01	Ti6Al4V	
No.	Name of a part	Quantity	Norm/ No of draw	Material	Comments

FILE NAME	Appendix 2	FSCM NO	SHEET	A3	SCALE	1:1
SIZE						
DRAWN						
CHECK						
APPR.						
ISSUED						
REV						
CONTRACT NO	DWG NO PFF-63 - C0					

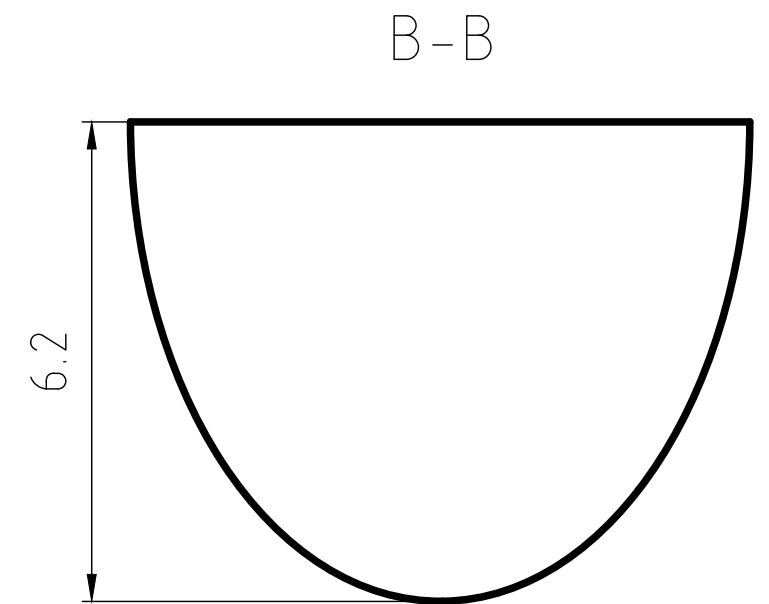
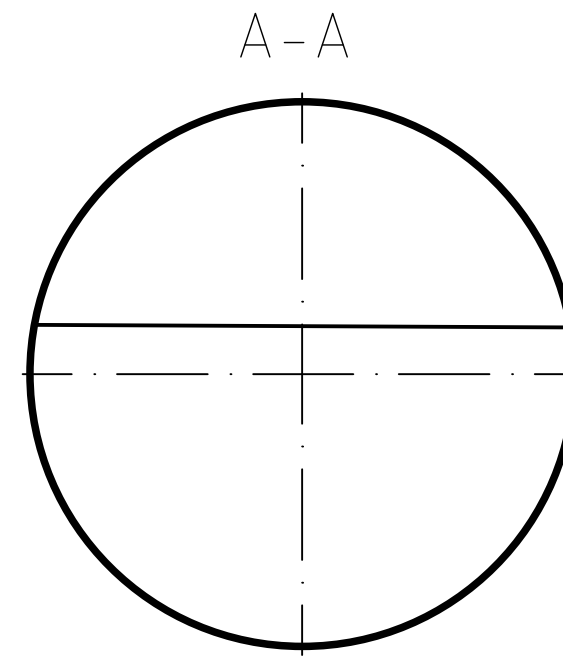
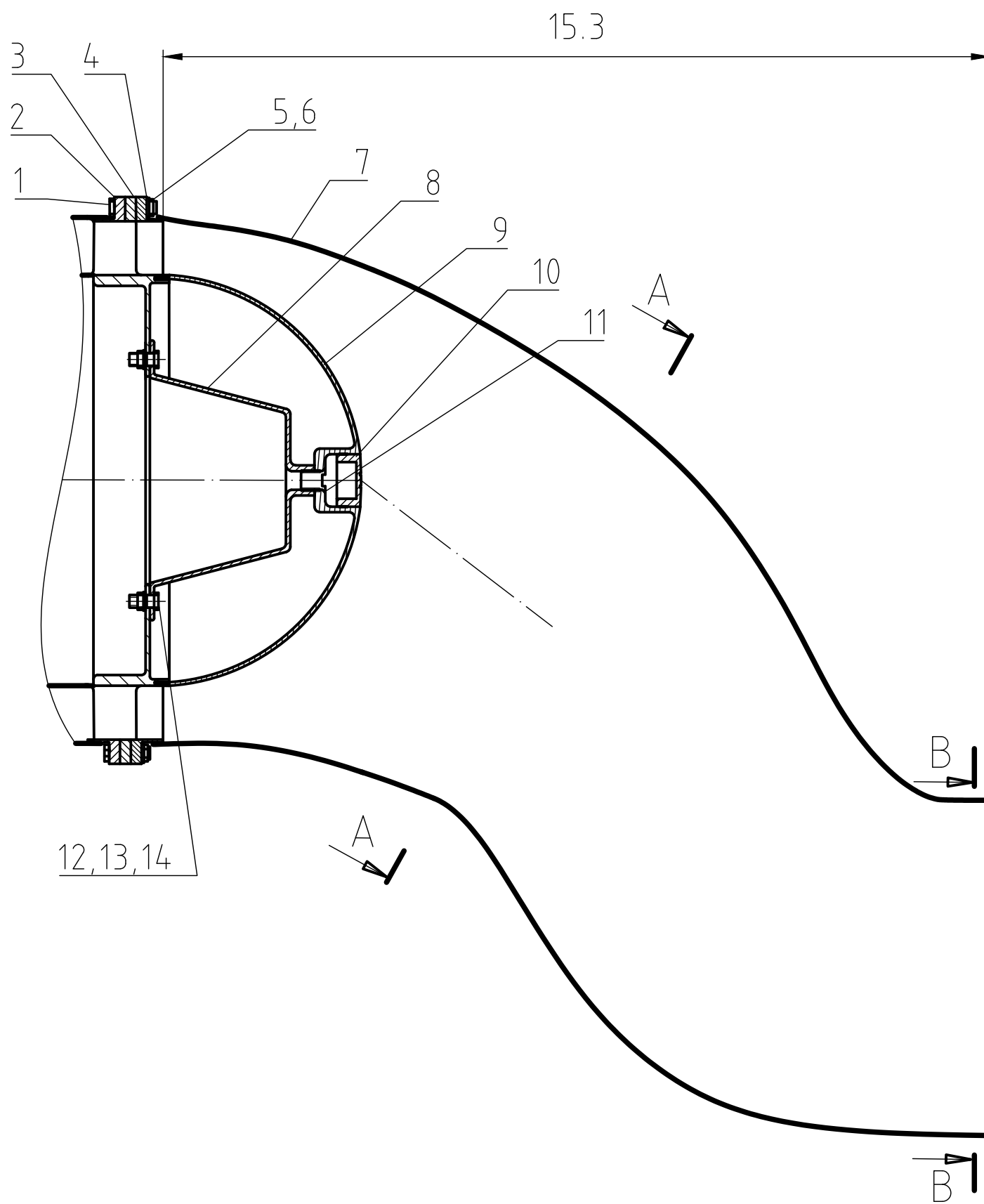
RevNo	Revision note	Date	Signature	Checked



No	Name of a part	Quantity	Norm/no of a draw	Material	Mass	Comments
34	Spring	1	Draw AS-3	Ti-5Al-2,5Sn	Mass	Comments
33	Pin	1	Draw AS-3	A-N720 CMC	Mass	Comments
32	Bearing nut	1	Draw AS-3	Ti-5Al-2,5Sn	Mass	Comments
31	Sealing ring	1	Draw AS-R1	A-N720 CMC	Mass	
30	HPT disk	1	Draw AS-D1	A-N720 CMC	0.73kg	Same for both stages
29	Bolt M6x10	11	ISO 4016	A-N720 CMC	0.93kg	
28	HPT disk	1	Draw AS-D1	A-N720 CMC	0.73kg	Same for both stages
27	PT disk	1	Draw AS-D2	A-N720 CMC	0.93kg	
26	Nut	1	Draw AS-S1	Ti-5Al-2,5Sn	0.001kg	
25	HPT bearing holder	1	Draw AS-3	Ti-5Al-2,5Sn	0.14kg	
24	PT bearing holder	1	Draw AS-3	Ti-5Al-2,5Sn	0.21kg	
23	Bolt M6x8	11	ISO 4016	Material	Mass	
22	Rib holder	1	Draw AS-3	Ti-5Al-2,5Sn	Mass	
21	Rib 2ed	3	Draw AS-2	H25N20S2	Mass	
20	Rotor blade 3rd	51	Draw AS-B5	A-N720	Mass	
19	Rib	3	Draw AS-2	Ti-5Al-2,5Sn	0.93kg	
18	Rotor blade 2ed	47	Draw AS-B4	A-N720 CMC	0.001kg	
No	Name of a part	Quantity	Norm/no of a draw	Material	Mass	

No	Name of a part	Quantity	Norm/no of a draw	Material	Mass	Comments
17	Nozzle blade 2nd	47	Draw AS-B3	A-N720 CMC		
16	Rotor blade	47	Draw AS-B2	A-N720 CMC		
15	Nut M4	24	ISO 4032	Carbon-steel		
14	Cover	6	Draw AS-2	H25N20S2		Cover must be assembled To join covers
13	Washer Ø4	24	EB 88494	Carbon-steel		
12	Nozzle blades	47	Draw AS-B1	A-N720 CMC		
11	Seal	6	Draw AS-2	Graphite		Sprayed in shown places
10	Nut M6	33	ISO 4032	Carbon-steel		For all M6 screws
9	Washer Ø6	33	EB 88494	Carbon-steel		For all M6 Screws
8	Bolt M6x8	22	ISO 4016	Carbon-steel		
7	Bearing holder	1	Draw AS-2	Ti-5Al-2,5Sn		
6	HPT top foil	1	Draw AS-AB1	18Cr9Ni		
5	PT top foil	1	Draw AS-AB1	18Cr9Ni		
4	HPT Airfoili bearing	1	Draw AS-AB1	Carbon		
3	Airfoil bearing	1	Draw AS-AB1	Carbon		
2	HPT shaft	1	Draw AS-S2	Carbon		
1	PT shaft	1	Draw AS-S1	Carbon		

FILE NAME	FSCM NO	SHEET	SCALE
Appendix 3	None	A3	1:1
SIZE			
DRAWN			
CHECK			
APPR.			
ISSUED			
REV		DWG NO	
CONTRACT NO		AS-1	

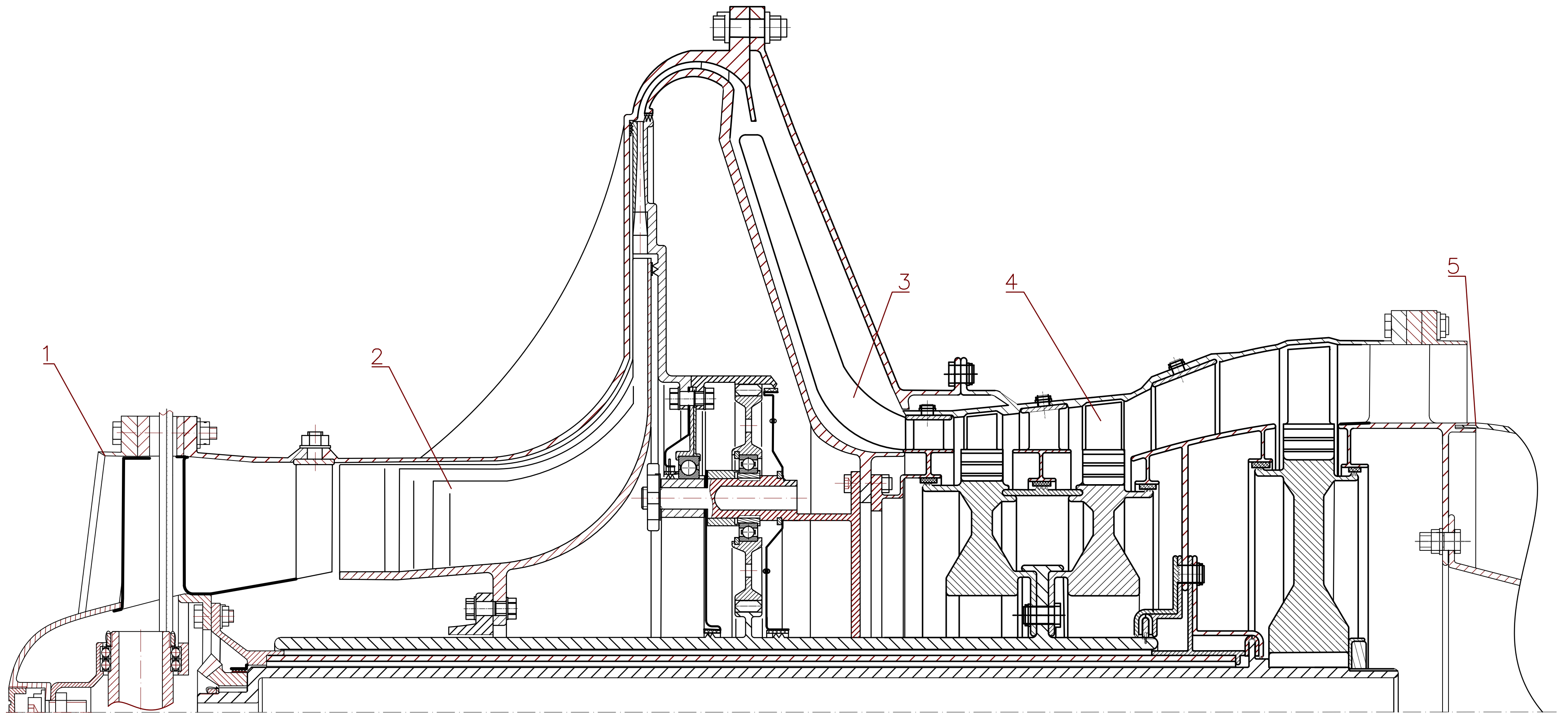


14	Bolt 5/16 x 5/32	11	Carbon steel	ASME B18.2.1	
13	Washer 5/16	11	Carbon steel	ASME B18.21.1	
12	Nut 5/16	11	Carbon steel	ASME B18.6.3	
11	Screw	1	Carbon steel	DI-SC1	
10	Plug	1	H25N20S2	DI-P	
9	Cone	1	H25N20S2	DI-C	
8	Cone strut	1	Ti-10V-2Fe-3Al	DI-CS	
7	Diffusor skin	1	H25N20S2	DI-S	
6	Washer $\phi 1/4$	20	Carbon steel	ASME B18.21.1	
5	Nut 1/4	20	Carbon steel	ASME B18.6.3	
4	Diffusor flange	1	Carbon steel	DI-DF	
3	Integrated rib ring	1	Carbon steel	DI-IRR	
2	Turbine cover flange	1	Carbon steel	DI-TCF	
1	Bolt 1/4 x 25/32	20	Carbon steel	ASME B18.2.1	

No.	Name of part	Quan.	Material	Standard	Coment
-----	--------------	-------	----------	----------	--------

Scale	Author	Surnames	Signs	Sheet A3	Name of drawing Appendix 4 Assembly drawing of the UAV diffuser
1:2.5	Checked by				

Company name	Material	Drawing number	Pap. /No. Pap
Military University of Technology	H25N20S2	PFF-63-DI	4/5



4	Diffusor	1		D.No. 4, DI	
3	Turbine	1		D.No. 3, ASS-1	
2	Compressor	1		D.No. 2, CO	
1	Inlet	1		D.No. 1, IN	
No.	Name of part	Quan.	Material	Standard	Coment
Scale	Author	Signs	Sheet	Name of drawing	
1:1	Checked by				
Company name			Material	Drawing number	Pap. /No. Pap.
Military University of Technology					5/5